# ADAMA SCIENCE AND TECHNOLOGY UNIVERSITY

## School of Mechanical, Chemical and Materials Engineering


# Design and modification of electric vehicle chassis frame for swapping mechanism of battery packs

*A thesis submitted in partial fulfillment of the requirements for the award of the degree of Master of Science in Automotive Engineering*


**By**

**DEREJE ARIJAMO**

Advisor: - Ramesh Babu Nallamothu (Associate Professor)

**DEPARTMENT OF MECHANICAL SYSTEMS AND VEHICLE ENGINEERING**



October, 2018

Adama, Ethiopia

# CANDIDATE'S DECLARATION

I hereby declare that the work which is being presented in the thesis entitled "Design and modification of electric vehicle chassis frame for swapping mechanism of battery packs" in partial fulfillment of the requirements for the award of the degree of Master of Science in Automotive Engineering is an authentic record of my own work carried out from October 2017 to October 2018 under the supervision of N. RAMESH BABU Department of Mechanical and Vehicle Engineering, Adama Science and Technology University, Ethiopia.

The matter embodied in this thesis has not been submitted by me for the award of any other degree or diploma. All relevant resources of information used in this thesis have been duly acknowledged.

| Name | Signature | Date |
|---|---|---|
| Dereje Arijamo | ____________ | 2018-10-09-GC |

Student

This is to certify that the above statement made by the candidate is correct to the best of my knowledge and belief. This thesis has been submitted for examination with my approval.

| Name | Signature | Date |
|---|---|---|
| N. Ramesh Babu | __________________ | ______________ |

Advisor

# ADAMA SCIENCE AND TECHNOLOGY UNIVERSITY

**SCHOOL OF MECHANICAL, CHEMICAL AND MATERIALS ENGINEERING**

**DEPARTMENT OF MECHANICAL AND VEHICLE ENGINEERING**

## Design and modification of electric vehicle chassis frame for swapping mechanism of battery packs

**By**

**Dereje Arijamo**

Approved by board of Examiners

Chairman, Department graduate committee

Advisor

Internal Examiner

External Examiner

## DEDICATION

*Dedication to my beloved family (Arijamo and Debebech) mom and dad, (Adanech, Daniel, Hanna, Tekle, Natnael) Sisters and brothers and sincerely for my little sisters Adanech Arijamo and Hanna Arijamo for their immeasurable support.*

ACKNOWLEDGEMENT

First of all, I would like to thank God for his endless blessings and gifts! I would like to thank my adviser Ramesh Babu Nallamothu (Associate Professor) for his scientific and technical guidance and support throughout this thesis, without his continuous corrections and constructive comments this thesis wouldn't have been successful. My advisor Ramesh Babu Nallamothu (Associate Professor) helped me through this thesis even starting from title selection.

I am grateful to all staff of ASTU, School of Mechanical, Chemical and Materials Engineering for giving me the opportunity to learn this M.Sc. program without tuition.

I would also like to thank my mother Debebech Derza, and my exhilarates (Dereje Gutema, W/ro Amakelech takele, W/ro Yeshi (RIP), Yared Wolde), for their endless comment, understanding, support and encouragement in my life. Last but certainly not least, I would like to thank all of my friends for their encouragement, and support with different materials and ideas. They helped me through the data collection by finding manuals as well as guidance through difficult steps.

## TABLE OF CONTENTS

**CONTENTS** **PAGES**

# LIST OF FIGURES

**FIGURES** **PAGES**

# LIST OF TABLES

**TABLES** **PAGES**

# ACRONYMS AND ABBREVIATIONS

| | |
|---|---|
| AISI 1020 | American iron and steel institute |
| BEV | Batteries of Electric Vehicles |
| BTMS | Battery Thermal Management System |
| CAE | Computer Aided Engineering |
| CFRP | Carbon fiber reinforced plastic |
| EVs | Electric Vehicles |
| FEM | Finite Element Method |
| FSAE-A | Formula Society of Automotive Engineers Australia |
| HBEFA | Handbook Emission Factors for Road |
| HEVs | Hybrid Electric Vehicles |
| IAA | Insurance Auto Auction |
| LCU | Load capacity utilization |
| NTM | Network for transport measures |
| PEV | Personal electric vehicle |
| PHEVs | Plug- In Hybrid Electric Vehicles |
| PEO | Polyethylene oxide |
| PVA | Polyvinyl alcohol manufacture |
| RAV4 | Recreational Activity Vehicle: 4-wheel drive |
| REV | Renewable energy vehicle |
| RHS | Rectangular tube high reputation |
| SAE | Society of Automotive Engineers |
| SLI | Starting, Lighting, and Ignition |
| SSM | Swapping Station Manager |
| SUV | Sport utility vehicle |
| TÜBİTAK | Scientific and technological research council turkey |
| UDL | Uniformly distributed load |
| UWA | University of western Australia |
| 6061-T6 | ‘T’ Temper or degree of hardness (heat treated) |

## Notations

| | |
|---|---|
| A | Area |
| C | Specific heat capacity |
| D | Diameter |
| E | Elasticity |
| $E_g$ | Power (energy generated) |
| F | Force |
| f | fluid |
| g | Gravity |
| h | Convective heat transfer coefficient |
| I | Moment of inertia |
| k | Thermal conductivity |
| L | Characteristic length |
| M | Bending moment |
| m | Mass |
| Nu | Nusselt number |
| Pr | Panditl number |
| t | Time |
| R | Reacrion |
| Re | Reynolds number |
| S | Displacement |
| $T_{air}$, $T_f$, $T_p$ | Temperature of (air, fluid, plate) |
| u | Speed |
| V | Volume |
| $V_s$ | Shear force |
| W | Weight |
| $w_n$ | Work ne |
| Y | Deflection |

## Symbols

| | |
|---|---|
| $\rho$ | Density |
| $\nu$ | Kinematic viscosity |
| $\Delta$ | Change |
| $\mu$ | Dynamic viscosity |
| $\sigma$ | Stress |
| $\dot{m}$ | Mass flow rate |
| $\Delta t$ | Change in time |
| Ixx | Mass moment of inertia |

# ABSTRACT

Automotive industries are moving towards the manufacturing of electric vehicles to reduce the consumption of fossil fuel and related harmful exhaust emissions from engines. In electric vehicle energy stored in the battery is the source of the energy to drive the electric vehicles. At the moment the size and the weight of the battery pack required for given mileage is very much high when compared to its counterpart IC engine. Size and shape of battery varies depending on the type of the battery selected and vehicle model. The electric vehicles impose additional requirements on chassis of the vehicle which is the load bearing frame of the vehicle. The chassis should be able to bear the heaviness of the battery pack and sustain load variation when swapping the battery. Provision of swapping electric vehicle battery helps in minimizing the wastage of vehicle time in waiting for charging the battery. The objective of this thesis work is to modify of the existing RAV4 EV 2014 electric vehicle chassis frame to swapping purpose rather than permanent battery pack on chassis frame. Material AISI 1020 and rectangular cross section in 80 mm x 40 mm x 4mm is selected to the electric vehicle chassis frame. The modeling was done by using CATIA V5 R20 the total deformation of chassis frame is 1.007 mm, equivalent stress is 115.88 MPa and the life of the chassis on full load is 130 days without deformation. In modal analysis and harmonic analysis there is no chance of resonance frequency existence in 10 modes of analysis after having this the weight of the electric vehicle battery pack is decreased from 383.51kg to 345.615Kg by shape minimization of the cooling plate and the BTMS fluid (water) inlet temperature is 20$^{o}$C, outlet temperature of fluid is 38$^{o}$C was done by transient analysis method on EXCEL. Finally prototype of a model of miniature size has prepared for exhibiting the shape of modified chassis.


Key words: - Chassis frame, Electric vehicle, Batteries pack, swapping and BTMS

# CHAPTER ONE

# 1 INTRODUCTION

## 1.1 General introduction

The automotive industry is facing tremendous engineering challenges over several years to meet the requirements generated by the fuel shortage, fuel cost, pollution control, raw material cost, and costumer safety. In meeting these challenges a wide variety of new models has been emerged or entered into the market in search for better strength and safety and fuel efficiency ***(Jean-Francois & Kamel, 2017)***. But now a day there was problem facing the fuel, problems like (global warming, availability of fuel, cost of fuel), in industries, locomotives and vehicles uses this fuel for their operation. Countries like Ethiopia spends more money for the purpose of importing the crude oil vehicles. Those vehicles also use oil for their operation, so need of finding other option to solve this problem. And adapting electric vehicle in the country is the first option because Ethiopia have developing electric power alternatives but it has no oil or fuel.

One of the possibilities is the electrification of our fleet of cars, vans, motorcycles, buses, trucks... Hybrid Electric Vehicles and Plug in Hybrid Electric Vehicles are the first steps to make the transition possible to the fullest electrification (Battery Electric Vehicles (BEVs)) of the automotive sector for the future. An Electric Vehicle is an alternative motor-vehicle (auto-mobile) propelled or driven by an electric motor, no need of fuel to propel the vehicle ***(Pesaran, Swan, & etal.., 2011)***.

Electrify vehicles then the challenges on electric battery packs instead of fuel, then researchers, universities and colleges contribute their knowledge on battery studies and related works. One contribution in this aspect is making the vehicles electric battery swappable. Swap (changing the discharged battery pack with the fully refueled battery pack) to make vehicles swappable, chassis should be design by considering swapping of battery pack.

The objective of this thesis work is to modify the existing RAV4 EV 2014 electric vehicle chassis frame to swapping mechanism of battery packs and design the modified chassis including all chassis parameters and checking thermal management system of electric vehicle battery after modified chassis frame. ****swap**** in this context changing the discharged (depleted) electric vehicle battery pack with charged one to propel the vehicle.

A ladder type chassis design was selected in this work, all the loadings and shape parameters are same with the existing one and only the changed part of the vehicle is the frame and coolant plate.

## 1.2 Background

The first Electric vehicle was built in between 1832 and 1839 in Scotland. Robert Anderson was the person, who built first crude electric carriage. Afterwards, Professor Stratingth of Groningen, Holland had started to design small scale electrical cars. In 1835, Electrical Car was produced by his assistance Christopher Becker. Those were the electrical cars based on the battery. American *Thomas Devenport and Scotsmen Robert Davidson* had used non rechargeable electrics cell. They built electric road vehicles in 1942. Storage battery based cars were produced till then, but the storage capacity of the battery was not so good. In 1965 Frenchmen Gaston plante made a new battery, which storage capacity was improved. Countrymen Camille Faure had further improved the capacity of battery in 1881. In 1964 GM‟s Engineering staff invented an Electro air. That car had a very good function and elements ***(Lovatt, 2008)***.

Each country government encourages the projects on electric vehicle but the projects as well as thesis are young for in any aspects of electric vehicle study. So project in this thesis sector is not done previously and there is no written document or journals on it but the projects on electric vehicle chassis frame for sport utility vehicles by SAE is done but it is not for swapping purpose and the papers on the battery is done. Battery thermal management system is also studding by many researchers all over the world but the swapping technology is very new and developing in same country's like USA, China, India other countries trying to adopt it.

In our country sugar factories, cargos and other huge industries for their indoor purpose use the forklifts which are driven by Battery cells. And the vehicles took long time to charge and they work for only 5-6 hrs and they stand for 8-10 hrs for charging purpose. In this case the workers carry those big loads instead of vehicles and there is need of lots of man power and the time is long to accomplish the duties.

According to the above reasons and to transfer technology the title Design and modification of electric vehicle chassis frame for swapping of battery packs was selected and done.

Finding the base line is also taken as a problem, those forklifts found in sugar factories are old in age and thesis is also not invited to the technology so as alternative finding the vehicles that made many in number and which have the problem like those fork lifts, then gating RAV 4 EV 2014 model is founded in this problem it takes 5-6 hrs. to charge the battery. Then taking it as base line and med its battery pack into swappable. BTMS after med of the battery swappable. BTMS by transient analysis.

## 1.3 Statement of the problem

In last decades, with the increasing development of battery technologies and concerns for the environment, electric vehicles (EVs) technologies got rapid development. However, EV drivers have to face the problem of battery refueling on a daily basis. Once the battery runs out, drivers can recharge it in the charging station. The battery takes 6-8hrs to full charge in AC charging according to the manufacturer specified time. That mean waiting long time to refuel the battery in permanently attached battery pack is as main problem. How to make those permanently attached battery packs with its chassis frame into swappable? And the other problem that face the electric vehicle battery is battery thermal management system, and how can the thermal management system cases the problem on permanently attached battery pack with chassis frame? And what BTMS look like in swappable battery pack?

## 1.4 Objectives

### 1.4.1 General Objective

The objective of this thesis work is to design and modify of the existing RAV4 EV 2014 model electric vehicle chassis frame for swapping mechanism of battery packs and check the thermal management system of the battery pack after design the chassis frame.

### 1.4.2 Specific Objectives

The specific objectives of the proposed thesis work are as follows:

- To select the base line model of electric vehicle and identify existing chassis frame problems
- To design and modify the chassis and making CAD modeling to show swappable chassis frame
- To perform static, dynamic, harmonic and static impact (crush analysis) on finite element (ANSYS)
- To identify battery thermal management system in transient analysis and ANSYS FLUIENT
- To prepare prototype for demonstration of the shape

### 1.5 Significance of the project

The significance of the proposed thesis work is as follows:

- Design and modification of RAV4 EV 2014 model electric vehicle chassis frame from mounted electric battery pack into swappable and make it minimize the time to waste the charging (by swapping the battery pack).
- Helps to cool a battery. As we know the main problem of batteries is heating (high temperature) or battery thermal management system. If we swapped the battery it tends to cool and ready for the next session and the need of coolant is only in the case of driving and charging.
- The way of gating alternative batteries and investigating new batteries are also open.
- Detail recommendation discussed and showing future works to the researchers.

### 1.6 Limitation of the thesis work

The main limitation on this thesis work is finding the base line electric vehicle in Ethiopia, the company found in legetafo/Ethiopia which is inaugurated in 2015 to assemble the Solarries eletra electric vehicles, but now is closed because of loss so, decide to work taking the electric vehicle manual from the Toyota company website (measuring the size of the RAV 4 2014 model vehicle for assurance) based on the problems that are shown in the sugar factories forklift and done on it.

The other limitation of this thesis was computer power. Because of this reason the explicit dynamic analysis is not done on this thesis work. The static impact analysis is done instead of explicit dynamic analysis and the remaining other all analysis are done on ANSYS 15.

### 1.7 Delimitation (scope)

This thesis is delimited to the modification of the chassis frame for RAV4 EV 2014 model electric vehicle, the chassis frames of other type of electric vehicles are not included, dynamic analysis like modal and harmonic analysis of chassis frame with selected materials is included, life of chassis frame is included, battery thermal management system is discussed, explicit dynamic analysis is not included but instead of this the crush analysis in static structure was done.

## 1.8 Structure of the Report

This report is consists of six chapters. The *first chapter* is introduction about the research study. It includes the background of study, problem statement, objectives, scopes, limitations, significant of the study and the structure of report.

*Next chapter* focuses on the literature review based on the previous convectional chassis frames, electric vehicle chassis frame and electric vehicle battery packs done.

*Chapter three* includes material and methods of the thesis and how was it done? And includes design process, design considerations for chassis frame Selection of chassis frame material, review and specification for the existing RAV4 EV 2014 model, EV vehicle overview and specification for rav4 EV 2014 model and finally the working of demonstrative prototype is described.

*Chapter four* includes design, modeling and analysis for the chassis frame, analytical calculation, CAD modeling for electric vehicle chassis, finite element analysis like meshing, loading and boundary conditions are included.

*Chapter five* includes result and discussion for the thesis work and static structural analysis for electric vehicle chassis frame, fatigue tool analysis for electric vehicle chassis frame, modal analysis for electric vehicle chassis frame, harmonic response for total deformation and static impact analysis (instead of explicit analysis).

*Chapter six* about the battery thermal management system the analysis was done by using the transient analysis and the graph indicates the average temperature throw the fluid and lintier coolant plate, the graph was done by using EXCEL and figures by fluent for visualization purpose.

*Chapter seven* the cost analysis of the chassis frame. Cost included the chassis frame cost and the plate that covers the chassis above and below to accommodate the battery pack.

*Final chapter* of this thesis consists of summery, conclusion, recommendation and future works of this thesis study. The overall conclusion with finalized details is discussed with some recommendation for improvements proposed.

# CHAPTER TWO

# 2 LITERATURE REVIEW

## 2.1 Introduction

This chapter focused on the research information those are done by other researchers and the outcome of the study about the related vehicle chassis and electric vehicle chassis. This literature used as the guideline to find the most suitable material and design based on the factor and the supported theory to finalize the design of the chassis for the electric vehicle to be developed.

## 2.2 Chassis frame

Chassis of Automotive or automobile helps keep an automobile rigid, stiff and unbending. Automobile chassis ensures less noise, vibrations and harshness throughout the automobile ***(Abhishek & Soni, 2014).***

The chassis can be classified roughly based on the frame type as ***(Rajput, 2007)***;

- **Ladder frame chassis -** ladder chassis resembles a shape of a ladder having two longitudinal rails inter linked by lateral and cross braces.
- **Space frame chassis** - A space-frame is analogous to a truss style bridge which is made up of small (generally straight) members in a triangular pattern which are always in pure compression or tension.
- **Backbone chassis -** Backbone chassis it has a rectangular tube type backbone, which is usually made up of glass fiber that is used for joining front and rear axle together.
- **Monocoque chassis -** Monocoque Chassis is a one-piece structure it is overall shape of a vehicle.

### 2.2.1 Longitudinal Torsion

Consequent upon the simultaneous rolling of the diagonally opposite front and rear road which over bumps, twist occurs in the chassis in opposite direction so that both the side and the cross member are subjected to longitudinal torsion. As a result, the chain distorts as shown in Fig 2-1.

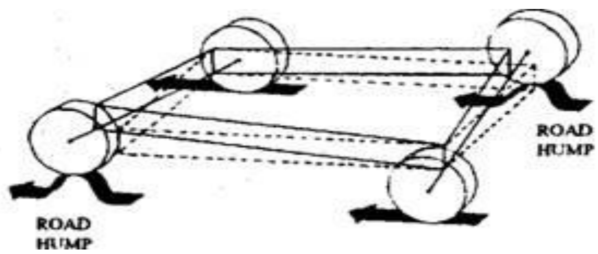


Figure 2-1 Longitudinal torsion

The camber of the road, side wind, centrifugal force while the tricycle negotiates a corner or collision with some object exposes the chassis to external (side) force. As the road wheel tyres opposes that external forces due to adhesion reaction, a nut bending moment acts on the chain side members so that the chassis frame tends to tow in the direction of the force. This reaction is called lateral bending and shown in Fig 2-2 ***(Adem, 2015)***.

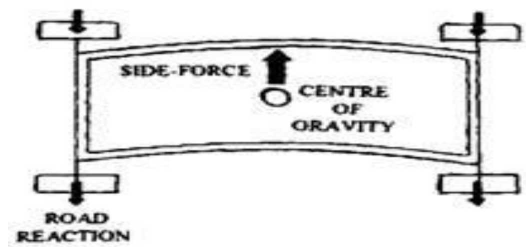


Figure 2-2 Lateral bending

A chassis frame if driven forward or backwards is continuously subjected to wheel impact with road obstacles such as pot holes, road joints, surface humps and curbs while other wheels produce the propelling thrust. These condition cause the rectangular chassis frame to distort to a parallelogram shape, known as lozenging as shown in Fig 2-3 ***(Adem, 2015)***.

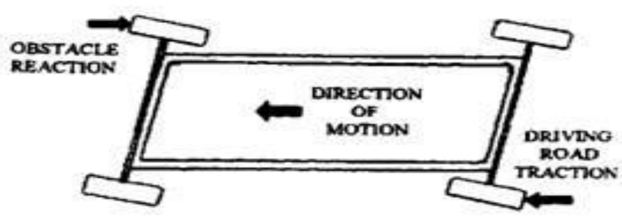


Figure 2-3 Lozenging

### 2.2.2 Vehicle chassis and frame design

One of the fundamental and most important stage during designing process is proper develop of chassis and frame of the vehicle, especially for special heavy vehicles. Design of the vehicle chassis has to be started from analysis of load cases. There are five basic load cases to consider Fig 2-4.

- Bending case: loading in vertical plane, the *x-z* plane due to the weight of components distributed along the vehicle frame which cause bending about the y-axis;
- Torsion case: vehicle body is subjected to a moment applied at the axle centerlines by applying upward and downward loads at each axle. These loads result in twisting action or torsion moment about the longitudinal x-axis;
- Combined bending and torsion loads;
- Lateral loading: generated at the tire to ground contact patch. These loads are balanced by centrifugal forces;
- Fore and aft loading: generated when vehicle accelerates and decelerates inertia forces ***(Szczesniak, Nogowczyk, & etal.., 2014).***

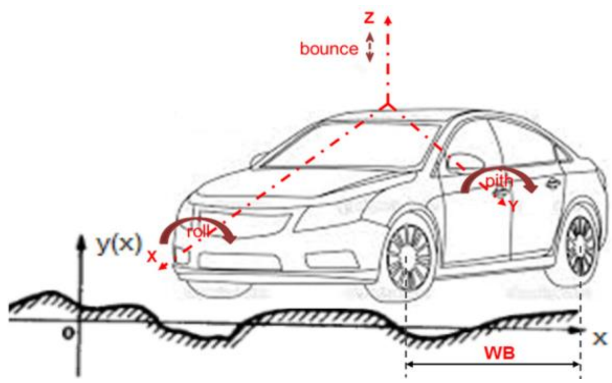


Figure 2-4 Axes of the vehicle and directions of basic movements

## 2.3 Chassis for electric vehicles

***(Dávila & Schönwald, 2013)*** the work on electric vehicle chassis. The chassis was conceived to provide the best compromise in terms of simplicity and cost effectiveness. Correspondingly it was decided to select two highly consolidated and thus affordable suspension archetypes, a McPherson for the front axle and a twist beam for the rear, each also offering a high level of integration and many advantages in terms of layout and packaging, being relatively easy to match with the modular powertrain developed. The aluminum casting solution has the advantage of requiring a single piece which is 30 % lighter and its cost although higher is still coherent with the vehicle category. but the final choice of the full steel solution emerged from the cost/benefit evaluation. And the CAD for the lateral and longitudinal dynamic analysis Chassis development for an EV follows a similar procedure to that of a conventional car. In this case, the dynamic behavior of the vehicle must be defined and for that reason, several types of suspension were considered. Each concept vehicle used a different type of suspension and both the lateral and longitudinal dynamics were evaluated through simulation.

## 2.4 Finite element modeling and analysis for electric vehicle chassis

Finite Element Analysis (FEA) is a powerful tool for analyzing any and all mechanical problems. To analyze a problem, first a geometry and material must be defined. Next, loads and boundary conditions are applied. Third, a mesh is applied, breaking the larger problem into a series of smaller problems. The mesh, in turn defines a large matrix of equations, which then must be solved simultaneously.

***(Prorok, 2016)*** Optimization of Formula SAE Electric Vehicle Frame with Finite Element Analysis. In the rules, the baseline material is AISI 1010 steel. Alternate materials are permitted, provided that structural equivalency to the baseline can be proved. For equivalency, tensile yield Strength, tensile Ultimate Strength and Buckling Modulus must be equivalent.

***(Taufik, Rashid, & etal.., 2014)*** The evolution of computer aided design (CAD) systems and related technologies has promoted the development of software for the east of chassis modeling. It visualizes the main outputs of the model, which consist in numeric data and graphic elements. This reduces the simulation time dramatically and enables the optimization process to come to successful results. This paper presents an electric car chassis design by using the commercial design software package, CATIA V5 R19. The design of the chassis with adequate stiffness and strength is the aim of this project. The material used is mild steel AISI 1018 with 386 MPa of yield strength and 634 MPa of ultimate strength. The result shows that the critical point of stress and displacement occurred in the middle of the side members in all loading conditions; maximum stresses are below the yield stress. The final products for the design have been fabricated successfully.

***(Behera & Kumar, 2016)*** In this paper the researchers work on the tile of static load analysis of ladder type chassis frame. In this research work the paper contains modeling, design & varies stress distribution for bending analysis of light vehicle chassis. The researchers use the materials like aluminum alloy and structural steel for the light weight chassis on different cross section of the chassis. And they select structural steel on the rectangular cross section because of its low deformation and cost.

***(Badgujar & Wankhade, 2015)*** This paper presents Static Analysis of Chassis Frame of Electric Tricycle. The model is created using CATIA V5 and imported to ANSYS 12 for static structural analysis. The stress plot includes Von Mises stress and shear stress along with displacement plot. The results are compared with analytical, calculated using bending of beam theory. As a conclusion The highest shear stress occurred is 75.571 MPa by FE analysis the calculated maximum shear stress is 81.9752 MPa. The result of FE analysis is 7.81 % lesser than the result of analytical calculation. The difference is caused by simplification of model and uncertainties of numerical calculation.

***(Damtie, 2013)*** It is significant to know the current strength situation of three wheeled vehicle frames to be confident on their load carrying capacity, service and use. They are antiquated, unsafe and highly polluting, so there is substantial room for improvement in this huge market. A new three wheeled vehicle is designed and achieved by modeling and analyzing the existing three wheeled vehicle model and by modeling a new three wheeled vehicle by using CATIA AND ANSYS. In the existing model all the total displacement values obtained were above 60mm. but in the new model designed using space frame the maximum displacement obtained was 2.07mm. This indicates that the stiffness value has been improved. Also in terms of the crash analysis the maximum von-misses stress obtained in the existing model was about 70 times larger than the results obtained in the new model. This shows that the new model can withstand impact loads so as the risk level has been minimized.

***(Zainuddin, Abidin, Ibrahim, & etal.., 2015)*** Stress Analysis of the Personal Electric Vehicle by taking base line vehicle GW15ZD/ DAIN Foldable bicycle. The power required to drive a personal electric vehicle can be reduced by reducing its weight. The structural frame of a PEV is a component that has great potential to be made lighter. However, it must be designed to withstand the payload and the dynamic load experienced in its operation. In this study, the stresses exerted on the chassis of a sit-on PEV subjected to impact loading condition is analyzed. A design of the chassis with reduced weight is also proposed. The success in the reduction of PEV frame mass by 63% is due to two major factors which are the material of the frame and the geometry of the frame. By selecting the right alloy material it enables significant mass reduction without compromising with the stiffness and strength requirement. The result of the stress analysis from the Finite Element Analysis shows the effectiveness of computer aided optimization technique.

***(Spanoudakis, 2010)*** The main target of this paper is to evaluate chassis deformation, based on static and modal analyses, in order to reduce weight and at the same time achieve adequate vehicle operation in a demanding low energy consumption race. By using the software’s like EPILYSIS solver and results are evaluated using META. A modal analysis is also set up and run, to determine the natural frequencies and the mode shapes of the chassis, so to partly understand the dynamic behavior of this structure. The design is carried out based on specific standards and limitations set by the competition regulations. All analysis are carried out for three different chassis models, respectively 2014, 2015 and 2016 (Louis vehicle), modeled in ANSA, solved with the Epilysis solver and evaluated using META post-processor. then after gathering the information of each model, it is evident that the new chassis (2016) can satisfy all design requirements and specifications set and at the same time provides lower weight, better stiffness to weight ratio and adequate response in bending and torsion frequencies.

***(Emre, 2015)*** This study is to design rigid and lightweight chassis for an electric vehicle. Design criteria and constraints are obtained from the TÜBİTAK electro mobile racing rules. Various chassis types with different geometries are considered and 18 units of chassis are designed using Computer Aided Design (CAD) software. Designs are analyzed using Finite Element Analysis (FEA) software and performance characteristics are parametrically and structurally optimized. Optimum design has aluminum 5042 H-19 space frame structure type and weighs 28.163 kg. Maximum von-Mises stress of the proposed design is 15.465 MPa and the value is far below the material's yield strength of 345 MPa. Torsional stiffness value of the chassis is generated from the result of 2.495 mm maximum torsional deformation and calculated as1828.289 Nm/deg.

***(Amin, 2009)*** The objective of this project is to design and analyze the chassis of an electric vehicle for use in campus condition. The design contain several specifications that were prescribed in the problem statement. In order to get to the objective, any information about electric vehicle and its chassis were gathered to get a better insight about the research. Information about software such as CATIA and COSMOS Works will also be gathered. And the dynamic and static analysis is hailed by that software's.

***(Waterman, 2011)*** Design and build a space-frame chassis for a race car to compete in the FSAE-A competition as part of the UWA REV team. The chassis design implements structural battery boxes which have the dual purpose of protecting the driver from the batteries and adding strength to the frame, this has not previously been used in any other FSAE car. Using these stressed battery boxes gives the chassis excellent torsional stiffness, yet the entire frame still weighs just over 40kg. Then a chassis design is complete and meets the FSAE rules. The chassis design is a unique one using the battery boxes as a structural component to stiffen the weaker, open cockpit section which has not been done before in FSAE.

***(Singh, 2017)*** Analysis of chassis frame for improving its payload. And also the paper analyzed the backbone frame for both dynamic and static load condition with the stress deflection bending moment on the electric car chassis frame. The finite element analysis over ANSYS is performed by considering the load cases and boundary conditions for the stress analysis of the chassis. The electric car chassis is being modelled in CATIA V5 and finite element analysis software-ANSYS. At present the weight of the chassis is 40 kg in this project they have reduced the weight of chassis by 50% and load capacity is still same. This has been carried out with the help of shape optimization. By considering different materials.

The Finite Element Analysis (FEA) is a computational technique used to obtain approximate solutions of boundary value problems in engineering ***(Contractor, Gaurav, & Rathod, 2015)***. An unsophisticated description of the FE method is that it involves dividing a structure into several elements (pieces of structure), describing behavior of each element in simple way, then reconnecting elements at nodes as if nodes were pins or drops of glue that hold elements together as shown in Fig 2-5 and 2-6. This process results in a set of simultaneous algebraic equations. In stress analysis equation are equilibrium equations of the nodes. There may several hundred or several thousand such equations, which mean that computer implementation is mandatory ***(Robert, 1995)***

### 2.4.1 General Procedure for FEA

There are three basic steps in formulating finite element analysis pre-processing, solution and post processing. The pre-processing (model definition) step includes: define the geometric domain of the problem, the element type(s) to be used, the material properties of the elements, the geometric properties of the elements (length, area, and the like), the element connectivity (mesh the model) as Fig 2-5 and Fig 2-6, the physical constraints (boundary conditions) and the loadings ***(David, 2004)***. The next step is solution, in this step the governing algebraic equations in matrix form and computes the unknown values of the primary field variable(s) are assembled. Computed results are then used by back substitution to determine additional, derived variables, such as reaction forces and element stresses. Actually the features in this step such as matrix manipulation, numerical integration and equation solving are carried out automatically by commercial software ***(Robert, 1995)***.

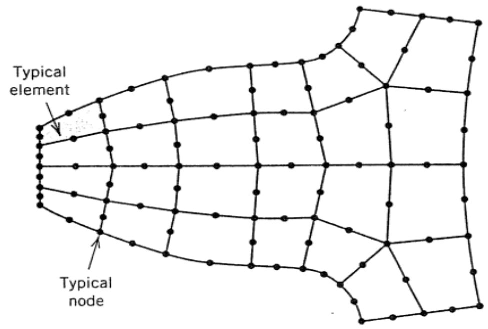


Figure 2-5 two-dimensional model mesh

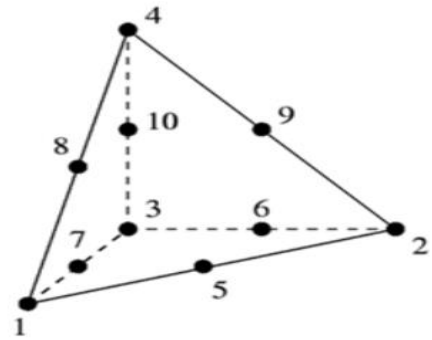


Figure 2-6 Node tetrahedral element

The final step is post processing, the analysis and evaluation of the result is conducted in this step. Examples of operations that can be accomplished includes ort element stresses in order of magnitude, check equilibrium, calculate factors of safety, plot deformed structural shape, animate dynamic model behavior and produce color-coded temperature plots. The large software has a preprocessor and postprocessor to accompany the analysis portion and the both processor can communicate with the other large programs. Specific procedures of pre and post processing are different dependent upon the program ***(David, 2004).***

### 2.5 Materials for electric vehicle chassis frame

***(Singh, 2017)*** The choice of materials for a vehicle is the first and most crucial factor for automotive design. There is a variety of materials that can be used in the automotive body and chassis, but the purpose of design is the main challenge here. The most important criteria that a material should meet are lightweight, economic effectiveness, safety, recyclability and life cycle considerations. The material that are taken into this work are described in the following Table 2-1.

Table 2-1 Properties of material

| **Properties** | **Structural steel** | **Aluminum Alloy** | **Magnesium Alloy** |
|---|---|---|---|
| Mass (kg) | 39.969 | 14.104 | 9.165 |
| Density (kg/mm^3) | 7.85*10^6 | 2.77*10^-6 | 1.8*10^-6 |
| Poisson’s Ratio | 0.3 | 0.33 | 0.35 |
| Young’s modulus (MPa) | 2*10^5 | 71000 | 45000 |
| Bulk Modulus (MPa) | 1.6667*10^5 | 69608 | 50000 |

Steel, the traditional building material for the structures of volume cars, has excellent property combinations if it can be exploited in structurally efficient designs, alloyed to produce high strength sheet, then formed and fabricated by such techniques as hydroforming and laser welded tailored blanking. Light alloys of aluminum, magnesium and titanium also have a place and advanced polymer composite systems have already been proven in race car and similar applications to provide ultra-light solutions. However, the future may lay in the wider meaning of composite construction, in a combination of metals and polymer compounds fulfilling complementary roles. Monocoque shell structures in high strength sandwich-construction polymer composites are considered against space-frame structures in aluminum alloy ***(Ren, Yu, & etal.., 2016).***

***(Lovatt, 2008)*** A lightweight chassis for a battery electric vehicle being developed at the University of Waikato. A chassis, built from 20mm thick aluminum honeycomb sandwich panel, was designed and built to LVVTA standards allowing the car to be driven on public roads. The car has been driven over 1800km with only one minor problem, indicating the chassis is reliable and well suited to its purpose. Titanium aluminide properties were researched to identify where titanium aluminides could be used in an automobile. Titanium aluminides have a specific strength and stiffness near to steel yet only half the density making it an ideal replacement for steel components. Automotive applications identified that could benefit from the use of TiAl include valves, brake rotors and inside ‘in-wheel’ electric motor.

### 2.5.1 AISI 1020 Structural Steel

AISI 1020 is a low hardenability and low tensile carbon steel with Brinell hardness of 119 – 235 and tensile strength of 410-790 MPa. It has high machinability, high strength, high ductility and good weld ability. It is normally used in turned and polished or cold drawn condition. Due to its low carbon content, it is resistant to induction hardening or flame hardening. Due to lack of alloying elements, it will not respond to nit riding. However, carburization is possible in order to obtain case hardness more than Rc65 for smaller sections that reduces with an increase in section size. Core strength will remain as it has been supplied for all the sections. Alternatively, carbon nitriding (heat treating process) can be performed, offering certain benefits over standard carburizing ***(Nunney, 2018).***

**Applications of AISI 1020**

AISI 1020 steel is used in case hardened condition. The applications of AISI 1020 steel are:

- It is used for simple structural application such as cold headed bolts.
- AISI 1020 steel also finds use in the following components:

Axles, chassis frames, general engineering parts and components, machinery parts, shafts, camshafts, gudgeon pins, ratchets, light duty gears, worm gears and spindles

### 2.5.2 6061-T6 Aluminum Alloy

**6061** is a precipitation-hardened aluminum alloy, containing magnesium and silicon as its major alloying elements. Originally called "Alloy 61S", it was developed in 1935. It has good mechanical properties; exhibits good weld ability, and is very commonly extruded (second in popularity only to 6063). It is one of the most common alloys of aluminum for general-purpose use ***(Shumaker, 2018)***.

**Applications of 6061-T6 is:**

Light weight vehicle frames, Bicycle frames and components, Many fly fishing reels, The Pioneer plaque was made of this alloy, The secondary chambers and baffle systems in firearm sound suppressors (primarily pistol suppressors for reduced weight and improved mechanical functionality), while the primary expansion chambers usually require 17-4PH or 303 stainless steel or titanium, Many aluminum docks and gangways are constructed with 6061-T6 extrusions, and welded into place, Material used in some ultra-high vacuum (UHV) chambers, Many parts for remote controlled model aircraft, notably helicopter rotor components.

Table 2-2 Description for those new listed materials ***(Shumaker, 2018), (Nunney, 2018)***

| Properties | AISI 1020 | 6061T-6 Aluminum Alloy |
|---|---|---|
| Density ($kg/m^3$) | 7900 | 2700 |
| Elastic modulus (GPa) | 200 | 69 |
| Yield strength (MPa) | 250 | 250 |
| Tensile strength (MPa) | 420 | 310 |
| Poisson’s Ratio | 0.29 | 0.33 |

## 2.6 Selection of material and cross section to the chassis frame

The materials used in the cage must meet certain requirements of geometry, and other limitations. The main criteria took into consideration when selecting the material for the roll cage safety, cost and durability ***(Satinder & Beant, 2014)***.

After conducting the analysis in ANSYS it was found that for structural steel equivalent stress value is highest for circular and lowest for square section. Total deformation are lowest for square cross section where as equivalent elastic strain is lowest for circular cross section and total deformation is lowest for rectangular cross section as shown on the below Table 2-3 and table 2-4. That is why the rectangular cross section of the steel selected for this electric vehicle chassis frame project.

The working material in this thesis for RAV4 EV 2014 model chassis frame structural steel AISI 1020 is the frame.

Table 2-3 Result analysis for aluminum alloy

| **Cross section** | **Equivalent stress** | | **Equivalent elastic strain** | | **Total deformation** | |
|---|---|---|---|---|---|---|
| | **Min.** | **Max.** | **Min.** | **Max.** | **Min.** | **Max.** |
| Rectangular | 3761.4 | 2.2949e7 | 5.2977e-8 | 0.00028732 | 0 | 0.001587 |
| Square | 5475.9 | 2.1284e7 | 7.7125 e-8 | 0.00026648 | 0 | 0.0012 |
| circular | 2811 | 2.3598e7 | 3.9592e-8 | 0.00033237 | 0 | 0.0017034 |

Table 2-4 Result analysis for structural steel

| **Cross section** | **Equivalent stress** | | **Equivalent elastic strain** | | **Total deformation** | |
|---|---|---|---|---|---|---|
| | **Min.** | **Max.** | **Min.** | **Max.** | **Min.** | **Max.** |
| Rectangular | 3344.7 | 2.93e7 | 1.6723e-8 | 0.00014662 | 0 | 0.00089456 |
| Square | 5447.7 | 2.542e7 | 2.7239 e-8 | 0.00012713 | 0 | 0.00060016 |
| Circular | 2100.2 | 3.0396e7 | 1.0501 e-8 | 0.00015198 | 0 | 0.0008462 |

## 2.7 Battery pack and electric vehicle chassis

EV battery packs are made up of multiple cell modules arranged in series and in parallel. Arranged around the battery pack and throughout the vehicle, the battery management system (BMS) is comprised of several components, including monitoring components close to the battery cells themselves, one or more power-conversion stages dictated by the needs of the vehicle, and intelligent controllers or embedded processors placed at strategic locations in the architecture to manage various aspects of the power subsystem.

### 2.7.1 Cell geometries

A battery is made of at least two electric cells which are connected together. The cells can be connected in series to give the overall voltage required. The main cell types to be found on the market are presented in Table 2-5.

Table 2-5 Main cell types on the market

| | Cylindrical | Prismatic | Pouch |
|---|---|---|---|
| **Geometry** |  |  |  |
| **Thermal dissipation [2]** | Unfavourable ratio of the outer surface, high radial temperature gradients | Good ratio of outer surface to volume, lower temperature gradients in depth (but still depending on cell thickness) | |
| **Packing density** | Poor | High | High |
| **Structure** | Robust | Robust | Vulnerable |
| **Cost** | Low in standard shapes | More expensive than cylindrical | Inexpensive |

***(Eitzinger, 2011)*** Works on Chassis, Drivetrain, and Energy Storage Layout for an Electric City Vehicle. The battery and thus also the battery frame does not need to be considered in the weight limit of 400 kg for the empty vehicle. Therefore it is obvious to use the structure of the battery frame also for other functions, besides carrying the battery modules. The weight of the frame is still relevant, because an increased vehicle weight results in decreased vehicle performance and increased energy consumption. Although a frame made from steel profiles will be heavier than a frame made from aluminum extrusion profiles, it was decided to make the frame from steel because of cost reasons.

***(Knutsen, 2013)*** Studies on electric vehicle charging patterns and range anxiety. Range anxiety is a relatively new concept which is defined as the fear of running out of power when driving an electric vehicle. To decrease range anxiety result that they got were that with bigger batteries but to get range anxiety just a few times a year you have to use battery sizes which aren't economical feasible today. Like increasing the numbers of charging stations, faster and better charging, conductive charging while driving and so on. However a lot of these solutions aren't economically or technologically possible right now and that makes electric vehicles a project in the innovator's state.

## 2.8 Electric vehicle battery swapping stations

Some concerns of vehicle users in switching from conventional internal combustion engine vehicles to Electric Vehicles, relate to distance range anxiety and the time required to recharge the EV batteries. The battery swapping station concept, which consists of replacing depleted batteries for fully charged batteries (in minutes) as shown in Fig 2-7 and 2-8, may incentivize EV adoption by having a similar role to that of petrol stations ***(Knutsen & Willén, 2013)***.

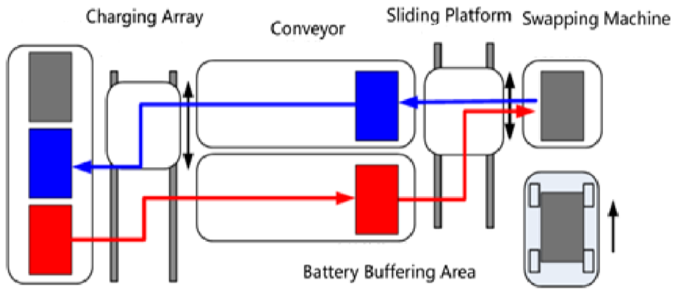


Figure 2-7 Swapping station configuration ***(Hua, 2017)***

Figure 2-8 Queued battery packs for swap

***(Unda, papadopoulos, & etal.., 2012)*** In this paper the operation of an EV battery Swapping Station Manager (SSM) is analyzed. A methodology is presented to calculate the number of chargers and batteries required to satisfy daily battery demand. The effects of the number of batteries and chargers on the swapping station's electricity load profile are shown. A JAVA software tool was developed for the calculation of the minimum number of batteries and chargers required to satisfy a swapping stations battery daily demand. The tool runs daily Simulations where the EVs arrival time and the depleted batteries' SoC are modeled as random numbers the simulated chargers are monitored allowing the tool to plot the swapping station's electricity load profile.

## 2.9 Thermal analysis for electric vehicle battery system

***(Pesaran, Swan, & etal.., 2011)*** Thermal management of battery packs in hybrid electric vehicles is essential to maximize pack performance and life. In this paper, they present results of thermal analysis and testing of a battery pack consisting of high-power lead-acid battery modules for the GM/DOE series HEV. Forced air was used as the medium for regulating module temperature the hybrid electric vehicle battery pack. A novel air manifold was used to deliver airflow uniformly to each module for even temperature distribution in the pack.

***(Samba, 2015)*** Lithium-ion batteries have emerged as a key energy storage technology and are now the main technology for portable devices. Due to their high potential and their high energy and power densities, and also their good lifetime, they are now the preferred battery technology, which has been able to provide longer driving range and suitable acceleration for electrically propelled vehicles such as Hybrid Electric Vehicles, Battery Electric Vehicles and Plug-In Hybrid Electric Vehicles ***(Axsen & Burke, 2008)***. However, cost, safety and temperature performance issues remain obstacles to its widespread application. As known, during the discharge or charge process, various exothermic chemical and electrochemical reactions occur. These phenomena generate heat that accumulates inside the battery and therefore accelerates the reaction between cell components. With higher discharge or charge current rates, the heat generation in a battery increases significantly. If heat transfer from the battery to the surroundings is not sufficient, the battery temperature can rise very fast and exceed the safe temperature range. In the worst-case scenario (Fig 2-9 and Fig 2-10) thermal runaway can occur.

The tables and figures are referred from ***(Samba, 2015)***. For optimal performance, safety and durability considerations, the battery must operate within the safe operating range of voltage, current and temperature as indicated by the battery manufacturer. The voltage range is between the maximum voltage (3.65V) and the minimum voltage (2V), the temperature range is depending on the operating mode (charge and discharge) and varies between [-20°C; 60°C] and [0°C; 40°C] during discharge and charge, respectively. These ranges can change according to the cell chemistry and battery manufacturer.

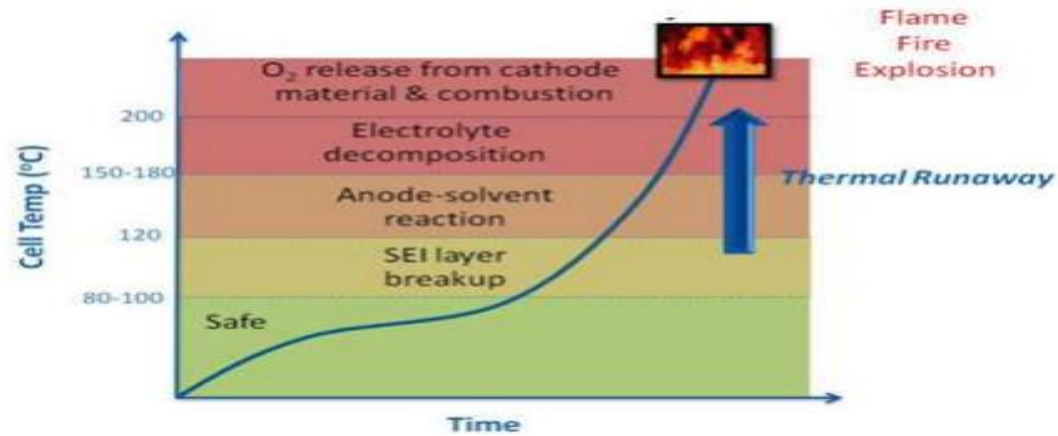


Figure 2-9 Thermal runaway process

Figure 2-10 Over temperature of the battery pack

The following Table 2-6 and Table 2-7 are describes that the electric vehicle different properties of its operating condition the first table is about the hybrid electric commercial vehicle and the second table is also describes about the model vehicle, battery type and show other parameters of plugin hybrid electric vehicle. Table 2-8 about cooling scheme for electric vehicle battery pack.

Table 2-6 Commercial HEVs

| **Model** | **Battery type** | **Energy content (KWh)** | **Electric motor power [KW]** | **Electric range [km]** | **Max vehicle speed in pure electric [km/h]** | **Battery thermal management** |
|---|---|---|---|---|---|---|
| Audi Q5 hybrid (Full HEV) | Li-ion(266 V/5Ah) | 1.3 | 40 | 3 | 100 | Air-cooling |
| BMW ActiveHybrid 3 (Full HEV) | Li-ion(317 V/2Ah) | 0.675 | 41 | 4 | 70 | Air-cooling |
| BMW ActiveHybrid 5 (Full HEV) | Li-ion(317 V/2Ah) | 0.675 | 40.5 | 4 | 60 | Air-cooling |
| BMW ActiveHybrid 7 (mild HEV) | Li-ion(120 V/6.6Ah) | 0.8 | 15 | 4 | 60 | Liquid cooling |
| Nissan infinity M35h (Full HEV)20 | Li-ion(346 V/3.7Ah) | 1.4 | 50 | No data available | 80 | Air-cooling |
| Mercedece S400 class hybrid | Li-ion | 0.8 | 20 | No data available | No data available | Air-cooling |

Table 2-7 Commercial PHEVs

| **Model** | **Battery type** | **Energy content (KWh)** | **Electric motor power [KW]** | **Electric range [km]** | **Max vehicle speed in pure electric [km/h]** | **Battery thermal mng’nt** |
|---|---|---|---|---|---|---|
| Mercedes Vision S500 plug-in (PHEV) | Li-ion | 10 | 85 | 33 | 140 | Water-cooling |
| Toyota prius plug-in (PHEV) | NiMH | 4.4 | 60 | 22 | 100 | Air-cooling |
| Volvo V60 plug-in hybrid (PHEV) | Li-ion | 11.2 | 51 | 49 | 112 | Water-cooling |

Table 2-8 Comparison between different cooling schemes BTMSs **(Khan & Swierczynski, 2017)**

| Cooling Scheme | Description | Application | Nominal Temperature Difference Allowed Between the Cells |
|---|---|---|---|
| Air | -Both cooling and heating is feasible;<br>-Good performance;<br>-Normally large space needed;<br>-Cheapest;<br>-Lower development effort is needed. | Application is limited but in most cases sufficient for HEV/48V/12V applications | Temperature difference between air and cells can be > than 15 °C limitation |
| Liquid | -Lowest temperature gradients;<br>-Cooling and heating is feasible;<br>-Best performance. | Liquid cooling can be found in EV, PHEV, HEV, 48V batteries | Cooling plate 1–3 °C |
| Refrigerant | -"Aggressive" cooling due to very low cooler temperatures. Intelligent thermal management and specific pack design needed to avoid a too-aggressive cooling and condensation of humidity. | HEV, 48V batteries | Cooling plate 3–8 °C |

# CHAPTER THREE

# 3 MATERIAL AND METHODS

## 3.1 Materials for electric vehicle chassis frame

The material AISI 1020 is selected for this electric vehicle chassis frame according to the literature discussion in the above section the material property of AISI 1020 shown below. This material selected based on the availability, cost and its mechanical properties that suit for chassis frame design and the rectangular cross section was taken in reference of literatures on related studies,

### 3.1.1 Steel AISI 1020 the properties from ANSYS 15. Workbench

The following data is took from the ANSYS workbench to show that the structural steel AISI 1020 as selected material, its mechanical properties on the ANSYS workbench in tables Table 3-1, Table3-2 and Table 3-3.

Table 3-1 Properties of Structural steel AISI 1020

| **Properties of Structural steel AISI 1020 which data's took from ANSYS** | |
|---|---|
| Compressive Yield Strength MPa | 250 |
| Tensile Yield Strength MPa | 250 |
| Tensile Ultimate Strength MPa | 460 |
| Reference Temperature C | 22 |
| Relative Permeability | 10000 |

Table 3-2 Strain-Life Parameters

| Strength Coefficient MPa | Strength Exponent | Ductility Coefficient | Ductility Exponent | Cyclic Strength Coefficient MPa | Cyclic Strain Hardening Exponent |
|---|---|---|---|---|---|
| 920 | -0.106 | 0.213 | -0.47 | 1000 | 0.2 |

Table 3-3 Isotropic Elasticity

| Temperature C | Young's Modulus MPa | Poisson's Ratio | Bulk Modulus MPa | Shear Modulus MPa |
|---|---|---|---|---|
| | 2.e+005 | 0.3 | 1.6667e+005 | 76923 |

## 3.2 Software’s used to this thesis work

This thesis work includes that same analytical calculations and different software to analysis. The software like CATIA V5 R20, ANSYS 15, and EXCEL were used. CATIA V5 R20 used for CAD modeling of the chassis frame and the electric vehicle battery cell and its cooling plate according to the calculations was done. ANSYS 15 was used for the analysis of structural, modal, harmonic and fluent flow for the new modeled chassis frame and battery cell. EXCEL was used for the iteration of temperature deference in time variation in battery cell coolant (used for battery thermal management system).

## 3.3 Review and specification for the existing RAV4 EV 2014 model

***(Dealer, 2014)*** Compared with other electric vehicles, the 2014 Toyota RAV4 EV is an impressive all-around package. Compared to conventional gasoline-fueled crossover SUVs, though, its high price and limited driving range are still tough sells.

### 3.3.1 Vehicle overview

The all-electric 2014 Toyota RAV4 EV is something of an odd duck in the company's extensive model lineup. Although the gas-powered RAV4 was recently redesigned, the all-electric version presses on still based on the previous-generation RAV4. of course, this means the RAV4 EV lacks the newer RAV4's various improvements. But that's not to say that being an odd duck is a bad thing ***(Dealer, 2014)***.

As a crossover SUV, the RAV4 EV is expected to offer abundant cargo capacity, and despite its need to accommodate a sizable battery pack, it does. Its 73 cubic feet of max capacity not only matches the redesigned gas-only RAV4, but makes it one of the most spacious compact SUVs. Performance is also impressive, as this electric SUV can scoot to 60 mph in just 7.2 seconds. Of course, "how far can it go on a charge" will likely be more of a concern than how quickly it charges forward. Although the RAV4 EV's 103-mile driving range may seem stingy by conventional vehicle standards, it's actually better than any other 2014 electric vehicle apart from the super advanced (and super expensive) Tesla Models. Add in this Toyota's high-tech yet user-friendly features and comfortable cabin and you've got an unusually well-rounded electric vehicle.

### 3.3.2 Specification for RAV4 EV 2014 model

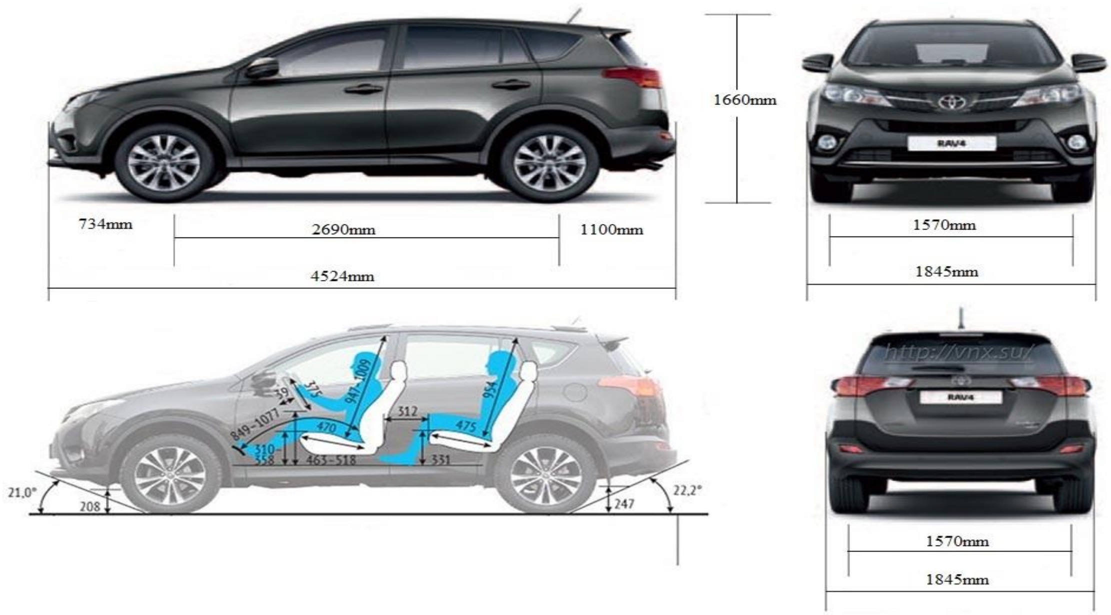


Figure 3-1 RAV 4 EV 2014 model internal and external spec

Table 3-4 Specification for RAV4 EV 2014 model **(Dealer, 2014)**

| **Mechanical and performance** | **RAV4 EV spesification** |
|---|---|
| **ELECTRIC MOTOR** | |
| Motor type (two drive modes; normal and sport) | AC induction motor with fixed gear open-differential transaxle; gear ratio 9.73 |
| Power output | 154 hp (115 kw) maximum |
| Max. torque | 218 lb, -ft/273 lb, -ft. |
| Max. speed | 85 mph/100 mph (160 kmh) |
| **TRACTION BATTERY** | |
| Type | Lithium ion (Li-ion) with to charge modes: normal and extended |
| Power output | 400 w max. |
| Voltage | 386v max. |
| Connecter | SAE J1772 connecter |
| **EMISSION RATING** | |
| Type | Zero emission vehicle (ZEV) |
| **STARTING SYSTEM** | |

| | |
|---|---|
| Type | Electronic push button start |
| **DRIVE TRAIN** | |
| Type | Front wheel drive |
| **SUSPENSION** | |
| Type | Independent MacPherson strut front suspension with stabilizer bar and hydraulic with coil springs. Trailing arms, stabilizer bar and hydraulic shock absorbers |
| Coefficient of drag (cd) | 0.30 |
| **WEIGHTS AND CAPACITIES** | |
| Curb weight (lb) | 4032 |
| Seating capacity | 5 |
| Passenger volume (cu. Ft.) | 108.2 (FR/RR; 57.4/50.8) |
| Cargo volume (cu. Ft.) behind front/second row | 73.0/36.4 |
| Gross vehicle weight rating (GVWR) (lb.) | 5005 |
| Battery capacity (kwh) (normal/extended) | 35.0/41.8 |
| Battery weight (lb.) | 845.5 |
| **TIERS** | |
| MPGe (city/highway/combined) | 78/74/76 |
| EPA-rated driving range | 103 miles |
| Charging time (normal/extended charge mode) | 12A/120V, 44hrs./52hrs.<br>16A/240V. 12hrs/15hrs.<br>30A/240V. 6.5hrs/8hrs |
| **HOME CHARGING STATION** | |
| Leviton UL-listed, level 2 (240v) 40-amp, 9.6 kw or 30-amp, 7.2 kw home charging station (EVSE) | available |

### 3.4 Design Process

The design process is a series of steps that is followed to come up with a solution to a problem. Steps of the design process involved in this study are shown in the Fig 3-2. At the beginning of the design process, design geometry has been defined according to the existing RAV4 2014 model specifications as shown in Table 3-4. Selected profile (cross section) done on CAD modeling and material be selected depending on the previous works.

Finite element analysis using ANSYS and analytical solution has been performed for analyzing of the existing frame and structure for the required results i.e. static analysis and crash simulation was done. After that, Re-modeling of the frame and structure using new size of components and new frame type has been done.

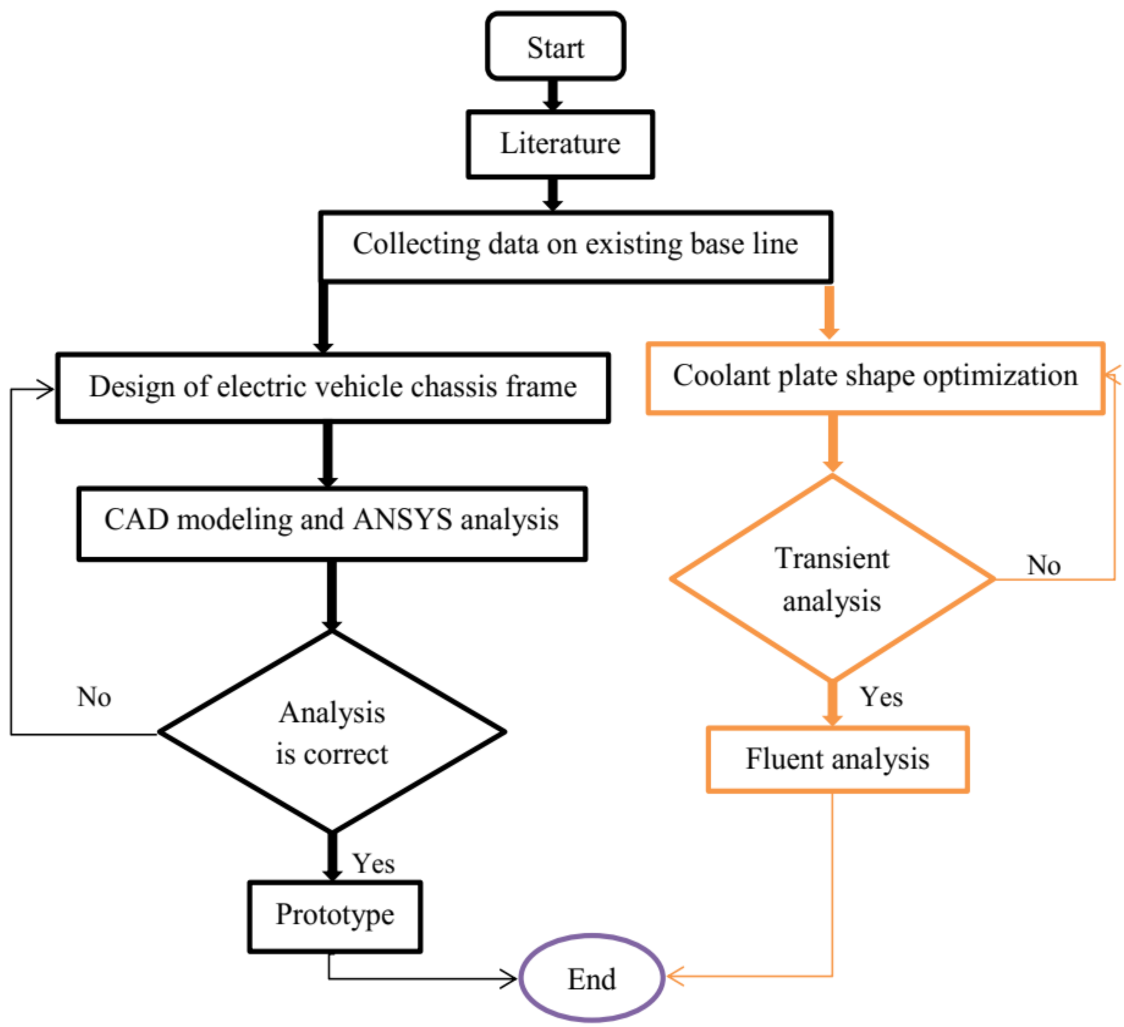


Figure 3-2 Flow chart for the working method of the thesis

### 3.5 Design Considerations for Chassis frame

The analytical calculations for the considered chassis were done using basic design calculations. The pre-required data considered are as follows, Materials for chassis frame must be rigid and achieve minimum deflection with minimum weight and cost.

In the existing RAV 4 EV the chassis was made from aluminum hard plate is used to accommodate the battery pack. In this study, two different materials were used for selection of material those material are selected from there availability, cost and mechanical properties. These are AISI 1020 Structural Steel and 6061-T6 Aluminum Alloy. Material properties seen in Table 3-1. when in case of design the chassis frame, different profile of cross sections are discussed and the rectangular profile is selected for this thesis work and the material AISI 1020 was selected according to section 2.5 & 2.6 discussion.

#### 3.5.1 Prototype preparation for electric vehicle chassis frame

The prototype Fig 3-4 is only for the demonstration purpose there is no need of test or taking results from it. The prototype is done in 1:1.5 scale of the actual one. It was done on the modified chassis frame.

Figure 3-3 Chassis frame for designed electric vehicle

# CHAPTER FOUR

# 4 DESIGN, MODELING AND ANALYSIS OF THE CHASSIS FRAME

## 4.1 CHASSIS DESIGN AND ANALYSIS

The chassis generally experiences four major loading situations; vertical bending, longitudinal torsion, lateral bending, and horizontal lozenging. These various conditions are represented diagrammatically in the figures below. Understanding these conditions is the key to designing a better chassis. When the chassis frame supported at its ends by the wheel axles and acted upon by an equivalent weight due to the tricycle's equipment, passengers and luggage around the middle of its wheel base, the side members are caused to sag in the central region. This sagging is known as vertical bending ***(Okpala, Charles, & Nwokeocha, 2017)***.

## 4.2 Analytical Verification

The following method is used as verification for the method used. The method is verified by using a simply supported overhanging beam of cross section used in the structure. Total load acting on chassis is the sum of weight of the body the battery and weight of the passengers, all loads described below in Table 4-1.

Table 4-1 Load factor from European environmental agency

| NTM Nomenclature | HBEFA Nomenclature | Max gross weight | Vehicle length | Load capacity | | | Load Capacity Utilisation | | | |
|---|---|---|---|---|---|---|---|---|---|---|
| | | tonne | m | tonne | pallets | m3 | LCU w% | LCU pallet% | LCU v% | LCU dimw% |
| Light commercial vehicle - Pick-up | LCV Petrol N1-II/LCV Diesel N1-II | 2,5 | 5,00 | 0,6 | 1 | 6 | 0,20 | 0,4 | 0,25 | 0,30 |
| Light commercial vehicle - Van | LCV Petrol N1-III/LCV Diesel N1-III | *3,5* | *7,00* | *1,5* | 4 | *17* | 0,20 | 0,4 | 0,25 | 0,30 |
| Rigid Truck <=7.5t | RT <=7,5t | 7,5 | 8 | 5 | 14 | 0 | 0,40 | 0,6 | 0,40 | 0,50 |
| Rigid Truck 7.5-12t | RT>7,5-12t | 12 | 11 | 6 | 20 | 0 | 0,40 | 0,6 | 0,40 | 0,50 |
| Rigid Truck 12-14t | RT>12-14t | 14 | 11 | 9 | 24 | 0 | 0,40 | 0,6 | 0,40 | 0,50 |
| Rigid Truck 14-20t | RT>14-20t | 20 | 12 | 12 | 24 | 0 | 0,40 | 0,6 | 0,40 | 0,50 |
| Rigid Truck 20-26t | RT>20-26t | 26 | 12 | 15 | 24 | 0 | 0,40 | 0,6 | 0,40 | 0,50 |
| Truck with Trailer 14-20t | TT/AT > 14-20t | 20 | 12 | 12 | 20 | 0 | 0,40 | 0,6 | 0,40 | 0,50 |
| Truck with Trailer 20-28t | TT/AT > 20-28t | 28 | 12 | 16 | 28 | 0 | 0,40 | 0,6 | 0,40 | 0,50 |
| Truck with Trailer 28-34t | TT/AT > 28-34t | 34 | 17 | 22 | 36 | 0 | 0,50 | 0,7 | 0,50 | 0,60 |
| Truck with Trailer 34-40t | TT/AT > 34-40t | 40 | 19 | 26 | 36 | 0 | 0,50 | 0,7 | 0,50 | 0,60 |
| Truck with Trailer 40-50t | TT/AT >40-50t | 50 | 16,50 | 33 | 33 | 110 | 0,50 | 0,7 | 0,50 | 0,60 |
| Truck with Trailer 50-60t | TT/AT >50-60t | 60 | 25,25 | 40 | 51 | 140 | 0,50 | 0,7 | 0,50 | 0,60 |

General calculations for considered load on chassis frame

- Curb weight = 1828.87 kg
- Gross vehicle Weight = 2270.22 kg
- Total load to be applied = 2270.22 x 9.81 = 22,270.86 N
- Considering an overload of 25% of total load = 22,270.86 x 1.25 = 27,838.57N.
- As the chassis frame has two members so load acing on each side member is half of the total load.
- Chassis has two beams. So load acting on each beam is half of the Total load acting on the hassis. Load acting on the single frame =27,838.57N./2 = 13,919.285N / Beam

Table 4-2 Considered loads of different components which causes bending in chassis frame

| Serial no | Component | Total load (kg) | Load/member (kg) | Load (N) /member | Types of load applied |
|---|---|---|---|---|---|
| 1 | Battery weight | 383.51 | 191.755 | 1,881.11 | Distributed load |
| 2 | Body wegiht | 2,000 | 1,000 | 9,810 | UDL |
| 3 | Passenger wegiht | 375 | 187.5 | 1,839.375 | UDL |

From the above Table 4-2 bending moment at different cross sections are calculated by analytical method By this method of simple bending different dimensions of the taken cross sections for the side member of ladder frame are calculated by considering highest bending moment.

$$\frac{M}{I} = \frac{\sigma}{\gamma} = \frac{E}{R} \qquad \text{4.1}$$

$$M = \frac{I}{\gamma} x\, \sigma = Zx\sigma \qquad \text{4.2}$$

In analytical calculation found that the values of shear force, stress, bending moment, moment inertia of the chassis frame and total deflection of chassis frame. The same to that in ANSYS analysis we found that total deformation, equivalent stress, shear force and dynamic analysis like modal and harmonic. Before going to show the calculations and analysis there are some theories on the strength of materials

### 4.2.1 Generally used theories for Ductile Materials

- Maximum shear stress theory

States that failure occurs when the maximum shear stress from a combination of principal stresses equals or exceeds the value obtained for the shear stress at yielding in the uniaxial tensile test.

- Maximum Equivalent (von-misses) stress theory

In this case, a material is said to start yielding when its von Misses stress reaches a critical value known as the yield strength. The von Misses stress is used to predict yielding of materials under any loading condition from results of simple uniaxial tensile tests.

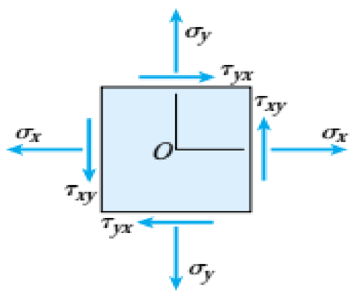


Figure 4-1 Two-dimensional view stress

To relate failure to two dimensional view of stress in Fig 4-1, three important stress indicators are derived: Principal stress, maximum shear stress, and Von-misses stress.

***Principal stresses*** is maximum and minimum value of the normal stress, in this case the shear stress become zero.

$$\sigma_1, \sigma_2 = \frac{\sigma_x+\sigma_y}{2} \pm \sqrt{\frac{(\sigma_x-\sigma_y)^2}{2} + \tau_{xy}{}^2} \quad \text{4.3}$$

Where, σ1 and σ2 are principal stresses, σx and σy are component stresses on their x and y respective axes and $\tau_{xy}$ is shear stress in the xy-plane.

***Maximum shear stress*** having found the principal stresses and their directions for an element in plane stress

$$\tau_{max} = \sqrt{\left(\frac{\sigma_x-\sigma_y}{2}\right)^2 + \tau_{xy}^2} \quad \text{4.4}$$

***Von Misses stress*** in this case, a material is said to start yielding when its von misses stress reaches a critical value known as the yield strength. The von misses stress is used to predict yielding of materials under any loading condition from results of simple uniaxial tensile tests.

$$\sigma_v = \sqrt{\frac{(\sigma_1-\sigma_2)^2+(\sigma_2-\sigma_3)^2+(\sigma_3-\sigma_1)^2}{2}} \text{.........................................................................................} 4.5$$

Where, $\sigma_v$ is von-misses stress and σ1, σ2, and σ3 are principal stress

### *Calculation for reaction*

Chassis is simply clamp with shock absorber and coil spring so chassis is simply supported beam with uniform distribution load. Load acting on entire span of beam is 13,919.285N (from above calculation in page 31) length of the beam is 4524mm (manual).

In Fig 4-2 uniformly distributed load is 13,919.285N/4,524mm=3.07N/mm now taking the reaction around support A.

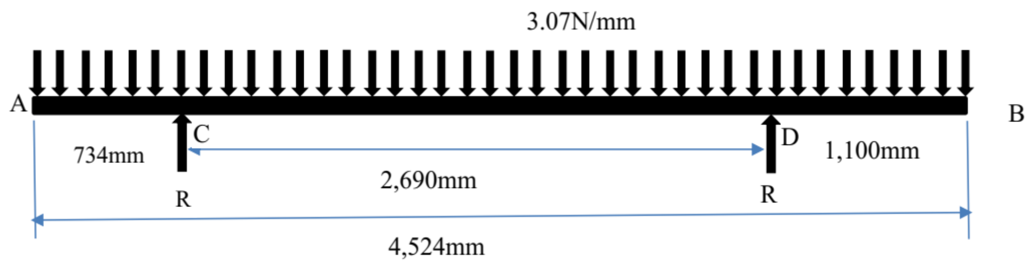


Figure 4-2 Chassis as simply supported beam with over hung

$$Rc + RD = 13{,}919.285N \text{..........................................................................................} 4.6$$

$$RC = \frac{Wl(l-2c)}{2b} \textit{ (Damtie, 2013)} \text{......................................................................................} 4.7$$

$Where, Rc\ is\ reaction\ force\ at\ point\ C, W\ is\ distributed\ load\ over\ the\ member, l\ is\ length$

$of\ the\ side\ member, (a, b, c) are\ lengths\ between\ the\ distance\ between\ the\ capital\ leters$

$$= \frac{3.07\frac{N}{mm}x4{,}524mm(4{,}524mm - 2x1100\ mm)}{2x2{,}690mm}$$

$$Rc = \frac{3.07\frac{N}{mm}x3{,}908.5mm}{2} = 5{,}999.5N$$

From equation (4.1)

$$RC + RD = 13{,}919.285N$$

$$RD = 13{,}919.285N - 5{,}999.5N$$

$$RD = 7{,}919.8N$$

*Calculation for shear force and bending moment*

Shear force

$V_A = Wa$ ..........4.8

$$= 3.07\frac{N}{mm}x917mm$$

$$V_A = 2{,}815.19N$$

$V_C = RC - V_A$ ..........4.9

$$V_C = 5{,}999.5N - 2{,}815.19N$$

$$V_C = 3{,}184.31N$$

$V_B = WC$ ..........4.10

$$V_B = 3.07\frac{N}{mm}x1{,}100N$$

$$V_B = 3{,}377N$$

$V_D = RD - V_B$ ..........4.11

$$V_D = 7{,}919.8N - 3{,}377N$$

$$V_D = 4{,}542.8N$$

Where V is shear force,

Bending moment

$M_{left} = -\frac{wa^2}{2}$ ..........4.12

$$= -\frac{3.07\frac{N}{mm}x(734mm)^2}{2}$$

$$= -1{,}290{,}764.615Nmm$$

$M_{right} = -\frac{wc^2}{2}$ ..........4.13

$$= -\frac{3.07\frac{N}{mm}x(1{,}100mm)^2}{2}$$

$$= -1{,}857{,}350Nmm$$

$M_{midd} = Rc(\left(\frac{Rc}{2w}\right) - a)$ ..........4.14

$$= 5{,}999.5N(\left(\frac{5{,}999.5N}{2x3.07Nmm}\right) - 734mm)$$

$$= 1{,}458{,}582.024Nmm$$

The shear force diagram for electric vehicle chassis frame based on the above calculations Fig 4-3 for shear force diagram and Fig 4-4 stands for bending moment.

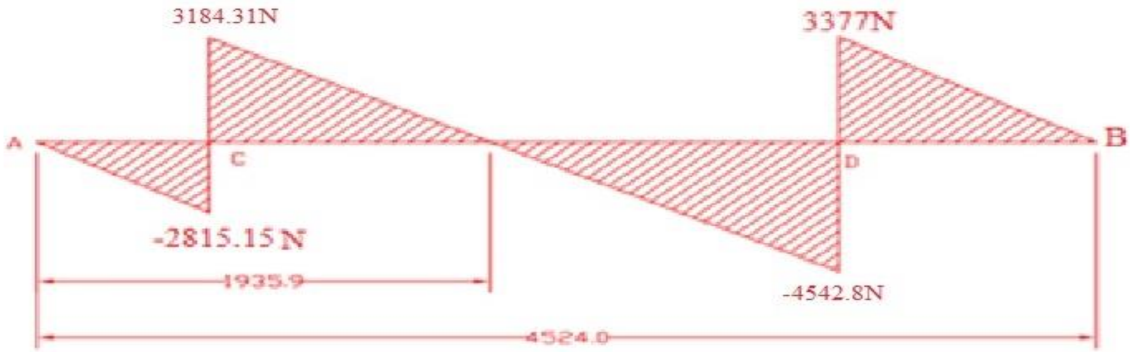


Figure 4-3 Shear force

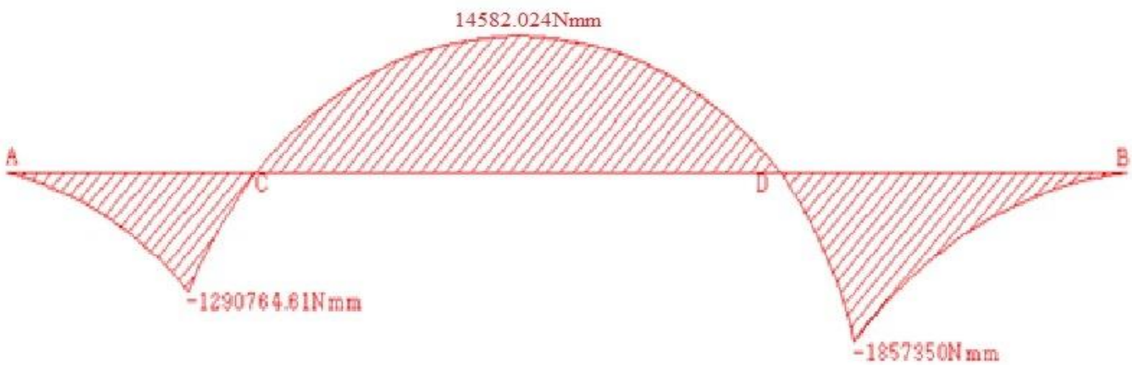


Figure 4-4 Bending moment

From the above Fig 4-3 and Fig 4-4 taking that the distance or position of the shear stress occur on the chassis frame and the position of bending moment. According to this reason position for both shear force and bending moment lies on the position 1935.9 mm distance from the front end of the chassis frame so this value is used to fine the deflection (Y) in the following equation.

Calculation for stress generated

$$M_{max} = 1{,}458{,}582.024Nmm$$

Moment of inertia around the x-x axis in the following Fig 4-5.

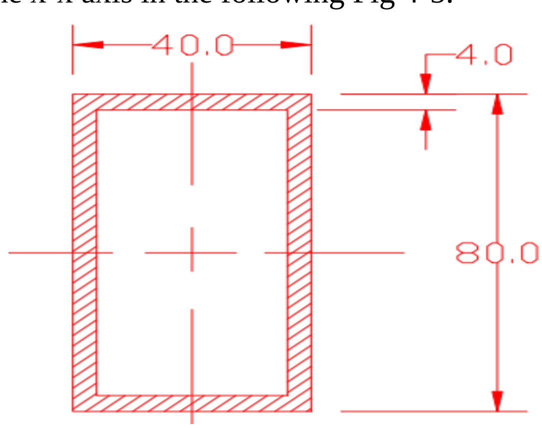

Figure 4-5 Cross section for the chassis frame

$$I_{xx} = \frac{bh^3 - b_1{h_1}^3}{12} \qquad \text{4.15}$$

$$= \frac{40mmx(80mm)^3}{12} - \frac{32mmx(72mm)^3}{12}$$

$$I_{xx} = 20{,}480{,}000mm^4 - 11{,}943{,}924mm^4$$

$$= 711{,}338.667mm^4$$

Deflection of chassis frame form equation (4.1)

$$Y = \frac{wx(b-x)}{24EI}[x(b-x) + b^2 - 2(c^2 + a^2) - \frac{2}{b}c^2x + a^2(b-x) \qquad \text{4.16}$$

$$Y = \frac{3.07 * 2262(2690 - 2262)}{24 * 2.1 * 10^5 * 157056084}[2262(2690 - 2262) + 2690^2 - 2(1100^2 + 734^2) - \frac{2}{2690}1100^2 * 2262 + 734^2(2690 - 2262)]$$

$$Y = 0.87mm$$

The deflection of the total chassis frame is 0.87mm from its normal position and the stress on the chassis frame is done in the following manner.

$$\frac{\sigma}{Y} = \frac{M}{I} = \frac{E}{R}$$

$$\sigma = \frac{MY}{I}$$

Where ‘M’ is bending moment, ‘Y’ is the distance between the xx section and the normal stress center line, ‘I’ is mass moment of inertia in xx cross section

$$\sigma = \frac{1{,}958{,}582.024Nmm * 38mm}{711{,}338.667mm^4} = 104.62MPa$$

And the centroid for the coordinate system for the chassis frame is not done yet because the ANSYS software is done very well and it done for each drawn parts on CATIA so the value of centroid of the chassis frame as it is and the mass moment of inertia is also took from the ANSYS software. And in appendix table C-0-3 and table C-0-4 the centroid, moment of inertia, mass of chassis frame and volume of each part is briefly described as shown.

### 4.2.2 CAD modeling for electric vehicle chassis

The chassis frame model created in CATIA V5 R20 as shown in Fig 4-6 is imported to ANSYS 15 on Fig 4-7. The meshed modal of chassis frame is shown in Fig 4-8.

Figure 4-6 Designed electric vehicle chassis frame (ladder type)

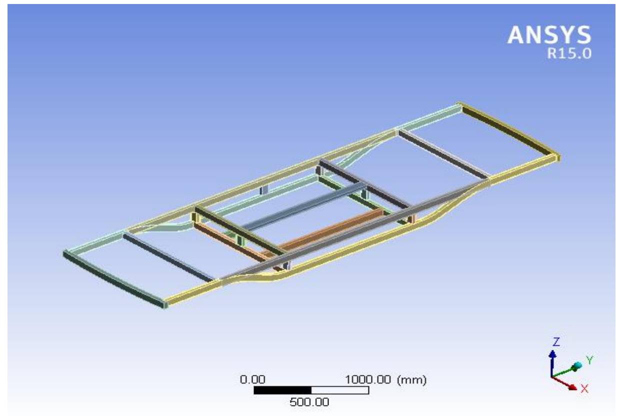


Figure 4-7 Geometry of chassis frame in ANSYS

### 4.2.3 Finite element analysis

The main objectives of the finite element analysis is stress and modal analysis of the electric vehicle chassis. The various sub objectives are listed as below:

- Static Structural Analysis:
  - Finding the Von Misses stresses, maximum shear stress
  - Finding maximum deflection and its position
- Modal Analysis:
  - Find the mode shapes of the chassis for the first ten natural frequencies
  - Resonance frequency
- Harmonic Analysis:
  - Obtaining the resonance frequency for the chassis by plotting the amplitude vs. frequency graph.
- Static Impact analysis

### 4.2.4 Meshing

FEA software typically uses a CAD representation of the physical model and breaks it down into small pieces called finite “elements”. This process is called “meshing”. Higher the quality of the mesh (collection of elements), enhanced the mathematical representation of the physical model. The meshing is done on the model using tetrahedral elements. Fig 4-8 shows meshing of the model and

243634 Nodes and 34528 elements. The meshing is converged b/c the analytic result and result from ANSYS is almost the same 104.62MPa and 115.88MPa respectively. The error is 9.7% of the ANSYS result on analytic one. The error is acceptable so the tetrahedral fine mesh was selected.

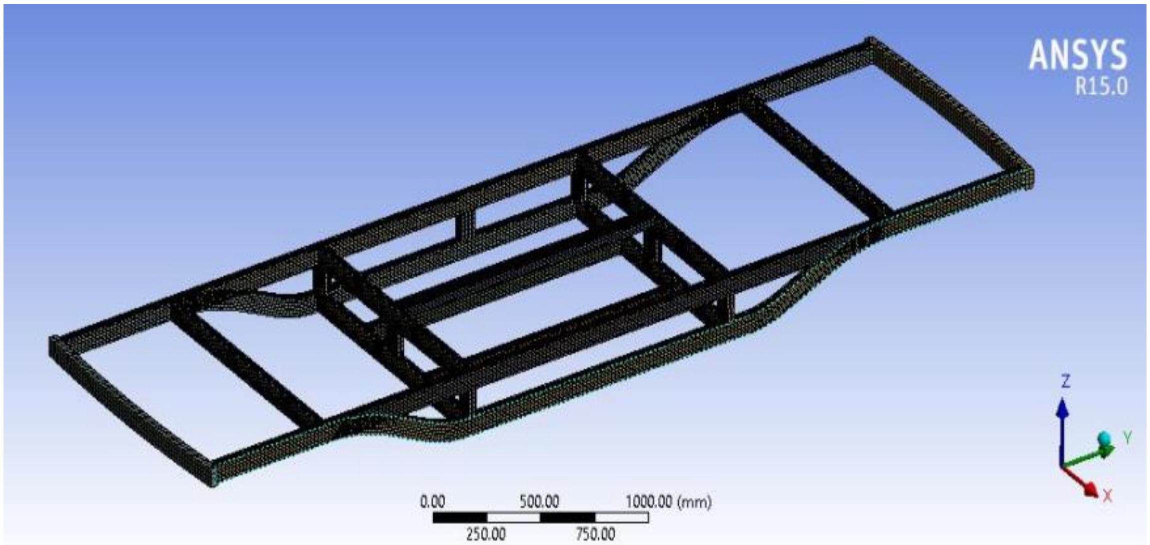


Figure 4-8 Meshed model of the designed electric vehicle chassis frame

### 4.2.5 Loading and boundary conditions

In this RAV4 EV 2014 model vehicle taking that of the existing vehicle load and the analysis is held by this load. The electric vehicle chassis model is loaded by static forces from the vehicle body, passengers and luggage. The magnitude of force on the upper side of chassis is 117720 N which is carried by distributed load on chassis frame on Fig 4-9.

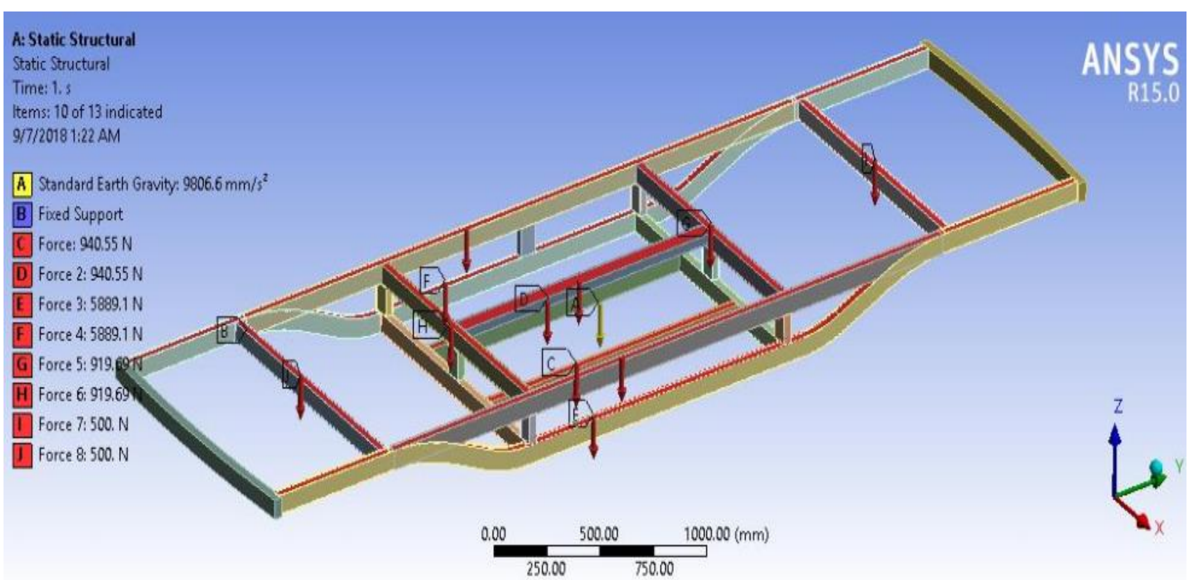


Figure 4-9 Static load (loads from battery, passenger and luggage) on chassis frame

### 4.2.6 Modal analysis

Modal analysis is an efficient tool for describing, understanding, and modelling structural dynamics. The dynamic behavior of a structure in a given frequency range can be modelled as a set of individual modes of vibration. The modal parameters that describe each mode are: natural frequency or resonance frequency, (modal) damping, and mode shape. The modal parameters of all the modes, within the frequency range of interest, represent a complete dynamic description of the structure. Modal frequency response analysis uses the mode shapes of the structure to reduce the size, uncouple the equation of motion (when modal or no damping is used), and make the numerical solution more efficient. Due to the mode shapes are typically computed as part of characterization of the structure, modal frequency response Analysis is a natural extension of a normal mode analysis ***(Santosh, Naresh, & etal.., 2016).*** In this analysis, the modal analysis has been done by the finite element packaged ANSYS 15. After making finite element model of chassis and appropriate meshing, model has been analyzed and first 10 frequencies that play important role in dynamic behavior of chassis, have been analyzed.

# CHAPTER FIVE

# 5 RESULT AND DISCUSSION

## 5.1 Static structural analysis for electric vehicle chassis frame

A static strength analysis calculates the effects of steady loading conditions on a structure, while ignoring inertia and damping effects, such as those caused by time-varying loads. This analysis determines the displacements, stresses, strains, and forces in structures or components caused by loads that do not induce significant inertia and damping effects. Member is assumed as perfectly connected before importing. Simplified CAD model of the designed electric vehicle frame is created using CATIA V5 R20 and it is imported in ANSYS R15 as an external geometry file.

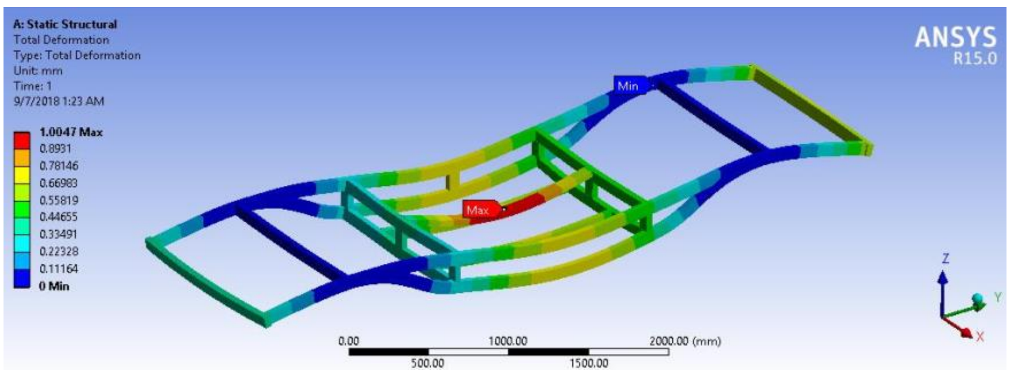


Figure 5-1 ANSYS static result of total deformation

In the above figure Fig 5-1 we understand that from the static structural analysis the total deformation is 1.0047mm it is the maximum deformation in this loading and it lies on the middle above the battery pack member at the center of the member.

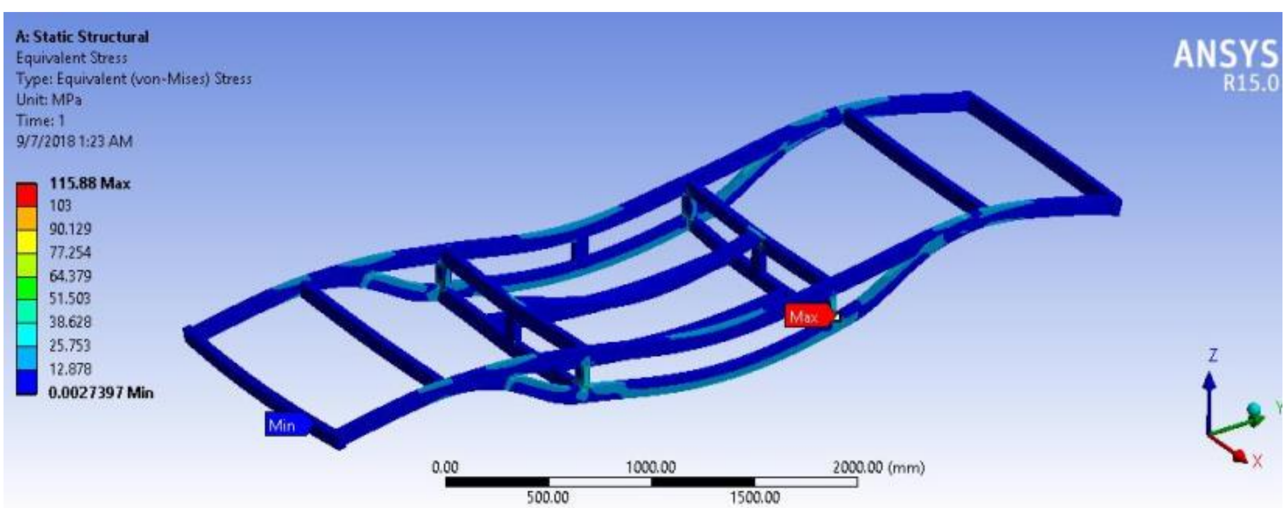


Figure 5-2 Static structural analysis for equivalent stress (von-misses stress)

In the above figure Fig 5-2 the static structural analysis for equivalent stress (von-misses stress) has been done on ANSYS 15 workbench and 115.88MPa is the maximum stress on the in the middle end right bottom part and the minimum von-miss stress 0.00273MPa lies on front end member of the chassis frame and the value of equivalent stress is better according to the yield stress of the structural steel AISI 1020 it has yield stress 250Mpa.

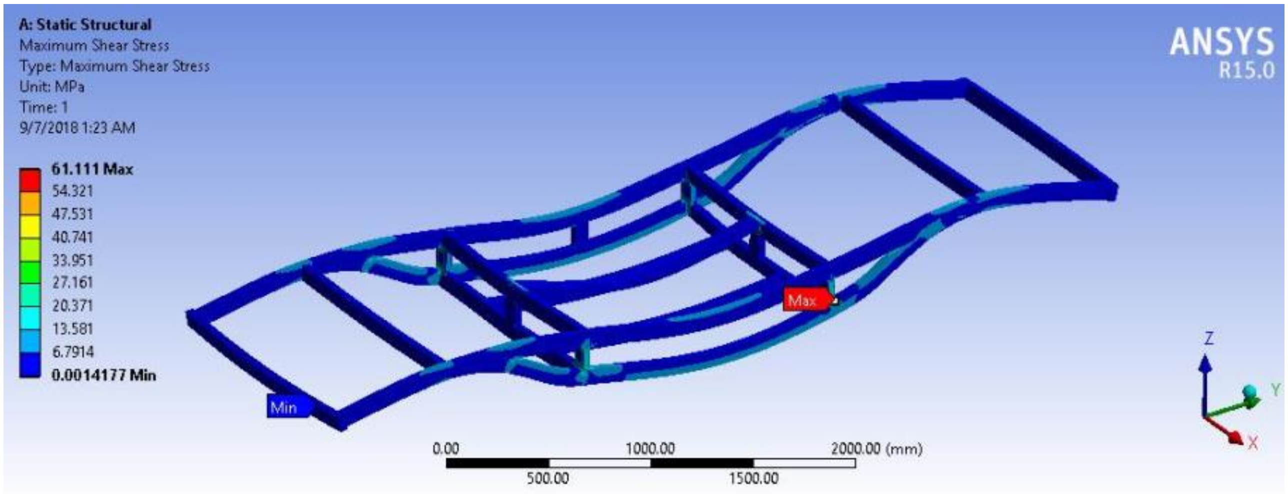


Figure 5-3 Static structural analysis of maximum shear stress

The Fig 5-3 express that the static structural analysis of shear stress on the chassis frame and the maximum shear stress is 61.111MPa which is found in that the von-miss maximum stress founds and the minimum shear stress is 0.001417MPa this also found the front end member of the chassis frame. The sequence is the same to that of von-miss stress analysis.

## 5.2 Fatigue tool analysis for electric vehicle chassis frame

Types of Results Just like some of the input decisions change depending upon whether to performing a Stress Life or a Strain Life analysis, calculations and results can be dependent upon the type of fatigue analysis. Results can range from contour plots of a specific result over the whole model to information about the most damaged point in the model (or the most damaged point in the scope of the result). Results that are common to both types of fatigue analyses are listed below:

- Fatigue life
- Fatigue damage at a specified design life
- Fatigue factor of safety at a specified design life

- Fatigue sensitivity chart

The following Constant amplitude shows, proportional loading is the classic, “back of the envelope” calculation describing whether the load has a constant maximum value or continually varies with time. Loading is of constant amplitude because only one set of FE stress results along with a loading ratio is required to calculate the alternating and mean values. The loading ratio is defined as the ratio of the second load to the first load (LR = L2/L1) the ration R in the following figure 5-4 is -1 according to the ANSYS done by the given data. Loading is proportional since only one set of FE results are needed (principal stress axes do not change over time). Common types of constant amplitude loading are fully reversed (apply a load, then apply an equal and opposite load; a load ratio of –1) shown in Fig 5-4. Since loading is proportional, looking at a single set of FE results can identify critical fatigue locations. Likewise, since there are only two loadings, no cycle counting or cumulative damage calculations need to be done.

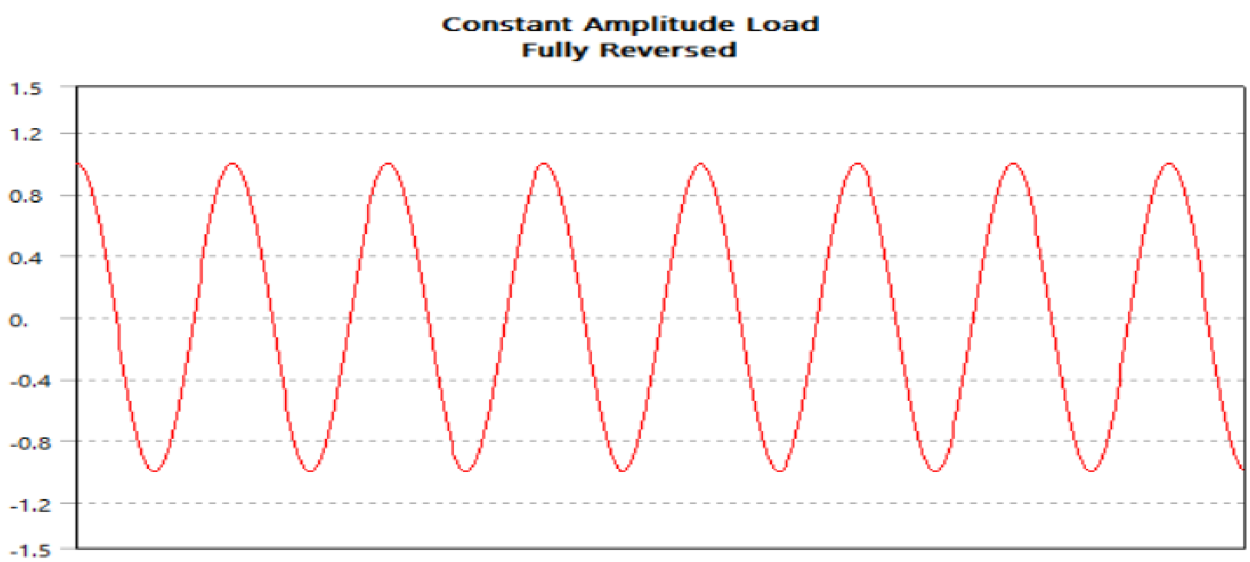


Figure 5-4 Constant amplitude loading.

### 5.2.1 Mean Stress Correction

Once we have made the decision on which type of fatigue analysis to perform, Stress Life or Strain Life, and have determined loading type, the next decision is whether to apply a mean stress correction. Cyclic fatigue properties of a material are often obtained from completely reversed, constant amplitude tests. Actual components seldom experience this pure type of loading, since some mean stress is usually present. If the loading is other than fully reversed, a mean stress exists and may be accounted for.

### 5.2.2 Mean Stress Corrections for Stress Life

For Stress Life, if experimental data at different mean stresses or r-ratio's exist, mean stress can be accounted for directly through interpolation between material curves. If experimental data is not available, several empirical options may be chosen including Gerber, Goodman and Soderberg theories which use static material properties (yield stress, tensile strength) along with S-N data to account for any mean stress expressed in the following Fig 5-5 and Table 5-1.

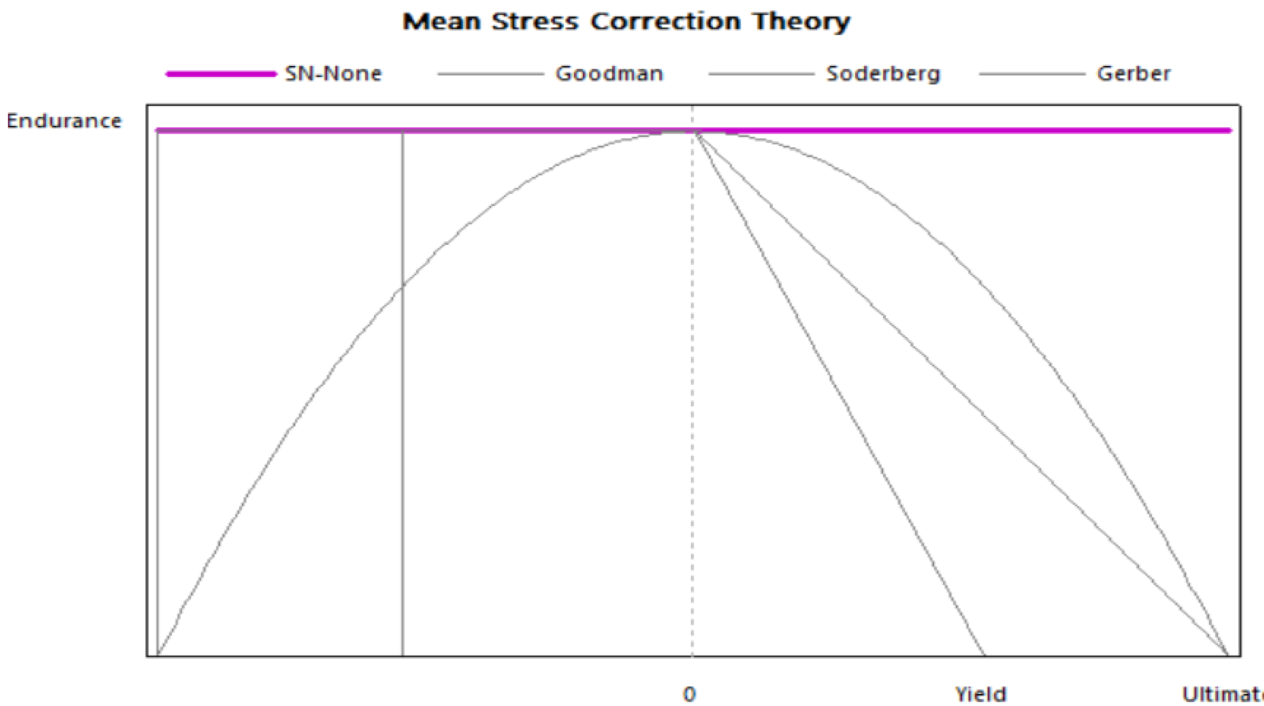


Figure 5-5 Representation of Soderberg Mean stress Correction for Stress Life Fatigue Analysis.

$$\frac{\sigma_{Alternating}}{S_{Endurance\_limit}} + \frac{\sigma_{Mean}}{S_{Yield\_strength}} = 1$$

Soderberg Equation

$$\frac{\sigma_{Alternating}}{S_{Endurance\_Limit}} + \left(\frac{\sigma_{Mean}}{S_{Ultimate\_Strength}}\right)^2 = 1$$

Gerber Equation

$$\frac{\sigma_{Alternating}}{S_{Endurance\_limit}} + \frac{\sigma_{Mean}}{S_{Ultimate\_strength}} = 1$$

Goodman Equation

Table 5-1 Comparison of mean stress correction theories **(Qasim & Emad, 2014)**

| **Theory** | **Features** |
|---|---|
| Goodman | • Most experimental data falls between Goodman and Gerber theories<br>• It is usually a good choice for brittle materials<br>• It is not bounded when using negative mean stresses |
| Soderberg | • Generally the most conservative<br>• It is not bounded when using negative mean stresses |
| Gerber | • It is usually a good choice for ductile materials<br>• It is bounded when using negative mean stresses. |

Table 5-2 Fatigue tool results

| Object Name | *Life* | *Damage* | *Safety Factor* |
|---|---|---|---|
| State | Solved | | |
| **Scope** | | | |
| Scoping Method | Geometry Selection | | |
| Geometry | All Bodies | | |
| **Definition** | | | |
| Type | Life | Damage | Safety Factor |
| Suppressed | No | | |
| Design Life | | 1.e+009 cycles | |
| **Results** | | | |
| Minimum | 1.8848e+005 cycles | | 0.74388 |
| Minimum Occurs On | Part 4 | | Part 4 |
| Maximum | | 5305.6 | |
| Maximum Occurs On | | Part 4 | |

### 5.2.3 Fatigue Life

As mentioned in the above Table 5-2 Fatigue Life can be over the whole model or scoped just like any other contour result in Workbench (i.e. parts, surfaces, edges, and vertices). This result contour plot shows the available life for the given fatigue analysis. The loading is of constant amplitude, this represents the number of cycle’s 1million cycle until the part will fail due to fatigue and the safety factor for this analysis is 0.743. The given load history represents 188,480 minutes of loading with this load condition and the chassis will fall after this minute this mean that it stays by this loading for 130 days without deformation shown in Fig 5-6. After that it tends to deform or fail.

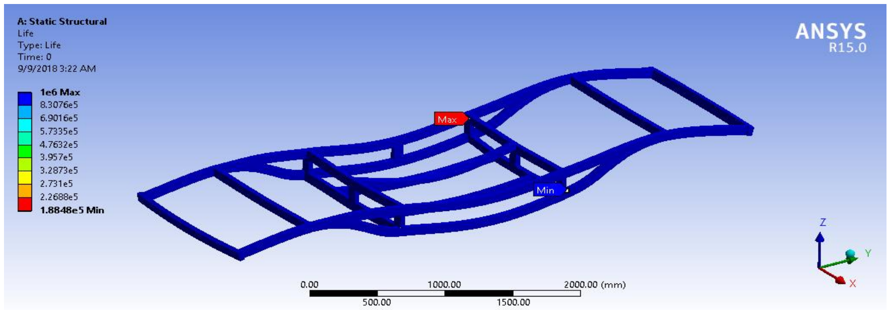


Figure 5-6 Fatigue Life over the whole model.

### 5.2.4 Fatigue Safety

Factor Fatigue Safety Factor is a contour plot of the factor of safety with respect to a fatigue failure at a given design life. The factor of safety indicated in the analysis is 0.74388 Fig 5-7. Like damage and life, this result may be scoped.

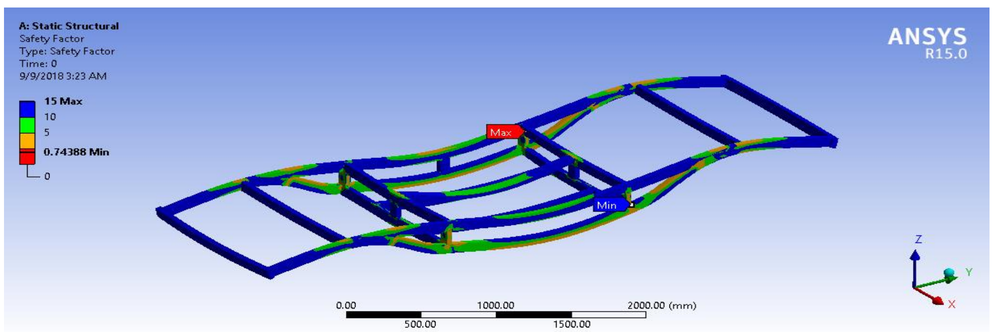


Figure 5-7 Fatigue Safety Factor over the whole model.

### 5.2.5 Fatigue Damage

Fatigue Damage is a contour plot of the fatigue damage at a given design life. Fatigue damage is defined as the design life divided by the available life. This result may be scoped. The default design life may be set through the Control Panel. For Fatigue Damage, values greater than 1 indicate failure before the design life is reached as shown in Fig 5-8.

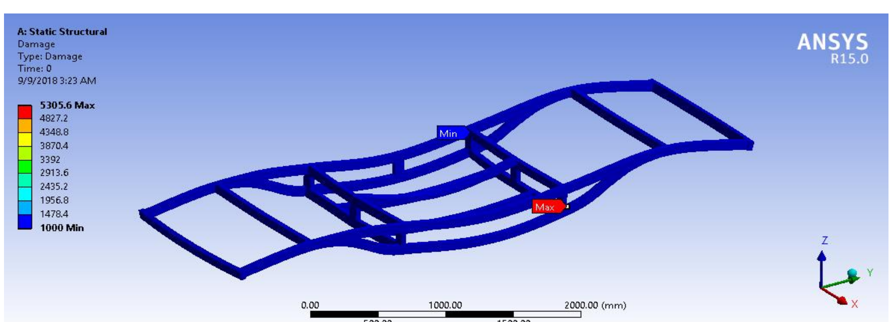


Figure 5-8 Fatigue Damage over the whole model.

### 5.2.6 Fatigue Sensitivity

Fatigue Sensitivity shows how the fatigue results change as a function of the loading at the critical location on the model. This result may be scoped. Sensitivity may be found for life, damage, or factor of safety. And in the following ANSYS result based on the applied loading up to 72% the frame has the same available life cycle after that when the percentage of loading is more the available life cycle decreased as shown in Fig 5-9. The value only 72% is that much not good but based on the considering safety factor of chassis frame is 0.743 this safe and taking the personal Wight as 75kg because of this there is no that much problem. Default values for the sensitivity options may be set through the Control Panel.

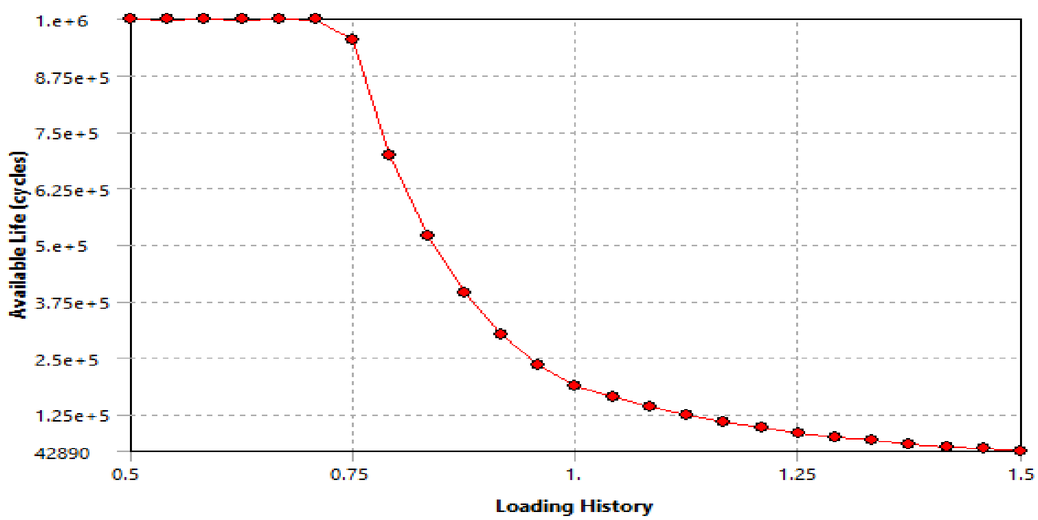


Figure 5-9 Fatigue Sensitivity curve.

## 5.3 Modal analysis for electric vehicle chassis frame

Modal analysis by using Finite Element Method (FEM) can be used to find natural frequencies and mode shapes. In this analysis, the modal analysis has been done by the finite element packaged ANSYS 15. After making finite element model of chassis and appropriate meshing, model has been analyzed and first 10 frequencies in global vibration play important role in dynamic behavior of chassis, have been analyzed.

There are two types of vibration, which are global and local vibrations. The global vibration means that the whole chassis structure is vibrating while local vibration means the vibration is localized and only part of the car chassis is vibrating ***(Pravin, 2012)***.

Table 5-3 Modal analysis results (total deformation results) for EV chassis frame

<table>
<tr>
<td>
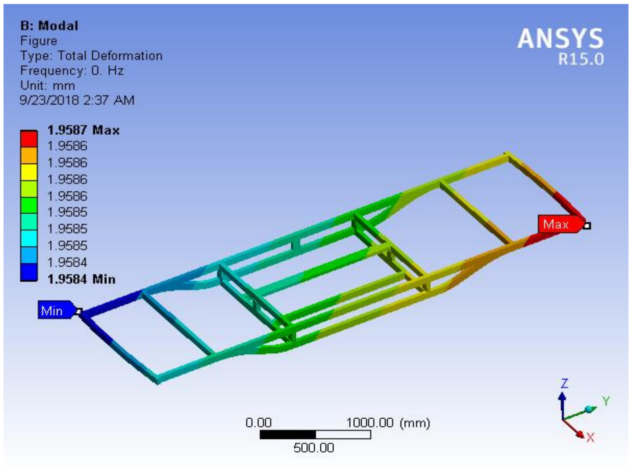


Total deformation 1

This first global mode shape of the electric vehicle chassis frame is at 0 Hz and the total deformation 1.95mm. The chassis Experienced up and down motion. The maximum translation was at the right back end of the vehicle chassis.
</td>
<td>
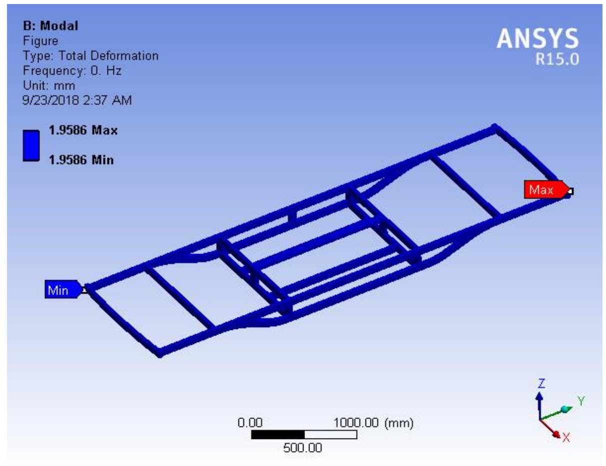


Total deformation 2

The second global mode shape of the electric vehicle chassis at 0 Hz and total deformation 1.95mm. The chassis Experienced left and right motion. The maximum translation was at the front left end of the vehicle chassis.
</td>
</tr>
<tr>
<td>
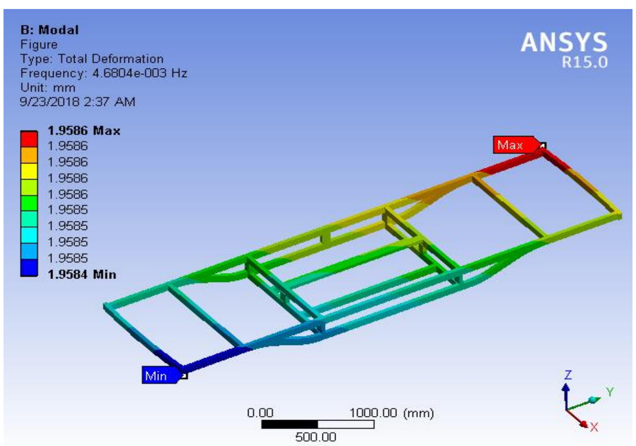


Total deformation 3

The third global mode shape of the electric vehicle chassis at 4.3835e-003 Hz. The chassis Experienced front and back mode. The maximum translation was at the left back end of the vehicle chassis.
</td>
<td>
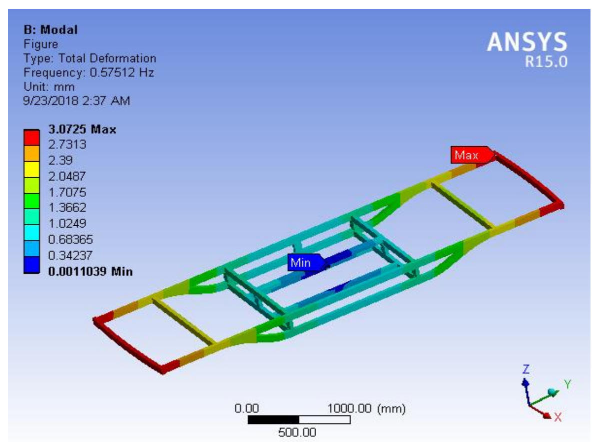


Total deformation 4

The fourth global mode shape of the electric vehicle chassis at 0.57 Hz. The chassis Experienced yawing mode along Z axis. The maximum translation was at the left back end of the truck chassis.
</td>
</tr>
</table>

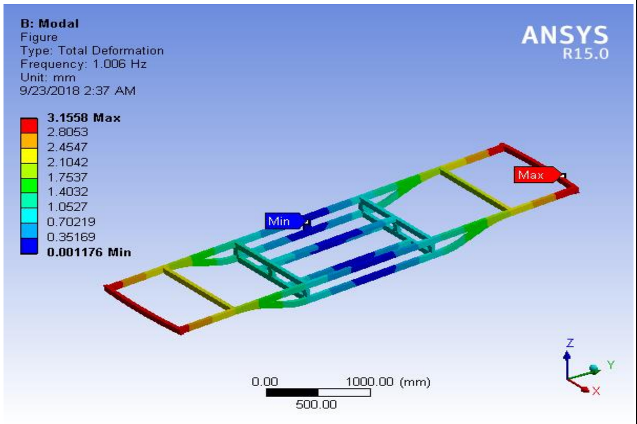


Total deformation 5

The fifth global mode shape of the electric vehicle chassis at 1.006 Hz. The chassis Experienced pitching mode along X axis. The maximum translation was at the back end of the vehicle chassis.

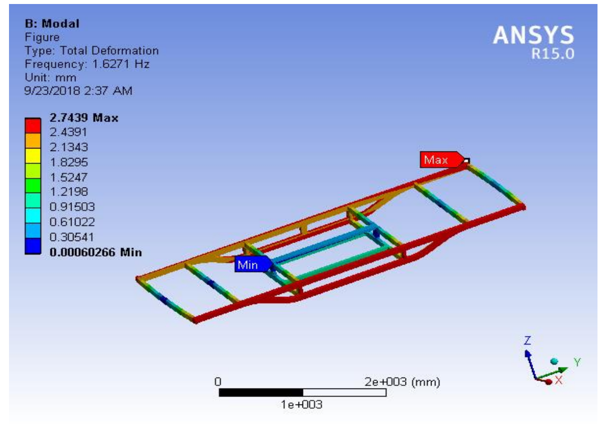


Total deformation 6

The sixth global mode shape of the electric vehicle chassis at 1.627 Hz. The chassis Experienced pitching mode along Y axis. The maximum translation was at the back left end of the truck chassis.

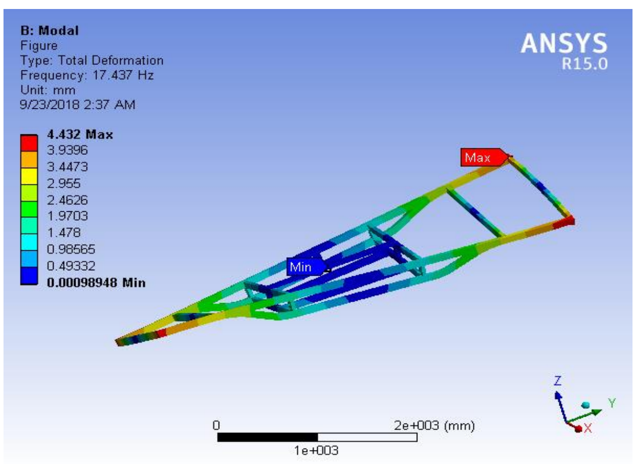


Total deformation 7

The seventh global mode shape of the electric vehicle chassis at 17.43 Hz. The chassis Experienced twisting mode along Y axis. The maximum translation was at the left back end of the vehicle chassis.

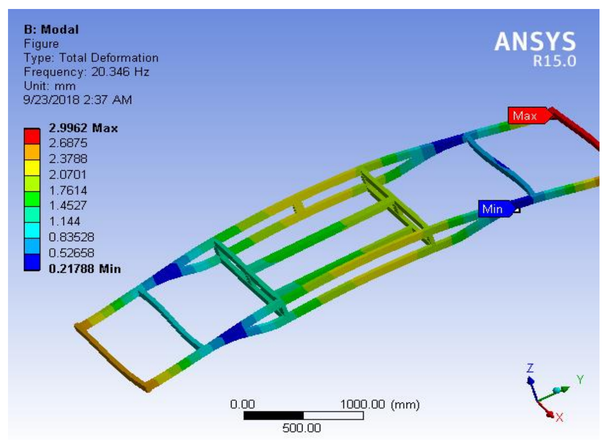


Total deformation 8

First global mode shape of the truck chassis at 20.346 Hz. The chassis Experienced the mode bending along lateral direction. The maximum translation was at the left back end of the vehicle chassis.

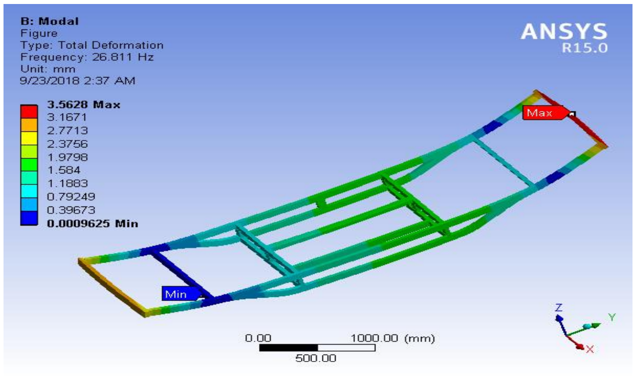


Total deformation 9

The ninth global mode shape of the electric vehicle chassis at 26.81 Hz. The chassis Experienced buckling on the middle part, and both overhang parts of the frame. The maximum translation was at the back end of the vehicle chassis.

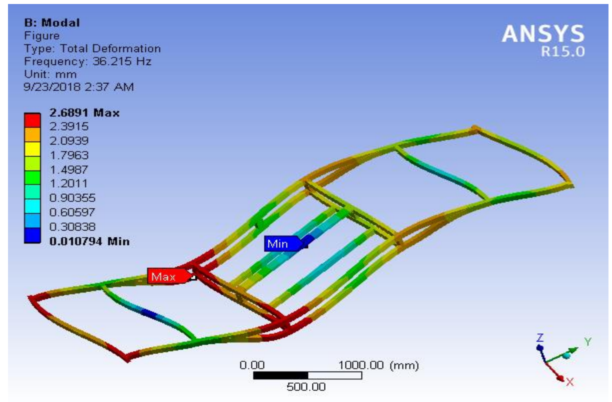


Total deformation10

The tenth global mode shape of the electric vehicle chassis at 36.21 Hz. The chassis Experienced twisting mode along Z and X direction. The maximum translation was at the front middle of the vehicle chassis.

The following bar chart and the frequency table indicates the frequency at each calculated mode.

Table 5-4 Frequency table for the modes

| Mode | Frequency [Hz] |
|---|---|
| 1. | |
| 2. | |
| 3. | 4.6804e-003 |
| 4. | 0.57512 |
| 5. | 1.006 |
| 6. | 1.6271 |
| 7. | 17.437 |
| 8. | 20.346 |
| 9. | 26.811 |
| 10. | 36.215 |

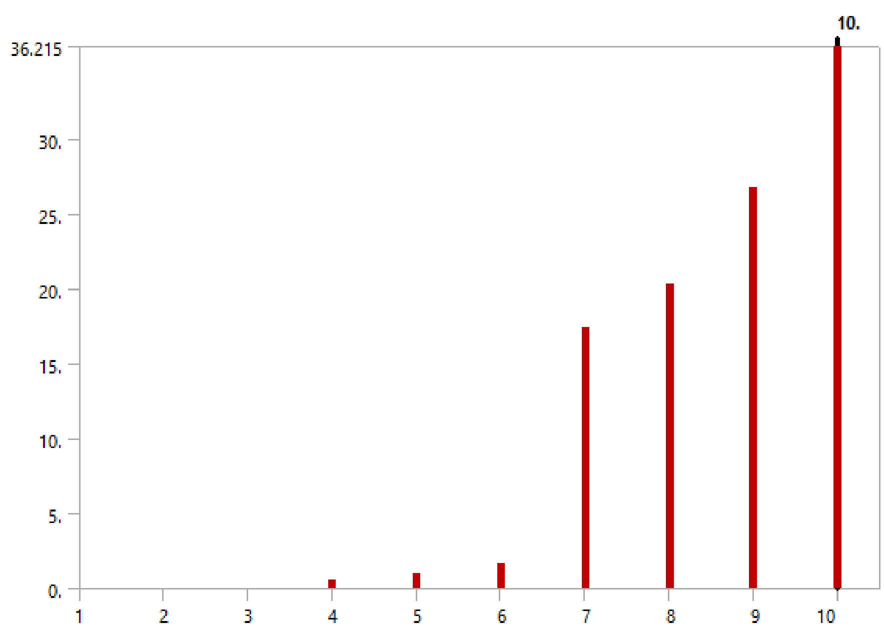


Figure 5-10 Chart of frequency for the modes

In general the natural frequency can be calculated using the equation

$$W_n = \sqrt{\frac{k}{m}}$$

Where K and m stand for stiffness and mass respectively the electric motor after reduction gear is known to have the operating speed varying from 6 to 25 revolutions per second ***(Dealer, 2014)***.

According to the above 10 modes of frequency there is no chance of occurrence of resonance frequency so it is safe.

The modal analysis is to avoid the damage of resonance to mechanical structure before it works in reality, the modal analysis is necessary to judge whether there is a resonance ***(Tang & Yu, 2017)***. Based on the results of modal analysis, the stability of device can be guaranteed through avoiding these frequencies or reducing the effect of excitation of these frequencies before the practical work of electric vehicle chassis frame.

In low speed idling condition, the speed range is about 6 to 8 rps. This translates into excitation frequencies varying from 24 to 30 Hz ***(Pravin, 2012)***. The main excitations are at low speeds, when the car is in the first gear. At higher gear or speed, the excitations to the chassis are much less. The natural frequency of the car chassis should not coincide with the frequency range of the axles, because this can cause resonance which may give rise to high deflection and stresses and poor ride comfort. Excitation from the road is the main disturbance to the car chassis when the car travels along the road. In practice, the road excitation has typical values varying from 0 to 100 Hz. At high speed cruising, the excitation is about 1481 rpm or 50 Hz. Mounting of vibration components of the vehicle on the nodal point of the chassis is one of the vibration attenuation methods to reduce the transmission of vibration to the car chassis ***(Pravin, 2012)***.

Regarding the above discussions about the electric motor speed before it reaches to the axle speed, we can say that natural frequencies are in critical range. Hence with decreasing the chassis length which increases the chassis stiffness, we increase the natural frequencies to place them in the appropriate range. By assembling the battery pack more center and also the electric motor more center, we can prevent coinciding the simulation force frequencies and natural frequencies. Otherwise resonance phenomenon occurs and if these two frequencies coincide, this phenomenon destroys the chassis. As a reminder it is mentionable that validity of the results has been verified by comparing the results from a similar model with the model proposed by Mr Foui and his cooperator.

Because the analysis is in free-free state, the first 3 modes that have almost zero frequency aren't considered and mode numbers 4 to 10 in Table 5-3 represent the first 3 modes of frequency. It is necessary to notice that in usual, the first 3 modes of frequency (mode numbers 4 to 10 in Table 5-3) play the main role in dynamic behavior of chassis and limited energy of motor to generate these frequencies can be ignored and these shows the safeness of chassis frame.

## 5.4 Harmonic analysis for electric vehicle chassis frame

Harmonic analysis result is used to verify the steady-state response of a linear structure, enabling researches, engineers and chassis designer to determine whether in which the chassis can withstand resonance, fatigue or other structural problems related to vibration during its operating life. Harmonic Analysis calculates the response of a structure to cyclic loads over a frequency range and plot the response on amplitude vs. frequency graph is shown in Fig 5-11.

### 5.4.1 Solution for frequency amplitude

Fig 5-11 shows in above that the highest amplitude recorded is at approximately 36.21 Hz with amplitude of 2.911 mm. Frequency at the highest peak amplitude illustrated in the plot is similar with the tenth mode shape frequency of the vehicle chassis and table 5-5 and Fig 5-12 shows the result of harmonic analysis.

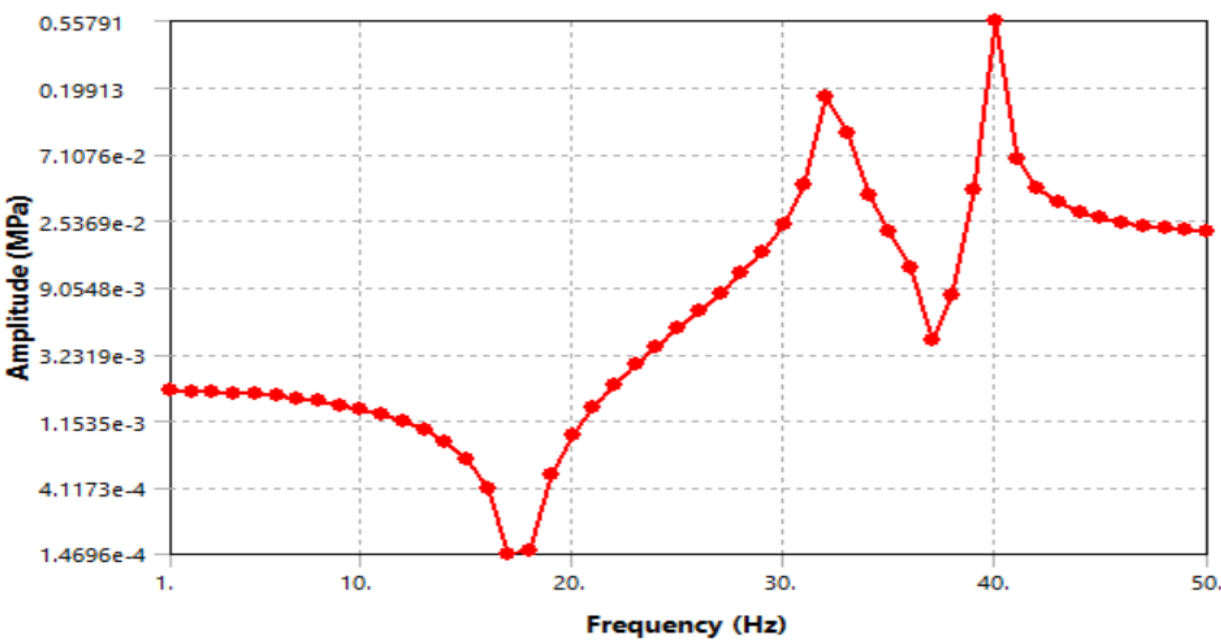


Figure 5-11 Frequency amplitude

Table 5-5 Harmonic Response Results

| Object Name | *Total Deformation* | *Equivalent Stress* |
|---|---|---|
| **Results** | | |
| Minimum | 0. mm | 5.7536e-003 MPa |
| Maximum | 2.0479 mm | 104.59 MPa |
| Minimum Occurs On | Part 21 | Part 17 |
| Maximum Occurs On | Part 10 | Part 1 |
| **Minimum Value Over Time** | | |
| Minimum | 0. mm | 5.7536e-003 MPa |
| Maximum | 0. mm | 5.7536e-003 MPa |
| **Maximum Value Over Time** | | |
| Minimum | 2.0479 mm | 104.59 MPa |
| Maximum | 2.0479 mm | 104.59 MPa |
| **Information** | | |
| Reported Frequency | 50. Hz | |

## 5.5 Impact force calculation & analysis images in case of Static analysis

### 5.5.1 Front impact

During front impact, the electric vehicle may hit a tree, another vehicle or a wall. Time of impact will be greater for deformable bodies as compare to that of rigid bodies so impact force in the case of wall will be more than that in case of another vehicle or tree. Impact time in case of impact with wall is taken as 0.13 seconds ***(Sati, Upreti, & & Tripathi, 2016)***. For analysis, the vehicle is considered to be in static state and force corresponding to velocity 160 km/h with impact time 0.13 seconds is applied to front part of the roll cage of vehicle keeping rear suspension members fixed.

Calculations:

Weight of the electric vehicle chassis frame, M =116.281 kg (from ANSYS)

Initial velocity before impact, $V_{initial}$ = 160km/h or 44.4m/s

Final velocity after impact, $V_{final}$ will be zero.

Impact time = 0.13 seconds

Impact Force Determination by Speed Limit:

According to the constraints in the rulebook, the maximum speed of the car is assumed to be 160km/hr. or roughly around 44.44m/s. For a perfectly inelastic collision, the impact force is as calculated as the flowing manner.

$$W_{net} = \left(\frac{m*v^2}{2}\right) final - \left(\frac{m*v^2}{2}\right) intial \quad \text{.......} 5.1$$

Where. $W_{net}$ is network done on account of an inelastic collision

$$W_{net} = -\left(\frac{m*v^2}{2}\right) intial \quad \text{.......} 5.2$$

$$W_{net} = -\left(\frac{116.281 * 44.44^2}{2}\right) intial$$

$$W_{net} = 114822.79Nm$$

But Wnet = impact force * s

$$Impact\ force = \frac{W_{net}}{s} \quad \text{.......} 5.3$$

$$s = Impact\ time * V_{max}$$

$$s = 0.13sec * 44.44m/s$$

$$s = 5.77m$$

So from equation (5.3) we get that $F = W/s$

Then $F = \frac{114822.79Nm}{5.77m} = 19899.9 = 19900N$

According to this calculated load apply as reaction force on the electric vehicle chassis frame to show the impact analysis and gate the results of total deformation, equivalent stress and safety factor on the frame. By taking the front object as rigid the load applied on the chassis frame from the rigid object is 19900N. The ANSYS simulation shows this occasion on Fig 5-13 to Fig 5-24

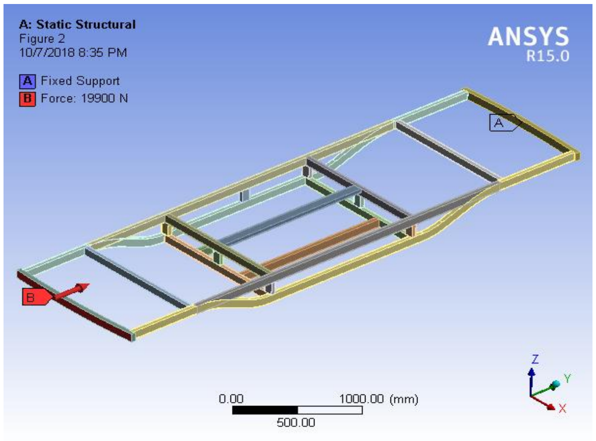


Figure 5-12 Impact applied load and fixed

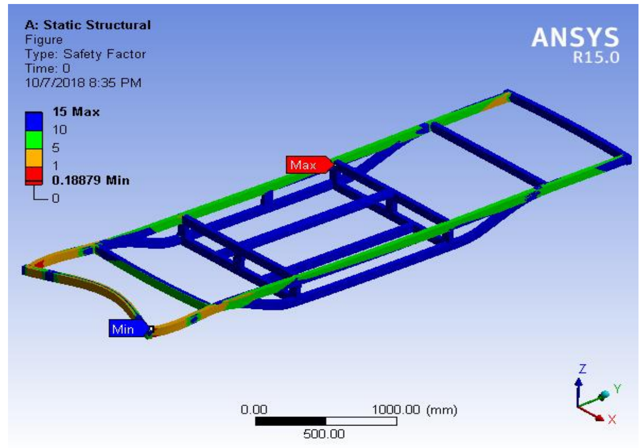


Figure 5-13 Front impact safety factor analysis

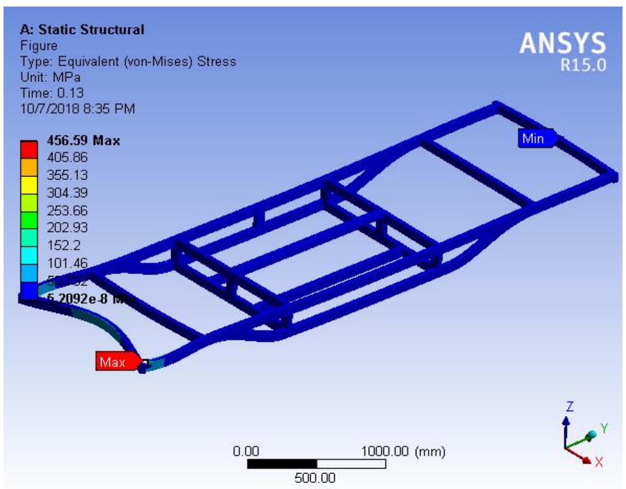


Figure 5-14 Front impact equivalent stress

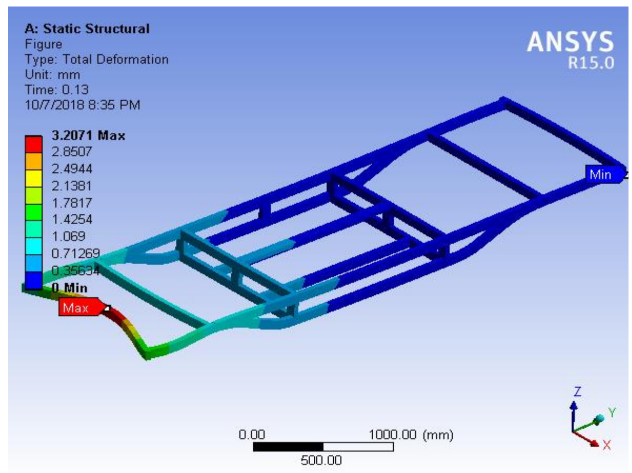


Figure 5-15 Front impact total deformation

The applied front impact force 19900N according the calculation and the maximum damage happens on the front right end of the chassis frame and the value is 456.59Mpa and the factor of safety is 0.1009 and the deformation on the chassis frame is 3.2071mm it lies on the front member in the middle of the chassis frame.

### 5.5.2 Rear impact

In actual condition during rear impact, another vehicle is going to hit this vehicle on its rear part. As the vehicle is a deformable body so the impact time is taken as 0.30 seconds. For analysis, vehicle is considered to be in static state and force corresponding to velocity 160 km/h with impact time 0.30 seconds is applied to rear part of the roll cage of vehicle keeping front members fixed.

$$work\ done = force * displacement = F * s$$

$$s = impact\ time * \ v_{max}$$

$$= 0.3sec * \frac{44.44m}{sec} = 13.332m$$

Therefor $$F = \frac{W}{S} = \frac{114822.79Nm}{13.332m} = 8612.57N = 8613N$$

According to this calculation applying the load 8613N on the electric vehicle chassis frame see the results from the ANSYS. Fig 5-16 to Fig 5-29 about rear impact of the frame.

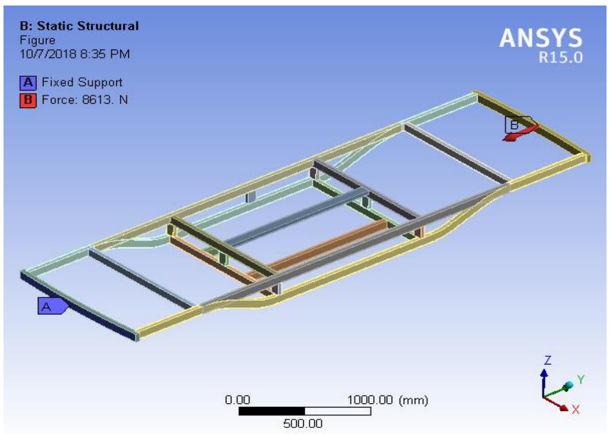


Figure 5-16 Applied load and fixed support

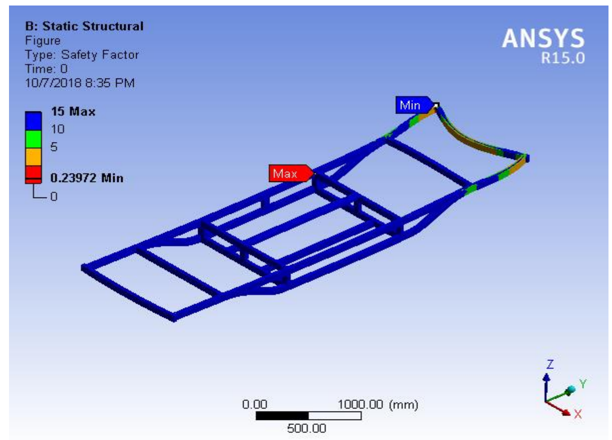


Figure 5-17 Rear impact safety factor analysis

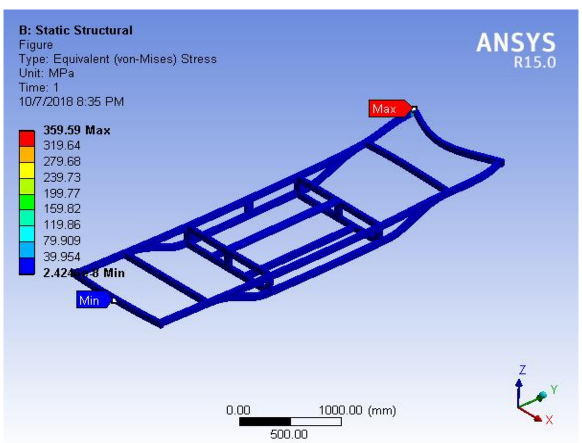


Figure 5-18 Rear impact equivalent stress

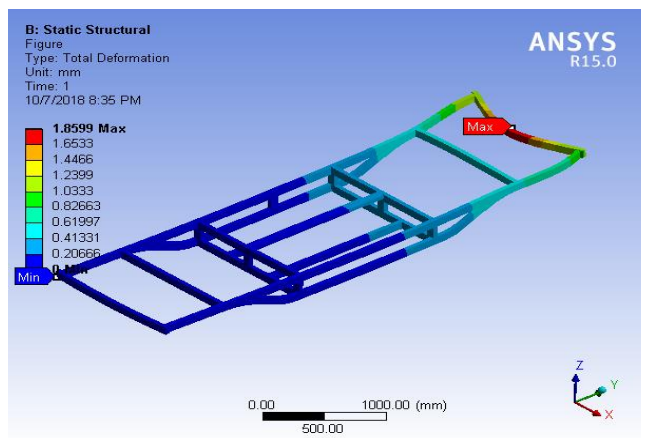


Figure 5-19 Rear impact total deformation

The applied rear impact force 8613N according to the above calculation and the maximum damage happens on the rear left end of the chassis frame and the value is 359.59Mpa and the factor of safety is 0.2397 and the deformation is 1.8599mm in the rear member in the middle of the chassis frame

### 5.5.3 Side impact

During side impact another electric vehicle will hit vehicle on side and as vehicle is deformable body, so the impact time is taken as 0.30 seconds ***(Sati, Upreti, & & Tripathi, 2016)***. For analysis, vehicle is considered to be in static state and force corresponding to velocity 160 km/h with impact time 0.30 seconds is applied to side of the roll cage of vehicle keeping suspension members of other side fixed.

$$work\ done = force * displacement = F * s$$

$$s = impact\ time * \ v_{max}$$

$$= 0.3sec * \frac{44.44m}{sec} = 13.332m$$

Therefor $$F = \frac{W}{S} = \frac{114822.79m}{13.332m} = 8613N$$

The calculated value load 8613N is similar that of the rear impact analysis because of its crushing time (second) 0.3sec and this analysis is also used to find the values like total deformation, equivalent stress and safety factor when the static impact occurs on the side of the electric vehicle chassis frame as shown from Fig 5-20 to Fig 5-23.

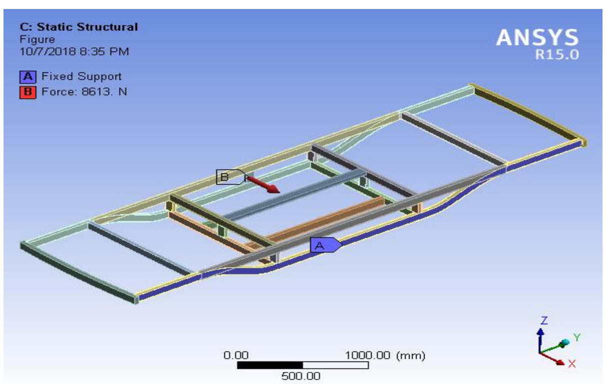


Figure 5-20 Applied load and fixed support

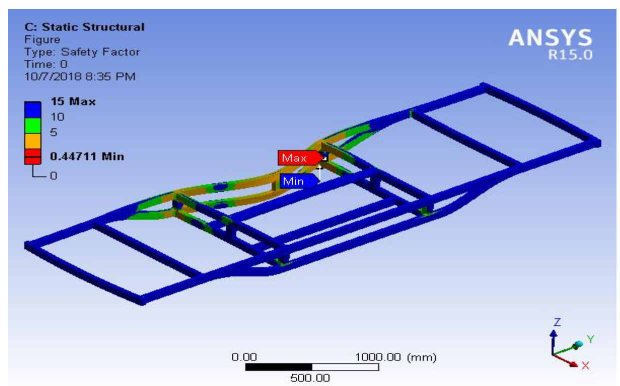


Figure 5-21 Rear impact safety factor analysis

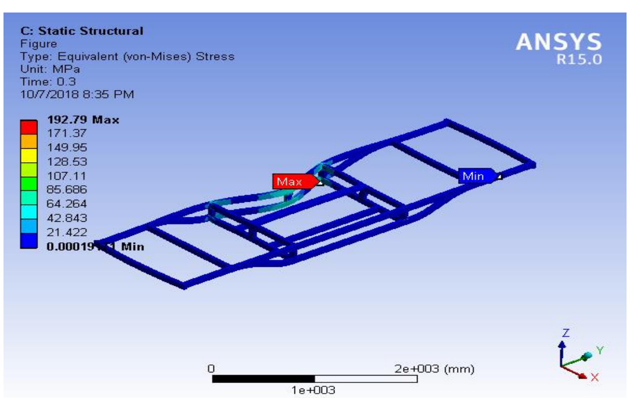


Figure 5-22 Side impact equivalent stress analysis

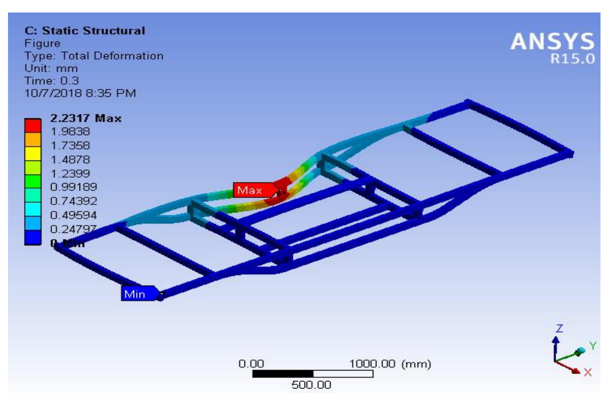


Figure 5-23 Side impact total deformation

The applied side impact force 38330N according to the above calculation and the maximum damage happens on the front right end of the chassis frame and the value is 192.78 Mpa and the factor of safety is 0.233 and the deformation is 2.3317mm at the left side member in the middle. Impact analysis are summarized in three cases on the following Table 5-6.

Table 5-6 Result for static impact analysis

| | **Force applied (N)** | **Max. stress (Mpa)** | **Max. deformation (mm)** | **Factor of safety** |
|---|---|---|---|---|
| Front | 19900 | 456.59 | 3.207 | 0.1889 |
| Rear | 8613 | 359.59 | 1.8599 | 0.2397 |
| Side | 8613 | 192.79 | 2.317 | 0.447 |

# CHAPTER SIX

# 6 ANALYSIS ABOUT BATTERY PACK AND THERMAL MANAGEMENT SYSTEM

## 6.1 The battery pack and its discussion

The vast majority of traction batteries in modern-day EVs are of lithium-ion chemistry. This is because, relative to other chemistries popular in other applications (such as lead-acid starter batteries), lithium-ion offers the right combination of attributes to make EVs competitive in the marketplace. These desirable attributes include:

- High performance:  enough energy density to provide a long driving range combined with enough power delivery to provide for fast acceleration
- Long life:  durability that provides reliable operation for many years (potentially a decade or more) and without much preventative maintenance needed to achieve this reliability
- Affordable cost:  such that EVs are projected to cost roughly the same as conventional vehicles, once manufactured in the same volumes (millions of vehicles per year).

To deliver this impressive combination of attributes, automotive manufacturers go to great lengths to select the right battery cells for their products and then to engineer them into high-performance, high-reliability, low-cost battery packs for mass-production in their quality-controlled factories. ***(James, 2017)***

Table 6-1 Value chain for electric-car batteries comprises seven steps

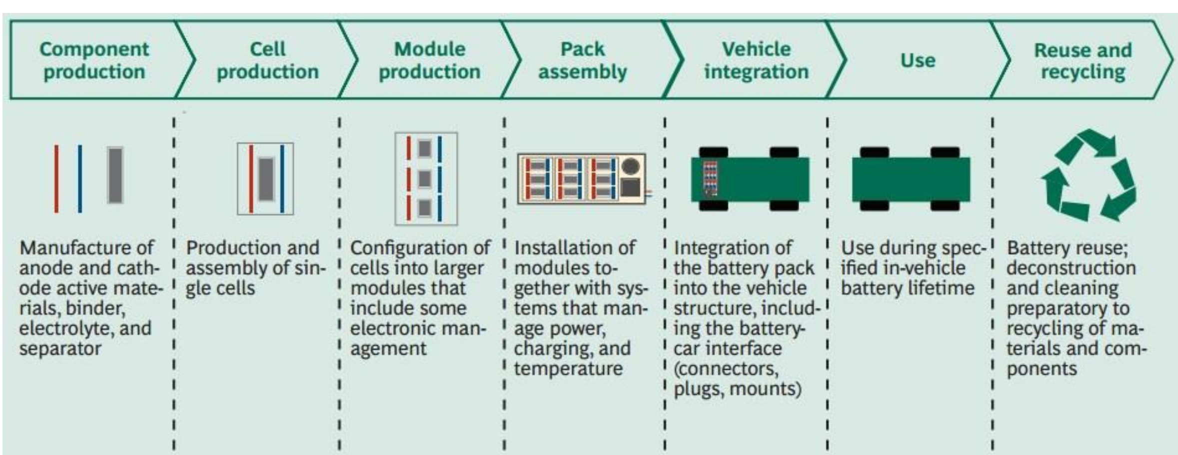


The electric vehicle‘s maintenance requirements are fewer and therefore the maintenance costs are lower. The electric motor has one moving part, the shaft, which is very reliable and requires little or no maintenance. The controller and charger are electronic devices with no moving parts, and they require little or no maintenance. State-of-the-art lead acid batteries used in current electric vehicles are sealed and are maintenance free. However, the life of these batteries is limited and will require periodic replacement. New batteries are being developed that will not only extend the range of electric vehicles, but will also extend the life of the battery pack which may eliminate the need to replace the battery pack during the life of the vehicle.

The comparison pf gasoline vehicle and electric vehicle is sown in Table 6-2 detail based on its functions of the related components

Table 6-2 Comparison of gasoline vehicle and electric vehicle

| GASOLINE VEHICLE | FUNCTION | ELECTRIC VEHICLE |
|---|---|---|
| Gasoline Tank | Stores the energy to run the vehicle | Battery |
| Gasoline Pump | Replaces the energy to run the vehicle | Charger |
| Gasoline Engine | Provides the force to move the vehicle | Electric Motor |
| Carburetor | Controls Acceleration and speed | Controller |
| Alternator | Provides Power to accessories | DC/DC converter |
| | Converts DC to AC to power AC motor | DC/AC converter |
| Smog Controls | Lowers the toxicity of exhaust gasses | |

### 6.1.1 Refueling for electrical vehicles

Due to the limited driving range of electrical vehicle, the refuel for a long distance driving is an essential prerequisite for EV development as shown in Table 6-3.

- AC charging: Easy but slow
- DC charging: Hi-power, impact to both battery and grid
- Battery swapping: standardization dilemma

Table 6-3 Refueling methods for electric vehicle battery packs

| | **AC plug-in charging** | **DC Fast charging 0.3C** | **DC Fast charging >1C** | **Battery swapping** |
|---|---|---|---|---|
| Time to finish | 8~13h | 3~4h | <1h | 2min |
| Grid network | Home plug | 16/vehicles/spot | 48vehicles/spot | 720vehicles/station |
| Infra-structure cost | Low | High | High | High |
| Operating cost | Low | Low | High | High |
| Driving Range/km | 100~200 | 100~200 | 100~200 | 100~200 |
| Maintenance cost | - | - | High | Low |
| Battery Maintenance | - | - | Fast charging shortness the life of batteries | Centralized charging and maintenance, longer life of batteries |

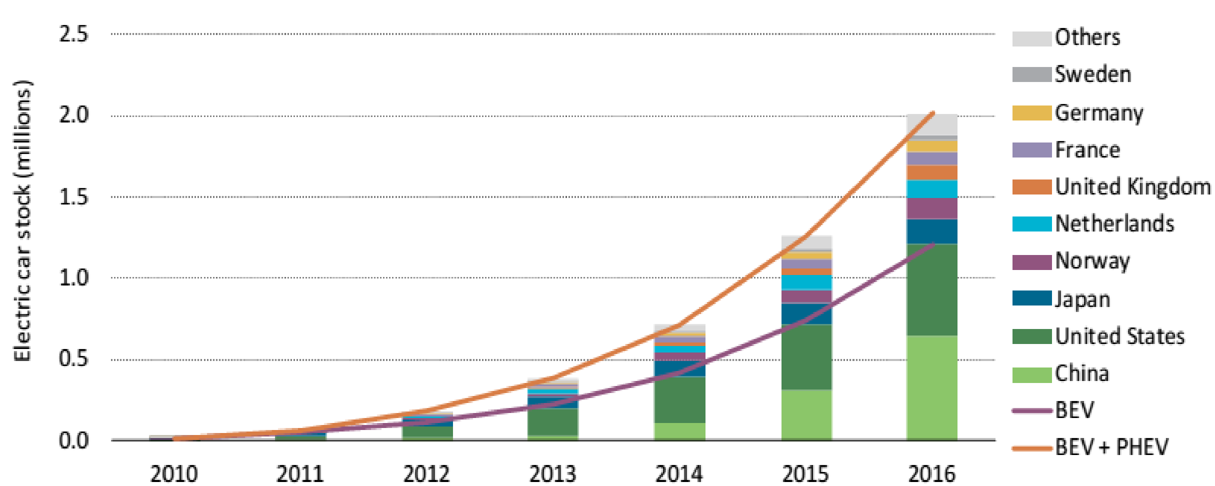


Figure 6-1 Evolution of the global electric car stock

***(Jean-Francois & Kamel, 2017)***, Notes: The electric car stock shown here is primarily estimated on the basis of cumulative sales since 2005. When available, stock numbers from official national statistics have been used, provided good consistency with sales evolutions Fig 6-1.

### 6.1.2 Battery specifications and price development

Battery specifications a number of manufacturers in the world already deliver commercially available EV batteries. Table 6-4 shows some of the commercially available batteries and their specifications. A few batteries currently under development are not yet commercially available, such as the Al-air and Li-air batteries. Also the batteries that are commercially available are still being developed. In table 5-14 the current and projected specifications of batteries suitable for EVs are given. The projected specifications are the predicted specifications that a type of battery will have by the year 2020. Some batteries are already nearing their maximum potential like the Pb-A and Ni-MH and probably will not improve much in the future.

Table 6-4 Battery specifications and price development

| | **Now** | | | **2020** | | | |
|---|---|---|---|---|---|---|---|
| | **Specific power (W/kg)** | **Specific power (W/kg)** | **Cycle life (deep cycles)** | **Specific power (W/kg)** | **Specific power (W/kg)** | **Cycle life (deep cycles)** | **sources** |
| Pb/A (VRLA) | 200 | 35 | 600 | 300 | 45 | 1500 | a,b |
| NiMH | 200 | 65 | 1000 | 300 | 75 | 1200 | C,d |
| NaNiCl2 | 150 | 100 | 1000 | 400 | 120 | 1500 | e |
| Lithium-ion | 300 | 100 | 1000 | 500 | 150 | 1500 | f,g |
| Zn/air | 90 | 100-200 | NA | 110 | 300 | 600 | h,i |
| Al/air | 10 | 200-300 | NA | 16 | 1300 | NA | C,j,d |
| Li/air | | | | low | 600-1000 | NA | K,l,m |
| Fe/air | 90 | 80 | 600 | 100 | 120 | 1000 | h,n |

## 6.2 Battery pack thermal management system

Temperature has a direct effect on the performance of a lead-acid battery. The concentration of sulfuric acid inside the battery increases and decreases with temperature. A battery being used in 32°F weather will only operate at 70% of its capacity. Likewise, a battery being used in 110°F weather will operate at 110% of its capacity. The most efficient temperature that battery manufacturers recommend is 78°F. Because the temperature factor is important in colder climates, insulated battery boxes or thermal management systems are used. (Bansal) Regular pack to operate in the desired temperature range for optimum performance/life 15ºC – 35ºC ***(Pesaran, Swan, & etal.., 2011)***

### 6.2.1 Battery Temperature affects battery pack:

Battery Thermal Management System should be:- Lightweight, Easily packaged, Reliable, Serviceable, Low-cost, Low parasitic power, Optimum temperature range, Small temperature variation

Temperature affects the battery pack in the following manners

- Operation of the electrochemical system
- Round trip efficiency
- Charge acceptance
- Power and energy availability
- Safety and reliability
- Life and life-cycle cost

### 6.2.2 Modification of cooling plate and discussion on the CFD result analysis

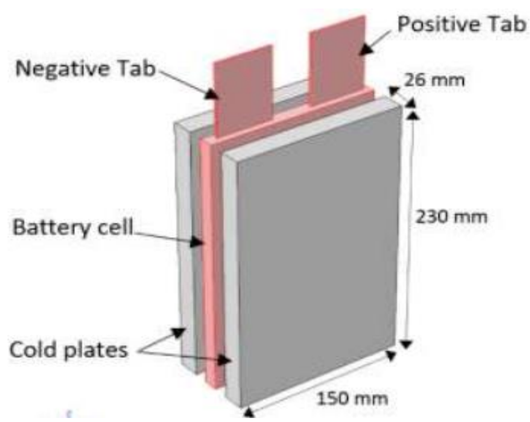


Figure 6-2 Battery cell cooled with two cold plates

The schematics of the different cold plate's designs are represented in Figure 6-3 and have the same dimensions of 70 mm in width, 12 mm in depth and 230 mm in height. The different cold plate designs differ from the structure of the cooling channels with an inner diameter of 9 mm:

Fig 6-3 (a): characterized by 5-straight cooling channels distributed equidistantly along the width of the cold plates. The inlet connector channel is placed at the middle in order to have more flow rate at the middle of the cold plate. The outlet connector channel is placed at the middle of the bottom to recover the hot liquid. This design has the advantage of reducing the pressure drop inside the cooling channel.

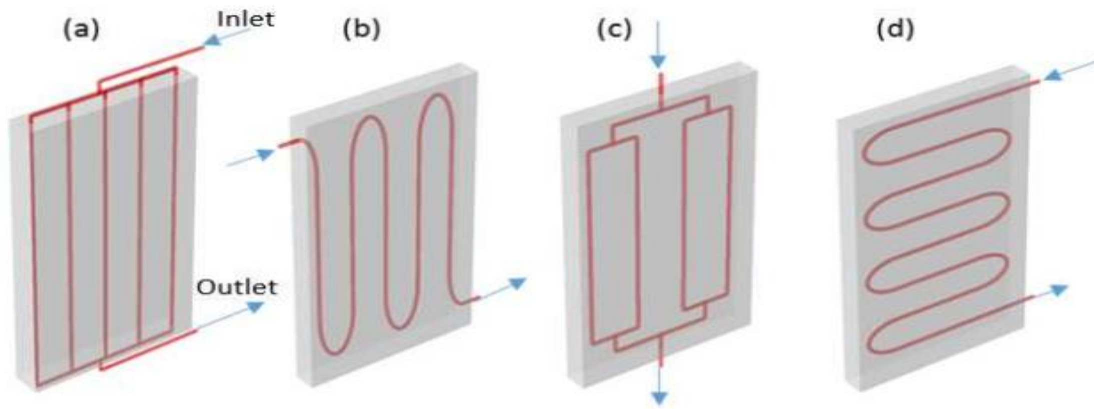


Figure 6-3 Different cold plate designs

Fig 6-3 (b): comprises one cooling channel having an inlet and outlet ends on the left and right sides of the cold plate, respectively. The intermediate portion with a sinuous pattern has arranged vertically. This design has the advantage of conducting the total flow rate into the cooling channel. Fig 6-3 (c): characterized by 4-straight cooling channels, where the total flow rate is split uniformly into the different lines. Fig 6-3 (d): have the same characteristic than the design 2, however the intermediate portion with sinuous pattern is arranged horizontally.

Table 6-5 Temperature distribution over the cell with different cold plate designs

| Water | Design 1 | Design 2 | Design 3 | Design 4 |
| --- | --- | --- | --- | --- |
| | Max=20.60 | Max=20.37 | Max=20.58 | Max=20.38 |

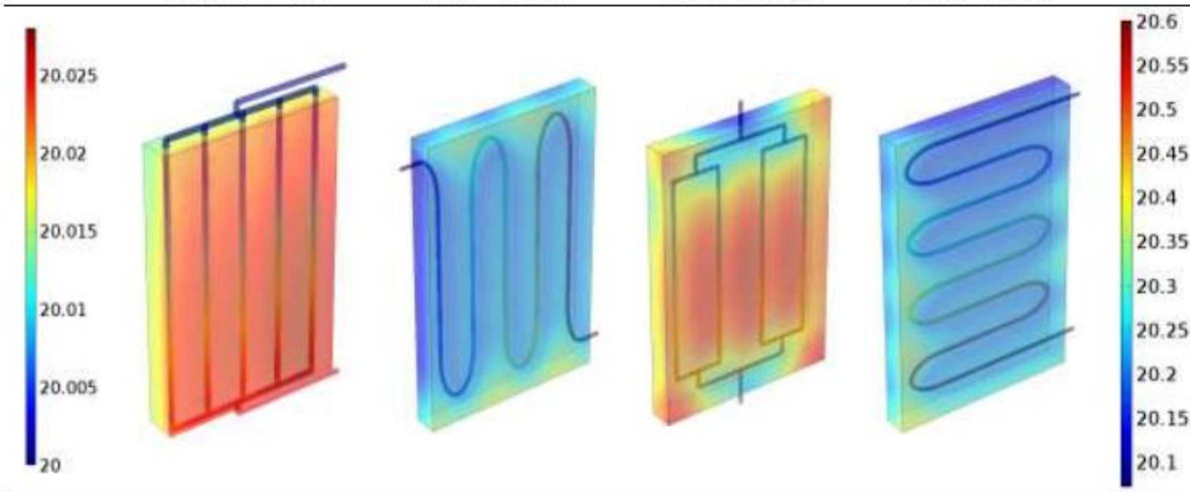


| | | | | |
| --- | --- | --- | --- | --- |
| | Min=20.33 | Min=20.07 | Min=20.10 | Min=20.07 |

Based on the above designed and measured discussion we prefer for this thesis CFD analysis and the cooling plate detail specification of the designed plate which is found in Fig 6-3 (d) and design 4 in Table 6-5 because of it is easy to design and bend the copper coil but the temperature is less than that of design 1 and design 3, in those design the need of welding to copper coils on its joint it must sharp weld and no need of linkage that is why I took design 4 from the above table 5-14.

Table 6-6 Thermal parameters of battery cells for CFD simulation

| **Parameters** | **Value** |
|---|---|
| Heat conductivity (length direction, W/m.K) | 4.323 |
| Heat conductivity (thickness direction, W/m.K) | 0.867 |
| Heat conductivity (length direction, W/m.k) | 5.02 |
| Heat capacity (kJ/k) | 1115 |

Table 6-7 Parameters of the cooling plate ***(Haifeng & Zechang, 2015)***

| **Parameters** | **Value** |
|---|---|
| Cooling plate material | Aluminum |
| Heat conductivity of cooling plate (W/m.K) | 202 |
| Specific heat capacity of cooling plate (J/kg.K) | 187 |
| Density (kg/m$^3$) | 2719 |
| Cooling liquid | Water |
| Viscosity (kg/m.s) | 0.001003 |
| Heat conductivity (W/m.K) | 0.6 |
| Specific heat capacity (j/kg.K) | 4182 |
| Density (kg/m$^3$) | 998.2 |
| Battery module number | 3 |
| Plate (mm*mm*mm) | 230x150x10 |
| Radius of fluid inlet and outlet (mm) | 12 |
| Power of heat source | 126000 |

The cooling plate takes the heat from battery cell away from the bottom of the battery cells and the size of the cooling plate is 230mm×150mm×12mm this dimension is the existing one and for the shape optimization 230mmx150mmx10mm and . Aluminum is selected EVS28 International Electric Vehicle Symposium and Exhibition 3 as the material of the cooling plate, and to simplify the simulation and analysis, water is selected as the heat medium.

### 6.2.3 Shape minimization of cooling plate

The existing battery cell on rav4 EV is pouch type and its arrangement by two layers 7 batteries (170mm) in vehicle track position and 7 batteries (position of 265mm) in parallel to vehicle base and 7 batteries are out of normal arrangement then the total number the battery cell is 105. The mass of the single battery cell is 1.4285kg and the mass of cooling plate in one side of battery cell before optimization is 1.1178kg.

Calculation

$$mass\ of\ electric\ vehicle\ battery\ pack = number\ of\ battery\ cell\ x\ mass\ of\ each\ cell$$

$$mass\ of\ pack = 105x1.42857kg = 150kg$$

The number of cooling plate is two for each battery cell, and total number cooling plate is 210 for this reason calculation to know the mass of cooling plate is

$$total\ mass\ of\ cooling\ plate\ is = number\ of\ cooling\ plate\ x\ mass\ of\ single\ cooling\ plate$$

$$mass\ of\ cooling\ plate = 210x1.1178kg = 234.738kg$$

Where, the grove in the cooling plate is not considered in mass calculation because it was cached by the fluid so it is negligible deference

$$total\ mass\ of\ battery\ pack = mass\ of\ battery\ cell + mass\ of\ cooling\ plate$$

$$mass\ of\ battery\ pack = 150kg + 234.738 = 384.73kg$$

this mass is the existing one and according to the chassis design the battery is swappable it is not permanently mounted with the vehicle for this reason there should be mass reduction to the pack and there is no need of that much cooling plate on the battery cell because when the battery will swap it is exposed to the atmospheric temperature and on time of charging the station has suitable charging place to the battery pack, the coolant is busy only in the case of charging and discharging.

As mentioned in the above, a battery being used in 32°F weather will only operate at 70% of its capacity. Likewise, a battery being used in 110°F weather will operate at 110% of its capacity. The most efficient temperature that battery manufacturers recommend is 78°F. Making this temperature variation by EXCEL and the thermal analysis is done and also the temperature feature on cooling plate by fluent (CFD) is shown below. The shape of the cooling plate 230mm x 150mm x 10mm only the thickness of the plate is minimized from 12mm to 10mm now we can see that the mass reduction to the entire battery pack.

$$mass\ of\ cooling\ plate = density\ of\ material\ x\ volume\ of\ material$$

$$volume\ of\ cooling\ plate = 0.23x0.15x0.01 = 0.000345m^3$$

$$mass\ of\ cooling\ plate = 2700\ {}^{kg}/_{m^3}\ x0.000345m^3 = 0.9315kg$$

$$total\ cooling\ plate\ of\ mass = 0.9315kg\ x\ 210 = 195.615kg$$

The battery mass as it is so the total mass of electric vehicle battery pack after optimization is

$$mass\ of\ battery\ pack = mass\ of\ total\ battery\ cell + mass\ of\ total\ cooling\ plate$$

$$mass\ of\ battery\ pack = 150kg + 195.615kg = 345.615kg$$

Then the mass reduction in the entire battery pack is from 384.738kg to 345.615kg this increases the life of the chassis frame and easy to swap the battery than the previous by reduction of 39.123kg and also the unknown reduction of cost on the battery pack.

### 6.3 Transient analysis for the BTMS

The derived differential equations, those represents the energy balance for the battery cell cooling plate, coolant plate and fluid equations are solved using the explicit finite difference method. The time derivative is replaced by the forward difference scheme. The transient temperatures are evaluated iteratively, using relations derived for the equation of energy balance (Duffie, 2013).

$$E_{generated} = heat\ absorbed\ by\ fluid + heat\ loss\ to\ the\ atmospher$$

Where, $E_{generated}$ is the generated energy (power) to the coolant plate

$$= h_{conv.fluid} x \frac{dT}{dx} + heat\ loss\ to\ the\ atomospher$$

Assume that Fig 6-4 plate of the coolant wall divided into two, one is top part from the horizontal diameter of the copper coil and naming it top plate (p1) and bottom plate (p2) respectively.

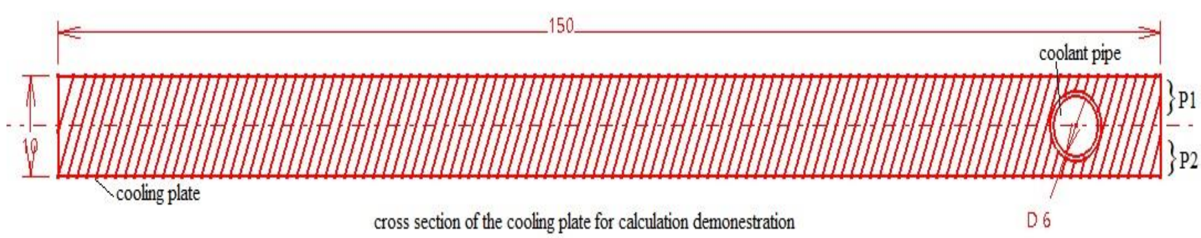


Figure 6-4 Cross section of the aluminum plate

***For p1 (Top part of the plate)***

$E_{in} - E_{out} = \Delta E$.....................................................................................................................5.1

$$heat\ coming\ from\ battery - heat\ transfer\ to\ fluid = \rho_p V_p C_p \frac{dT_{p1}}{dt}$$

By discretizing the above energy balance we gave the following equation for the section 1 or the above plate

$heat\ generated - h_{fluid} A(T_p - T_f) = \rho_p V_p C_p \frac{dT_{p1}}{dt}$............................................................. 5.2

***For fluid***

$-\dot{m}_f C_f \frac{\partial T_f}{\partial x} + h_f \pi D(T_{p1} - T_f) - h_f \pi D(T_f - T_{p2}) = \rho_f A_f C_f \frac{\partial T_f}{\partial t}$............................................5.3

***For p2 (bottom part of plate)***

$h_f A(T_f - T_{p2}) - h_{air} A_s(T_{p2} - T_{air}) = \rho_{p2} V_{p2} C_{p2} \frac{dT_{p2}}{dt}$.............................................................5.4

The explicit finite-difference method is proposed to solve the system of equations. The time derivatives are replaced by a forward difference scheme, whereas the dimensional derivative is replaced by a backward difference scheme.

***For p1 (Top part of the plate)***

$E_g - h_f A(T_p^t - T_f^t) = \rho_p V_p C_p (T_f^{t+\Delta t} - T_f^t)$ .........................................................................5.5

$T_{pj}^{t+\Delta t} = \frac{\Delta t}{\rho_p V_p C_p} E_g - \frac{\Delta t h_f}{\rho_p V_p C_p}(T_p^t - T_f^t) + T_f^t$..........................................................................5.6

***For fluid***

$-\dot{m}_f C_f \frac{\left(T_{fj}^t - T_{f_{j-1}}^t\right)}{\Delta l} + h_f \pi D\left(T_{p1j}^t - T_{f_j}^t\right) - h_f \pi D(T_{fj}^t - T_{p2j}^t) = \rho_f A_f C_f (\frac{T_{fj}^{t+\Delta t} - T_{fj}^t}{\Delta l})$ ......................5.7

Therefore, equation for iteration is as follow

$T_{fj}^{t+\Delta t} = \frac{h_f x \Delta t}{\rho_f V_f C_f}(T_{fj}^t - T_{p2j}^t) - \frac{\dot{m}_f C_f \Delta t}{\rho_f V_f C_f}\left(T_{fj}^t - T_{f_{j-1}}^t\right) - \frac{h_f x \Delta t}{\rho_f V_f C_f} x(T_{fj}^t - T_{p2j}^t) + T_{fj}^t$......................5.8

Where, j=1, 2, 3, …………………………299 (j is natural number and number of iteration)

***For p2 (bottom part of plate)***

$$\rho_{p2}V_{p2}C_{p2}\left(\frac{T_{p2}^{t+\Delta t}-T_{p1}^{t}}{\Delta l}\right)=h_fA\left(T_f^t-T_{p2}^t\right)-h_{air}A_s(T_{p2}^t-T_{air}^t) \qquad 5.9$$

$$T_{p2}^{t+\Delta t}=\frac{h_fA\Delta t}{\rho_{p2}V_{p2}C_{p2}}\left(T_f^t-T_{p2}^t\right)-\frac{h_{air}A_s\Delta t}{\rho_{p2}V_{p2}C_{p2}}\left(T_{p2}^t-T_{air}\right)+T_{p2}^t \qquad 5.10$$

From the EXCEL transient analysis the following figures founded the indicates that the temperature variation cooling plate in each minute and there are same assumptions for this analysis

These are

- Average speed of the vehicle 90km/hr (25m/sec)
- Average temperature of the environment 25°C the day average temperature in Adama
- Assume that the driver drives the vehicle for 5hr (300 minute) without rest
- Taking the bending of the copper coil as the node then the analysis have 10 nodes

Constants and calculated values for the EXCEL input are as follow

| | | | |
|---|---|---|---|
| $\rho_f$(kg/m$^3$) | = 997 | $k_f$(w/m.k) | = 0.607 |
| $\rho_{air}$(kg/m$^3$) | = 1.225 | $h_f$ | = 257.3290266 |
| $\rho_p$(kg/m$^3$) | = 2700 | $E_g$(kw) | = 645 |
| $C_f$ (J/kg. k) | = 4185.5 | $T_{air}$ | = 25 |
| $C_p$ | = 921 | $D_p$ | = 0.007 |
| $h_{air}$(W/m$^2$ k) | = 52.09 | L(m) | = 1.4 |
| $P_{rf}$ | = 6.14 | $\mu\_f$ | = 0.000891 |
| $f_{inlet}$ | = 20 °C | $T_{initial}$ | = 25 °C |

The values like renould number, volume of plate and volume pipe, volume of fluid and area are calculated values the constants took from the thermodynamics table of cengele in 25°C

The Nusselt, Rayleigh, and Prandtl numbers are given by ***(Duffie, 2013)***:

$$R_l=\frac{\rho_{air}V_{air}L}{\mu} \qquad 5.11$$

$$R_l=3.682x10^5$$

$$P_r\ from\ termo\ table \qquad 5.12$$

$$N_u=0.56R_l^{1/2}P_r \qquad 5.13$$

$$N_u=469.66$$

Fig 6-5 shows that the average temperature on plate facing on the battery cell (P1) of ten node in 300 minuet then the temperature is 38°c to 47°c smoothly increasing in each minute, the average fluid temperature of ten node is between 20°C and 29.5°C and the upper part of a plate (P2) average temperature is 21°C to 28.08°C. The correct mass flow rate for gating this temperature is the mass flow rate of 0.001kg of the fluid. And the following graph describes the relations and features of the three case temperature in ten nodes and 300 minute.

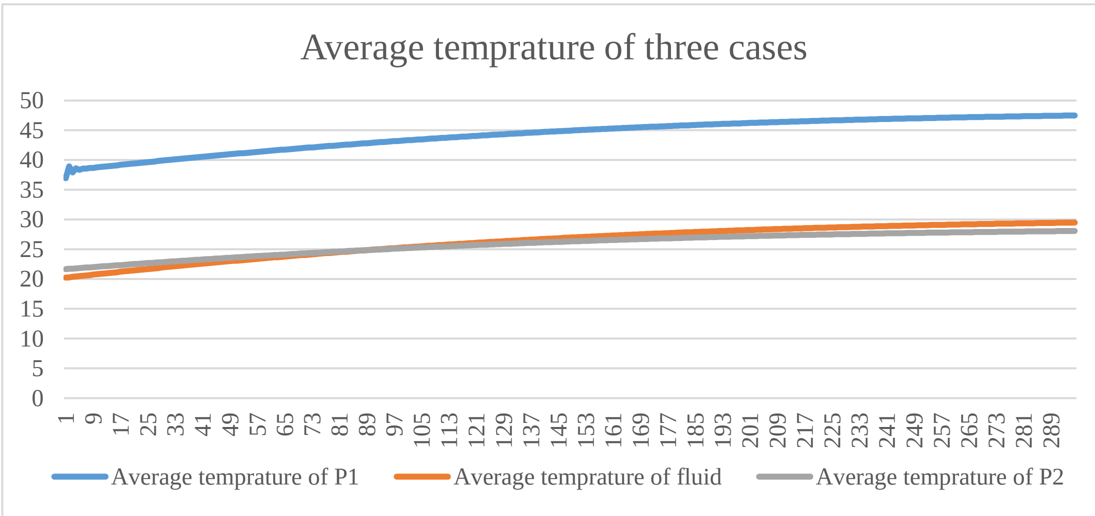


Figure 6-5 Average temperature of $p_1$, fluid and $p_2$

### 6.3.1 CAD modeling to cooling plate

CAD modeling using the CATIA v5 software for the 3D modeling in Fig 6-6 according to the minimized shape of the plate. And the next software is ANSYS used for the fluent (CFD) analysis as shown in Fig 6-7.

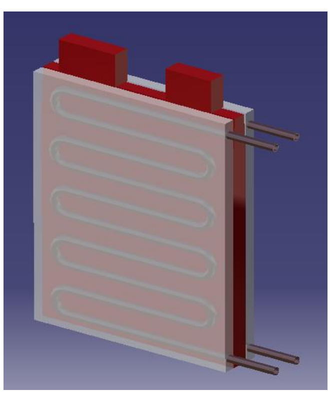

Figure 6-6 cooling plate with the battery pack

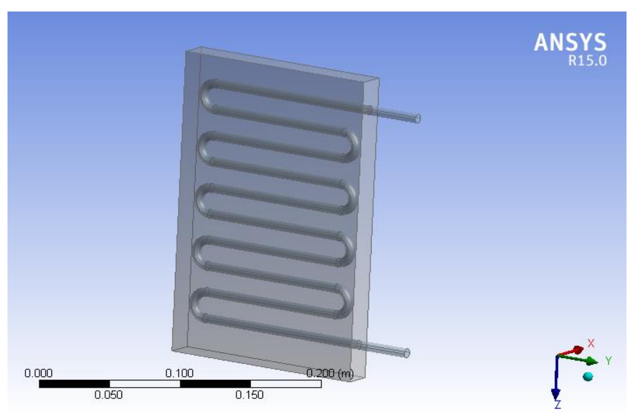


Figure 6-7 Modified cooling plate

The only changed parameter on the above battery cell is minimizing the thikness of coolant plate from 12mm to 10mm and the copper coil diameter from 9mm to 7mm diameter. According to the excel result we can see the effect of the fluent result on the cooling plate the tamprature of the intier plate with the coolant fluid is 46.2$^o$C. lets see the feature of the cooling plate when in operating as shown in Fig 6-8 and Fig 6-9.

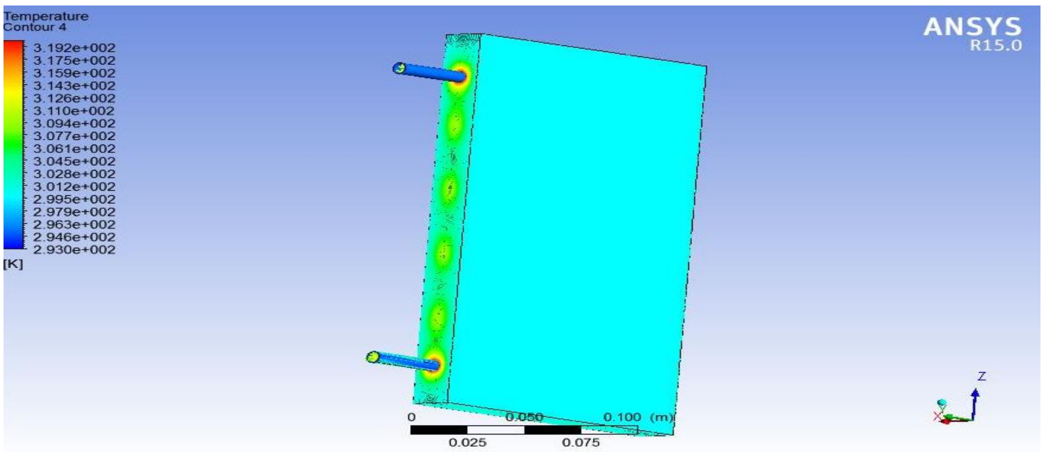


Figure 6-8 Temperature contour result for the new plate 3D view

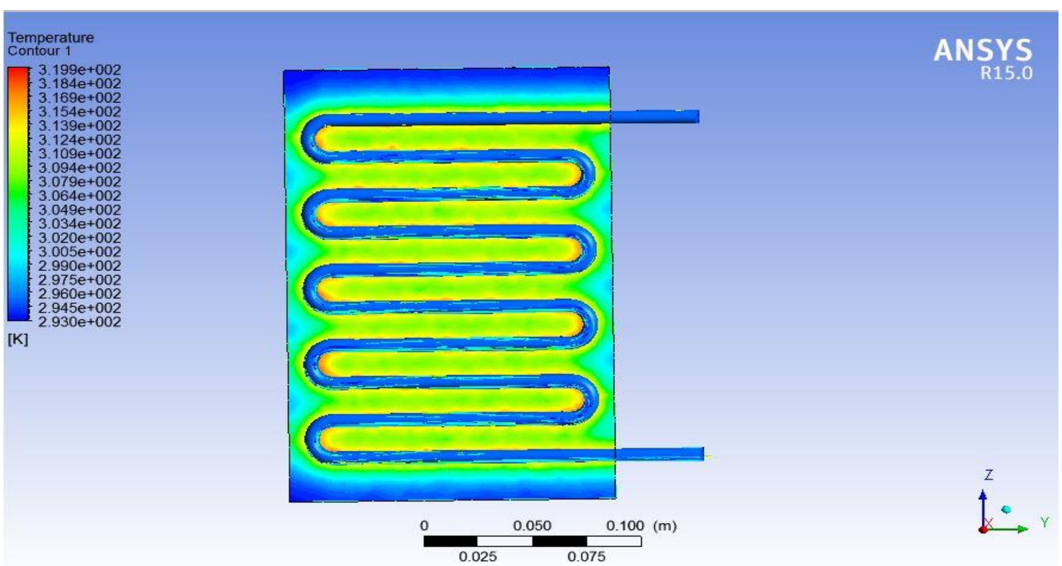


Figure 6-9 Temperature contour result for the new plate sectioned view

The maximum temperature in the optimized plate is 319.2K changing to degree Celsius it is

$$C^o = K - 273$$

$$C^o = 319.2 - 273$$

$$= 46.2C^o$$

# CHAPTER SEVEN

# 7 COST ANALYSIS

## 7.1 Cost estimation

Cost analysis is carried in order to estimate the cost of the new three wheeled vehicle model. The analysis is based on the current cost of the materials in the market. Figure 7-1 shows the numbers given to each parts of the space frame to identify each other. Members have the same cross section but they are different in their length. Each member has a rectangular hallow cross section of $80mm \ x \ 40mm \ x \ 5mm$

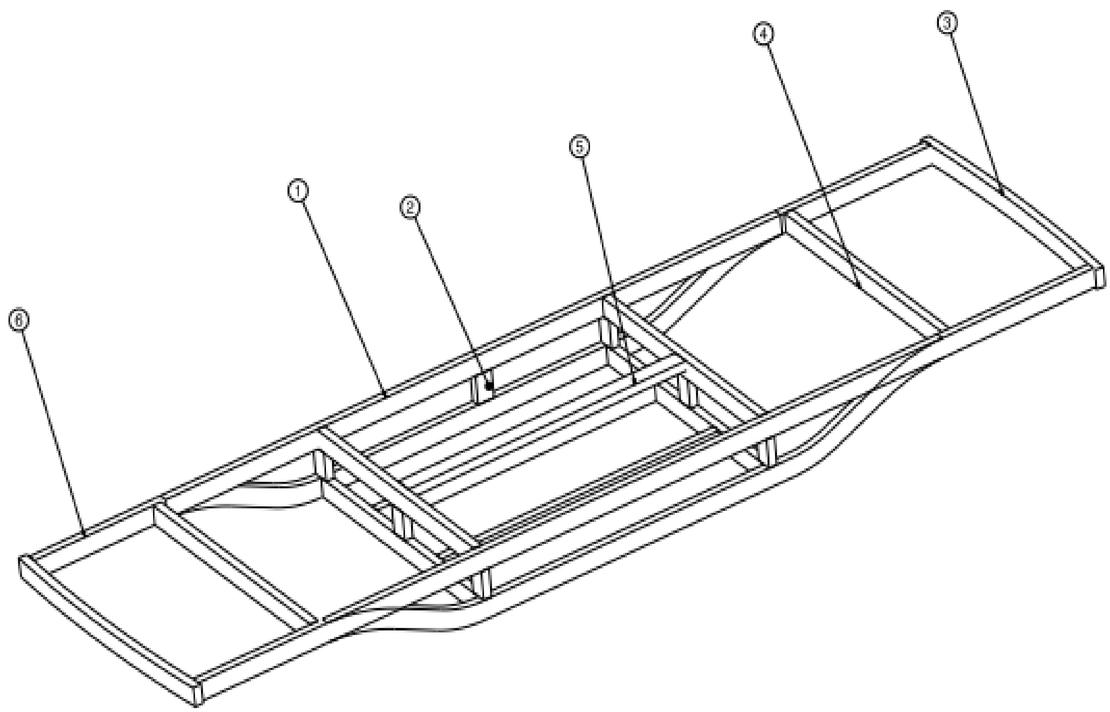


Bill of Material: Product1

| Number | Part Number | Quantity | Type |
|---|---|---|---|
| 1 | Top side member | 2 | Part |
| 4 | cross member | 6 | Part |
| 3 | Edge cross member | 2 | Part |
| 5 | battery box support | 3 | Part |
| 6 | Botom & long side member | 2 | Part |

Figure 7-1 Designed frame of the vehicle

In order to estimate cost, we need to find the total length of beam used in the electric vehicle chassis frame structure. To do this we have make a table by grouping members with the same length in one column. Table 7-1 bellow shows grouped members and their total length.

Table 7-1 Cost analysis table

| Number | Bill number | Unit length | Quantity of members | Total length |
|---|---|---|---|---|
| 1 | 1 | 2490mm | 2 | 4980mm |
| 2 | 4 | 1200mm | 6 | 7200mm |
| 3 | 6 | 4524mm + 240mm | 2 | 9528mm |
| 4 | 3 | 1300mm | 2 | 2600mm |
| 5 | 2 | 120mm | 7 | 840mm |
| 6 | 5 | 1400mm | 3 | 4200mm |
| | | Total length in mm | | 29348mm |

From the above table the total lengths of the rectangular hallow cross section with 80mm x 40mm x 5mm required is 29348mm. The current cost of the steel with the above cross section obtained from market is 108.35 Birr per meter. Now multiplying the total lengths of the steel required with its cost per meter the total cost of the EV chassis frame can be obtained.

$$Total\ cost\ estimation = 29.348m\ x\ 108.35 birr/m$$

$$= 3179.36\ birr$$

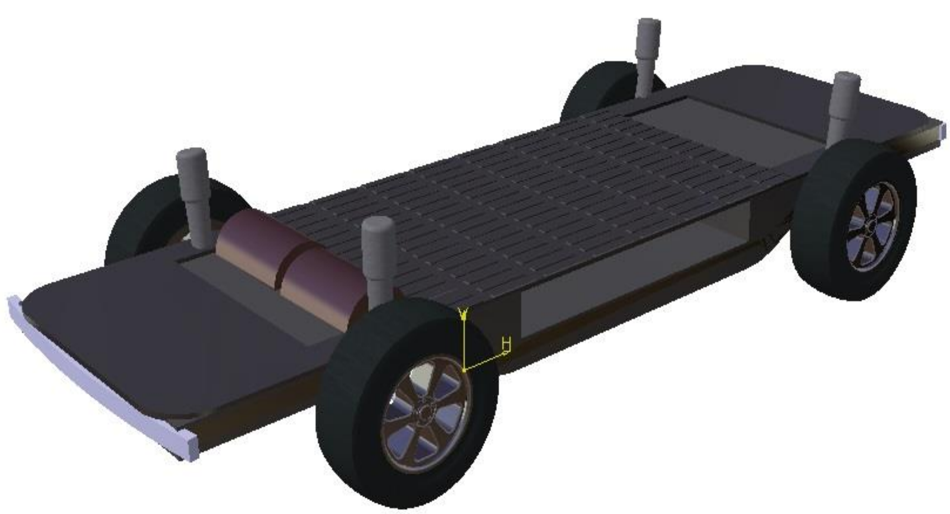

Figure 7-2 Plates mounted on the chassis frame to accommodate battery pack

The plate on the frame is used to make a box and to accommodate a battery pack on the chassis frame and its material type is the upper one is mild steel and the bottom plate is aluminum plate used to easily exchange or transfer temperature from the surrounding the battery pack.

Table 7-2 sheet metals to cover the frame

| Number | Part name | Dimension | Material type |
|---|---|---|---|
| 1 | Upper cover plate | 4764mm x 1280mm x 2.5mm | Mild steel plate |
| 3 | Bottom cover plate | 4524mm x 1280mm x 3mm | Aluminum plate |

The upper cover plat is mild steel plat and its cost is 750 ETB per square meter in current market and the upper cover of the chassis is plate is 6.09792 meter square and its total cost is

$$= 6.09792x750ETB$$

$$= 4573.44ETB$$

The bottom cover plat is aluminum plat and its cost is 975 ETB per square meter in current market and the bottom cover of the chassis is plate is 5.79072 meter square and its total cost is

$$= 5.79072x975ETB$$

$$= 5645.952ETB$$

The cost Table 7-3 for to manufacture the chassis frame includes electrodes, cutter disc, labor coast and others

$$= 2500ETB$$

Table 7-3 Total cost for chassis frame

| No | Material Items | Material specification | Total price ETB | Remark |
|---|---|---|---|---|
| 1 | Structural steel | RH S 80x40x5mm | 3179.36 | |
| 2 | Upper cover plate (Mild steel) | 4764mm x 1280mm x 2.5mm | 4573.44 | |
| 3 | Bottom cover plate (Al) | 4524mm x 1280mm x 3mm | 5645.952 | |
| 4 | Manufacturing cost | | 2500 | |
| | Total cost for the chassis frame | | 15898.754 | |

# CHAPTER SIX

# 8 SUMMERY, CONCLUSION AND RECOMMENDATION

## 8.1 Summary

This summery reports that the overall work of this thesis paper and it is short and summarized description about the aim of this thesis up to the goal that was achieved in in this thesis work.

The title of the thesis is '*Design and modification of electric vehicle chassis frame for swapping of battery packs'* when at the starting the thesis title selected based on according to the world need of the electric vehicle now a days. And then study on what are the problems on the electric vehicles? And taking the problems like the time it takes to charge the electric vehicle battery pack and taking the thermal management system as the second problem and also there are other problems also that should be study by other researchers but I took those the above two problems and tried to solve on those.

For the first problem this thesis took the solution as making the battery's that are attached to the chassis frame would be swappable by taking RAV 4 EV 2014 model as a base line. To make the attached battery pack to swappable the first problem there is a need of making a chassis frame to swapping. And the study is done on this baseline by finding the specification on vehicle and gating form the company website above in table 3-4 and finding the appropriate material according to the literatures so the material for the chassis frame is AISI 1020. And the analysis are hailed by using the analytical by calculation to find the basic parameters like shear force, bending moment, moment of inertia and static impact reaction on the chassis frame. And the modeling is done on CATIA V5 and the shear and bending moment diagram on AUTOCAD. The analysis like static, dynamic, harmonic and static impact analysis were done on the ANSYS 15 workbench.

The second problem mentioned on the above and in statement of problem is the thermal management system it was done based on the existing battery cell feature the main idea on this BTMS is shape optimization on the cooling plate on each battery cell and testing the battery and coolant temperature on EXCEL and it was checked and the average temperature from the battery is 47$^oC$ and out the plate is 38$^oC$. The existing battery cell type is pouch type and the battery thermal management system is done on this type. And the calculations for transient analysis were done. The parameters that are used to the analysis are took from the literature ***(Haifeng & Zechang, 2015)***.

Those all of mentioned on this summery are done in six chapter and the manufacturing cost of the chassis frame is mentioned on chapter seven and the conclusion includes the result of all designed parameters of chassis frame and the results of parameters of battery thermal management system and the recommendations and future works are listed on this chapter after the summery and conclusion part. In the future works there is advice to the future researchers to do their project or thesis on the electric vehicle because of the future of the world is making all vehicles to electric vehicle reason of existence fuel (the current situation of oil).

And finally this thesis work is includes the reference and the appendix of the entire document. The appendix includes the specification of RAV 4 EV 2014 model, that of the detail drawing of the chassis frame that was done on CATIA V5 and the battery cell cooling plate drawing and also the ANSYS result that was not include on the above

### 8.2 Conclusion

This thesis work is done on the title of design and modification of electric vehicle chassis frame for swapping of battery packs. It was done by the flow chart mentioned in Fig 3-1. As discussed in the chapter three the material selected for this chassis frame AISI 1020 according to its durability and cost. The mathematical conclusion is in this thesis is classified in to two parts the first part is includes the electric vehicle chassis frame analysis in the ANSYS 15 workbench. The analysis includes the structural analysis, modal analysis, harmonic analysis and static impact analysis. The second discussion for the conclusion is about the electric vehicle battery cell thermal management system.

- The structural analysis includes the total deformation of the chassis frame on ANSYS 15 and the analytical work of the result. So the total deformation on the ANSYS 15 workbench is 1.0047mm. And the von-misses stress is 115.55Mpa on the ANSYS result it shows the chassis is in safe mode. The maximum shear stress on the ANSYS is 61.111Mpa occurs on the right rear part of the battery set. The fatigue life of the designed chassis frame is 130 days with full load without deformation and sensitivity of the electric vehicle chassis frame able to 72% additional weight in 10e6 cycle beyond this percentage the sensitivity cycle tends to decrease.
- The modal analysis is discussed in 10 mode and its frequency and the main purpose of the modal analysis is used to fine the excitation frequency (resonance frequency). According to frequency amplitude diagram from the harmonic analysis in Fig 5-11 there is no resonance

on the chassis so it is safe. The static impact of front, rear and side impacts by applying a force was done and the value total deformation, stress and safety factors was done analysis is used to done. And the cost of the chassis frame according to this design is 15898.754ETB

- That what is done in this thesis work on the BTMS is shape minimization of the cooling materials like a plate and cooper coil of the coolant the previous size of the cooling plate is 230mmx150mmx12mm and the diameter of the coil is 9mm and after shape optimization the size changed to 230mmx150mmx10mm and the copper coil diameter is 7mm. the need of this minimization is to reduce the weight of the battery pack from 383.51Kg to 345.61Kg.

## 8.3 Recommendation

Investors in all over the world and the new companies that will open in Ethiopia, researchers as a new research topic, it needs many thesis and research works on electric vehicle, the universities also initiate their students work on this electric vehicle chassis frame and related electric vehicle parts and so on.

Some recommended work opportunities are as follow

- Building battery swapping stations it use for energy-refueling of battery packs in addition to this Plug charging options as auxiliary energy-refueling
- Dynamic distribution of batteries to stations and vehicles that are stack with the reason of battery charge give out.
- Batteries renting for customers because alternative batteries are needed to swap.
- Producing vehicles that are without battery pack like that of OEM Company.

## 8.4 Future works

- Detail work on material selection to chassis frame
- The chassis frame life time for different types of road cases
- The sheet metal (the upper and bottom plate cover) it needs detail study and thermal conductivity
- Stability analysis should be performed.
- Transient analysis for battery cell in the case of charging.

# REFERENCES

Abhishek, S., & Soni, V. (2014). Structural Analysis of Ladder Chassis for Higher Strength. *International Journal of Emerging Technology and Advanced Engineering*.

Adem, S. (2015). Structural Analysis of FAW Dump Truck Chassis Frame Made of Composite Materials. *Adama Science and Technology University*.

Amin, I. (2009). Design and Analyze the Chassis of an Electric Vehicle for use in Campus Condition. *university Technical Malaysia Melka*.

Axsen, J., & Burke, A. F. (2008). Batteries for PHEVs: Comparing Goals. In J. Axsen, *Electric and Hybrid Vehicles* (pp. 406-429). California at Davis: Copyright 2010, Elsevier B.V.

Badgujar, A., & Wankhade, P. (2015). Static Analysis of Chassis Frame of Electric Tricycle. *International Journal of Engineering Research & Technology (IJERT)*.

Beall, j. (2017). Intelligent Battery Management and Charging for Electric Vehicles. *Texas Instruments,USA.*

Behera, D., & Kumar, R. (2016). Design, Static and Dynamic Analysis of an All-Terrain Vehicle Chassis and Suspension System. *Volume 4, Issue 2. Gandhi Institute of Engineering and Technology, Gunupur*.

Bhaskar, E., & Muneiah, T. (2014). Static and Dynamic Analysis of Chassis. *International Journal of Research (IJR), Vol-1 Issue-6*, ISSN 2348-6848.

Contractor, A., Gaurav, P., & Rathod, &. G. (2015). Design and Analysis of Ladder Frame Chassis Considering Support at Contact Region of Leaf Spring and chassis frame. *Mechanical Engineering, LDRP-ITR Gandhinagar/Kadi Sarva Vishwavidyalaya, INDIA.*

Damtie, E. (2013). Strength Analysis of Three Wheeled Vehicle's Chassis and Body Frame Assembled in Ethiopia. *School of Graduate Studies,Addis Ababa University, Ethiopia.*

David, V. (2004). *Fundamentals of Finite Element Analysis.* Mc Graw Hill.

Dávila, A., & Schönwald, C. (2013). Advanced Electric Vehicle Architectures Collaborative Project. *ELVA, RWTH Aachen University, Germany.*

Dealer, e. p. (2014). *Toyota RAV4 EV 2014 Model Owner's manual.*

Dinger, A. (2010). Batteries for Electric Car. *The Boston Consulting Group*.

Duffie, J. A. (2013). *Solar Engineering of Thermal Process.* canada.

Eitzinger, s. (2011). Chassis, Drivetrain, and Energy Storage Layout for an Electric City Vehicle.

Emre, k. (2015). Design, Analysis and Optimization of Chassis for an Electric Vehicle. *Ç.Ü Fen veMühendislik BilimleriDergisiYıl*.

Ganhaar, S. (2013). A simple Eightweight EV Platform Ready for Your body design. *IAA*.

Haifeng, D., & Zechang, S. (2015). Design and Simulation of Liquid-cooling Plates for Thermal Management of EV Batteries. *EVS28 KINTEX, Korea*.

Hodkinson, R., & Fenton, J. (2016). Lightweight Electric/Hybrid Vehicle Design. *Reed Educational and Professional Publishing Ltd*.

Hua, J. (2017). Progress in Battery Swapping Technology and Demonstration in China.

James, E. (2017). Electric Vehicle Battery Life for the New Zealand Energy Efficiency and Conservation Authority . *EECA*.

Jean-Francois, & Kamel, N. (2017). Evolution of the Global Electric Car Stock. *Global Outlook International Agency*.

Khan, M. R., & Swierczynski, M. J. (2017). Towards an Ultimate Battery Thermal Management System. *Department of Energy Technology, Aalborg University, Pontoppidanstræde 101, Aalborg DK-9220, Denmark*.

Knutsen, D., & Willén, O. (2013). A Study of Electric Vehicle Charging Patterns and Range Anxiety. *ISSN: , UPTEC STS13 015*, 1650-8319.

Lark, J. (2012). The Anatomy of an Urban Modular Electric Vehicle. *Massachusetts Institute of Technology*.

Lovatt, R. (2008). The Development of a Lightweight Electric Vehicle Chassis and Investigation into the Suitability of TiAl for Automotive Applications. . *Hamilton, New Zealand*.

Marlay, R. C. (2013). Electric Vehicle Charging Models and Implementation. *U.S. and China. U.S. Department of Energy*.

Marzuki, M. A. (2015). Determination of Natural Frequencies through Modal and Harmonic Analysis of Space Frame Race Car Chassis Based on ANSYS. *American Journal of Engineering and Applied Sciences*.

Nunney, T. (2018, Janury 4). Retrieved from AZom.com: https://www.azom.com/article.aspx.aspx?articleID=6114

Okpala, Charles, C., & Nwokeocha, T. O. (2017). Design and Analysis of Chassis and Spring. *P.M.B. 5025 Awka, Anambra State, Nigeria.*

Ottaviano, D. (2012). Technical Assessment and Modeling of Lithium-Ion Batteries for Electric Vehicles. *Zurich*.

Pesaran, A., Swan, D., & etal.. (2011). Electric Vehicle Battery Thermal Issues and Thermal Management Techniques. *Alternative refrigerant and system efficiency symposium*.

Prajapati, U. (2017). Comparison of Electric Vehicle to the Internal Combustion Engine Vehicle and its Future Scope. *International Journal of Electrical and Electronics Engineers,*.

Pravin, A. R. (2012). Dynamic Analysis Of A Car Chassis. *International Journal of Engineering Research and Applications*, pp.955-959.

Prorok, A. (2016). Optimization of Formula SAE Electric Vehicle Frame with Finite Element Analysis. . *Honors Research Projects. 251*.

Qasim, B., & Emad, K. (2014). Mean Stress Correction Effects on the Fatigue Life Behavior of Steel Alloys by Using Stress Life Approach Theories. *International Journal of Engineering & Technology IJET-IJENS Vol:14 No:04*.

Rajput, R. (2007). *A Textbook of Automobile Engineering.* Laxim.

Ren, Y., Yu, Y., & etal.. (2016). Finite Element Analysis and Optimal Design for the Frame of SX360 Dump Trucks. *13th Global Congress on Manufacturing and Management*.

Robert, D. (1995). *Finite Element Modeling for Stress Analysis.* New york: John willay, inc.

Samba, A. (2015). Battery Electrical Vehicles-Analysis of Thermal. *MOBI (the Mobility, Logistics and Automotive Technology Research Centre)*.

Santosh, H., Naresh, K., & etal.. (2016). Modal Analysis of Two Wheeler Chassis. *IJESR*.

Sati, B. K., Upreti, P., & & Tripathi, A. (2016). Static and Dynamic Analysis of the Roll Cage for an All-Terrain Vehicle. *Imperial Journal of Interdisciplinary Research (IJIR)*.

Satinder, S., & Beant, S. (2014). Design Optimization and Statical Crush Analysis of Chassis Frame for Off Road Vehicle. *International Journal of Automobile Engineering Research and Development (IJAuERD)*.

Shumaker, A. (2018, July 9). Retrieved from Wikipedia: https://en.m.wikipedia.org/wiki/6061_aluminium_alloy

Singh, N. (2017). Dynamic Analysis and Shape Optimization of Electric Car Chassis. *International Journal of Aerospace and Mechanical Engineering, Volume 4 – No.4,ISSN (O)*, 2393-8609.

Spanoudakis, p. (2010). Design and Development of a Prototype Electric Vehicle’s Chassis. *7th BETA CAE International Conference, Greece*.

Szczesniak, G., Nogowczyk, P., & etal.. (2014). Some Basic Tips in Vehicle Chassis and Frame Design. *JME 43-346 Bielsko-Biała, Poland*.

Tang, Y., & Yu, Y. (2017). Modal and Harmonic Response Analysis of Key Components of Robotic Arm Based on ANSYS. *Zhengzhou, 450002, China*.

Taufik, A., Rashid, N., & etal.. (2014). Electric Car Chassis Design and Analysis by Using CATIA V5 R19. *IOSR Journal of Mechanical and Civil Engineering (IOSR-JMCE), e-ISSN:*, 2278-1684.

Unda, I., papadopoulos, P., & etal.. (2012). Management of Electric Vehicle Battery Charging in Distribution Networks. *Institute of Energy School of Engineering Cardiff University*.

Wankhad, P., & Badgujar, A. (2015). Static Analysis of Chassis Frame of Electric Tricycle. *international jornal of engineering research and technology (IJERT)*.

Waterman, B. (2011). Design and Construction of a Space-frame Chassis. *University of Western Australia*.

Zainuddin, A., Abidin, K., Ibrahim, I., & etal.. (2015). Stress Analysis of the Personal Electric Vehicle Frame. *Conference Paper*.

# APPENDIX A

CAD modeling of electric vehicle chassis frame

Figure A-0-1 New chassis frame with its battery pack

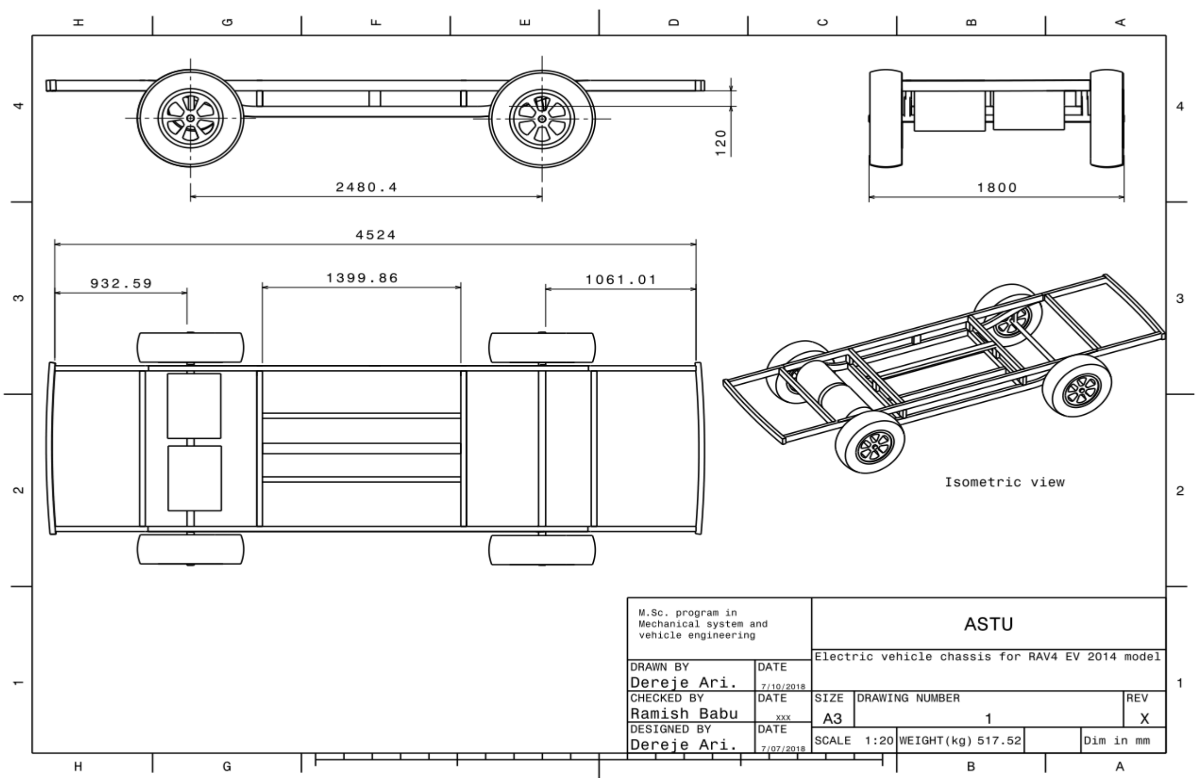


Figure A-0-2 Designed chassis frame and its external dimension

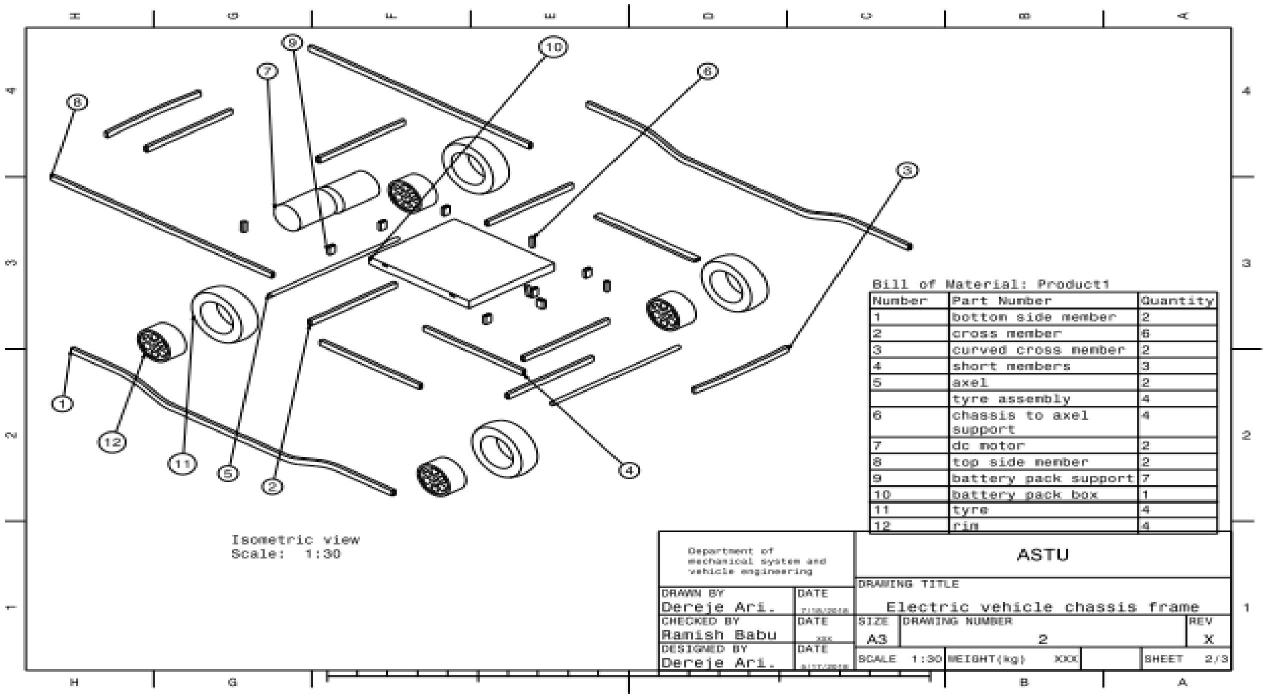


Figure A-0-3 Parts of the electric vehicle chassis frame

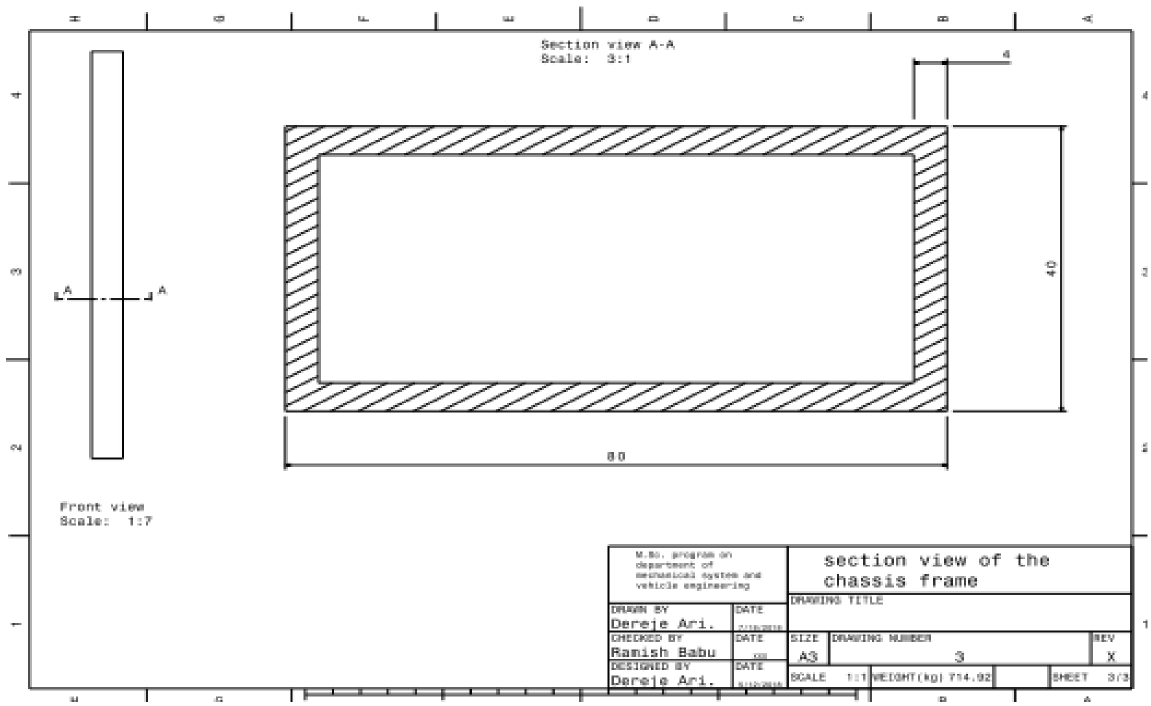


Figure A-0-4 Section view of the chassis frame all member have same section

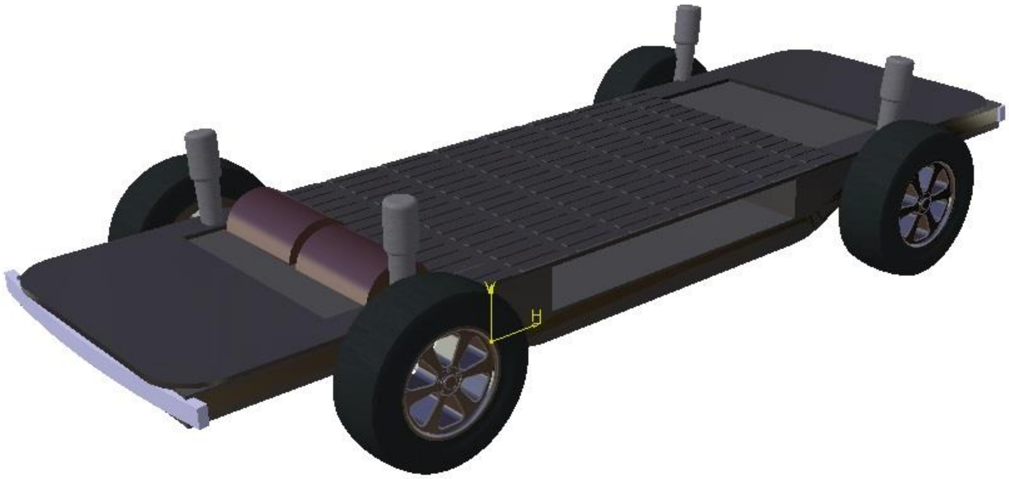

Figure A-0-5 Electric vehicle chassis frame without battery pack

Figure A-0-6 Electric vehicle chassis frame with battery pack

Figure A-0-7 Actual RAV4 EV 2014 chassis model

# APPENDIX B

CAD modeling of electric vehicle battery cell design and the battery cell ANSYS discussion

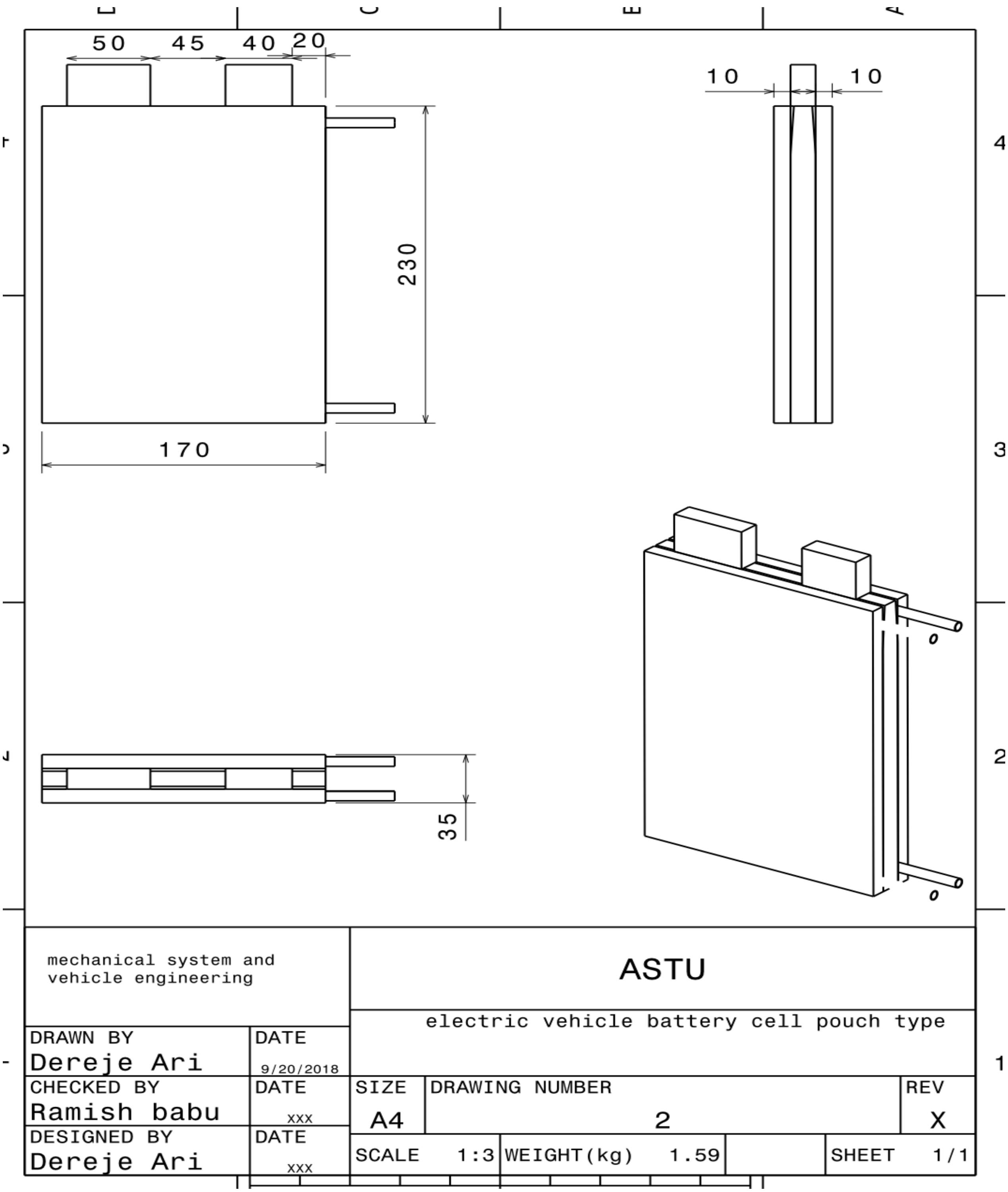


Figure B-0-1 Modified CAD modeling of battery cell and cooling plate

# APPENDIX C

Results and discussion of electric vehicle chassis frame in table form

Table C-0-1 Modal analysis for the chassis frame

| | |
|---|---|
| Object Name | *Frequency Response* |
| State | Solved |
| **Scope** | |
| Scoping Method | Geometry Selection |
| Geometry | 31 Faces |
| Spatial Resolution | Use Maximum |
| **Definition** | |
| Type | Directional Deformation |
| Orientation | Z Axis |
| Suppressed | No |
| **Options** | |
| Frequency Range | Use Parent |
| Minimum Frequency | 0. Hz |
| Maximum Frequency | 50. Hz |
| Display | Bode |
| **Results** | |
| Maximum Amplitude | 2.9118 mm |
| Frequency | 35. Hz |
| Phase Angle | 17.546 ° |
| Real | 2.7764 mm |
| Imaginary | 0.87783 mm |

Table C-0-2 properties of the imported geometry into ANSYS

| | |
|---|---|
| Object Name | *Geometry* |
| State | Fully Defined |
| **Definition** | |
| Source | C:\Users\CHU\Desktop\project files\catia working files\New folder\new chassis.igs |
| Type | Iges |
| Length Unit | Meters |
| Element Control | Program Controlled |
| Display Style | Body Color |
| **Bounding Box** | |
| Length X | 1328. mm |
| Length Y | 4648. mm |
| Length Z | 283.29 mm |
| **Properties** | |
| Volume | 3.321e+007 $mm^3$ |
| Mass | 260.7 kg |
| Scale Factor Value | 1. |
| **Statistics** | |
| Bodies | 22 |
| Active Bodies | 22 |
| Nodes | 39612 |
| Elements | 6316 |
| Mesh Metric | None |

Table C-0-3 Properties for imported geometry parts

| **Object Name** | ***Part 1*** | ***Part 2*** | ***Part 3*** | ***Part 4*** | ***Part 5*** | ***Part 6*** | ***Part 7*** | ***Part 8*** | ***Part 9*** | ***Part 10*** | ***Part 11*** |
|---|---|---|---|---|---|---|---|---|---|---|---|
| State | Meshed | | | | | | | | | | |
| **Material** | | | | | | | | | | | |
| Assignment | Structural Steel | | | | | | | | | | |

<table>
<tr><th colspan="12">Bounding Box</th></tr>
<tr><td>Length X</td><td>80. mm</td><td>40. mm</td><td colspan="5">80. mm</td><td colspan="2">40. mm</td><td>80. mm</td><td>40. mm</td></tr>
<tr><td>Length Y</td><td>40. mm</td><td>80. mm</td><td colspan="5">40. mm</td><td colspan="2">3103.5 mm</td><td colspan="2">1400. mm</td></tr>
<tr><td>Length Z</td><td colspan="7">120. mm</td><td colspan="2">80. mm</td><td>40. mm</td><td>80. mm</td></tr>
<tr><th colspan="12">Properties</th></tr>
<tr><td>Volume</td><td colspan="7">1.0752e+005 mm³</td><td colspan="2">2.7808e+006 mm³</td><td colspan="2">1.2544e+006 mm³</td></tr>
<tr><td>Mass</td><td colspan="7">0.84403 kg</td><td colspan="2">21.829 kg</td><td colspan="2">9.847 kg</td></tr>
<tr><td>Centroid X</td><td>649.8 mm</td><td>629.8 mm</td><td>1248.7 mm</td><td>1849.6 mm</td><td>1248.7 mm</td><td>649.8 mm</td><td>1849.6 mm</td><td>629.8 mm</td><td>1869.6 mm</td><td>1248.7 mm</td><td>996.02 mm</td></tr>
<tr><td>Centroid Y</td><td>622.48 mm</td><td>-4.5138 mm</td><td>-817.46 mm</td><td>622.51 mm</td><td>622.55 mm</td><td>-817.43 mm</td><td>-817.48 mm</td><td>-48.608 mm</td><td>-52.711 mm</td><td colspan="2">-97.463 mm</td></tr>
<tr><td>Centroid Z</td><td colspan="7">129.27 mm</td><td colspan="2">229.27 mm</td><td>249.27 mm</td><td>29.168 mm</td></tr>
<tr><td>Moment of Inertia Ip1</td><td colspan="7">886.8 kg·mm²</td><td colspan="2">22935 kg·mm²</td><td colspan="2">10346 kg·mm²</td></tr>
<tr><td>Moment of Inertia Ip2</td><td colspan="7">1682.9 kg·mm²</td><td colspan="2">1.7539e+007 kg·mm²</td><td colspan="2">1.6162e+006 kg·mm²</td></tr>
<tr><td>Moment of Inertia Ip3</td><td colspan="7">1229.6 kg·mm²</td><td colspan="2">1.7527e+007 kg·mm²</td><td colspan="2">1.6109e+006 kg·mm²</td></tr>
<tr><th colspan="12">Statistics</th></tr>
<tr><td>Nodes</td><td colspan="7">1128</td><td colspan="2">26328</td><td colspan="2">11880</td></tr>
<tr><td>Elements</td><td colspan="7">144</td><td colspan="2">3744</td><td colspan="2">1680</td></tr>
</table>

Table C-0-4 Properties of the imported geometry part 2

| **Object Name** | ***Part 12*** | ***Part 13*** | ***Part 14*** | ***Part 15*** | ***Part 16*** | ***Part 17*** | ***Part 18*** | ***Part 19*** | ***Part 20*** | ***Part 21*** | ***Part 22*** |
|---|---|---|---|---|---|---|---|---|---|---|---|
| State | Meshed | | | | | | | | | | |
| **Graphics Properties** | | | | | | | | | | | |
| Visible | Yes | | | | | | | | | | |
| Transparency | 1 | | | | | | | | | | |
| **Definition** | | | | | | | | | | | |
| Suppressed | No | | | | | | | | | | |
| Stiffness Behavior | Flexible | | | | | | | | | | |
| Coordinate System | Default Coordinate System | | | | | | | | | | |
| Reference Temperature | By Environment | | | | | | | | | | |
| **Material** | | | | | | | | | | | |
| Assignment | Structural Steel | | | | | | | | | | |
| **Bounding Box** | | | | | | | | | | | |
| Length X | 40. mm | 1326.8 mm | 1326.5 mm | 1200. mm | | | | | | 40. mm | |
| Length Y | 1400. mm | 72.511 mm | 68.028 mm | 40. mm | | | | | | 4524. mm | |
| Length Z | 80. mm | 86.442 mm | 80. mm | | | | | | | 280. mm | |
| **Properties** | | | | | | | | | | | |
| Volume | 1.2544e+006 mm³ | 4.2305e+006 mm³ | | 1.0752e+006 mm³ | | | | | | 4.1101e+006 mm³ | |
| Mass | 9.847 kg | 33.21 kg | | 8.4403 kg | | | | | | 32.264 kg | |
| Centroid X | 1487.6 mm | 1248.2 mm | 1247. mm | 1250. mm | 1249.6 mm | 1249.7 mm | | | | 629.67 mm | 1869.7 mm |

| | | | | | | | | | | | |
|---|---|---|---|---|---|---|---|---|---|---|---|
| Centroid Y | -97.463 mm | -2293.1 mm | 2293.1 mm | 622.48 mm | -817.38 mm | 1542.6 mm | -1643.6 mm | 622.54 mm | -817.46 mm | -1.0022 mm | |
| Centroid Z | 29.168 mm | 229.07 mm | 229.15 mm | 229.27 mm | | 229.17 mm | 229.27 mm | 29.168 mm | | 127.5 mm | 127.61 mm |
| Moment of Inertia Ip1 | 10346 kg·mm² | 4.8563e+006 kg·mm² | | 8868. kg·mm² | | | | | | 5.5133e+007 kg·mm² | |
| Moment of Inertia Ip2 | 1.6162e+006 kg·mm² | 24082 kg·mm² | | 1.0195e+006 kg·mm² | | | | | | 2.9879e+005 kg·mm² | |
| Moment of Inertia Ip3 | 1.6109e+006 kg·mm² | 4.8676e+006 kg·mm² | | 1.015e+006 kg·mm² | | | | | | 5.4851e+007 kg·mm² | |
| **Statistics** | | | | | | | | | | | |
| Nodes | 11880 | 3521 | | 10200 | | | | | | 39600 | |
| Elements | 1680 | 536 | | 1440 | | | | | | 5640 | |
| Mesh Metric | None | | | | | | | | | | |